

Julius-Maximilians-Universität Würzburg



Studies on the function and regulation of CD84,
GPVI and Orai2 in genetically modified mice

Untersuchungen zur Funktion und Regulation von CD84,
GPVI und Orai2 in genetisch veränderten Mäusen

Doctoral thesis for a doctoral degree

at the Graduate School of Life Sciences

Section Biomedicine

submitted by

Sebastian Hofmann

from

Coburg

Würzburg, 2013

Submitted on:

Office stamp

Members of the *Promotionskomitee*:

Chairperson: Prof. Dr. Manfred Gessler

Primary Supervisor: Prof. Dr. Bernhard Nieswandt

Supervisor (Second): PD Dr. Heike Hermanns

Supervisor (Third): Prof. Dr. Guido Stoll

Date of Public Defence:

Date of Receipt of Certificates:

Summary

Platelet activation and aggregation at sites of vascular injury are essential processes to limit blood loss but they also contribute to arterial thrombosis, which can lead to myocardial infarction and stroke. Stable thrombus formation requires a series of events involving platelet receptors which contribute to adhesion, activation and aggregation of platelets. Regulation of receptor expression by (metallo-)proteinases has been described for several platelet receptors, but the molecular mechanisms are ill-defined.

The signaling lymphocyte activation molecule (SLAM) family member CD84 is expressed in immune cells and platelets, however its role in platelet physiology was unclear. In this thesis, CD84 deficient mice were generated and analyzed. In well established *in vitro* and *in vivo* assays testing platelet function and thrombus formation, CD84 deficient mice displayed phenotypes indistinguishable from wild-type controls. It was concluded that CD84 in platelets does not function as modulator of thrombus formation, but rather has other functions. In line with this, in the second part of this thesis, a novel regulation mechanism for platelet CD84 was discovered and elucidated. Upon platelet activation, the N-terminus of CD84 was found to be cleaved exclusively by the α disintegrin and metalloproteinase 10 (ADAM10), whereas the intracellular part was cleaved by calpain. In addition, regulation of the platelet activating collagen receptor glycoprotein VI (GPVI) was studied and it was shown that GPVI is in contrast to CD84 differentially regulated by ADAM10 and ADAM17. A novel role of CD84 under pathophysiological conditions was revealed as CD84 deficient mice were protected from ischemic stroke in the model of transient middle cerebral artery occlusion and this protection was based on the lack of CD84 in T cells.

Ca^{2+} is an essential second messenger that facilitates activation of platelets and diverse functions in different eukaryotic cell types. Store-operated Ca^{2+} entry (SOCE) represents the major mechanism leading to rise in intracellular Ca^{2+} concentration in non-excitabile cells. The Ca^{2+} sensor STIM1 (stromal interaction molecule 1) and the SOC channel subunit protein Orai1 are established mediators of SOCE in platelets. STIM2 is the major STIM isoform in neurons, but the role of the SOC channel subunit protein Orai2 in platelets and neurons has remained elusive. In the third part of this thesis, Orai2 deficient mice were generated and analyzed. Orai2 was dispensable for platelet function, however, Orai2 deficient mice were protected from ischemic neurodegeneration and this phenotype was attributed to defective SOCE in neurons.

Zusammenfassung

Die Aktivierung und Aggregation von Blutplättchen sind wichtige Prozesse um Blutverlust nach Gefäßverletzungen zu vermeiden. Diese Prozesse spielen aber auch eine Rolle in der arteriellen Thrombose, die zu Herzinfarkt und Schlaganfall führen kann. Die Bildung stabiler Thromben setzt eine Reihe von Vorgängen voraus, an denen Blutplättchenrezeptoren beteiligt sind, welche zur Adhäsion, Aktivierung und Aggregation der Blutplättchen beitragen. Für einige Blutplättchenrezeptoren wurde eine Regulation der Expression durch (Metallo-)Proteinasen beschrieben, jedoch sind die molekularen Mechanismen weitgehend unbekannt.

CD84, ein Protein das zur *signaling lymphocyte activation molecule* (SLAM) Familie gehört, wird sowohl in Immunzellen als auch in Blutplättchen exprimiert. Jedoch war die Rolle von CD84 in der Physiologie der Blutplättchen unklar. In der vorliegenden Arbeit wurden CD84 defiziente Mäuse generiert und analysiert. In etablierten *in vitro* und *in vivo* Test, welche die Blutplättchenfunktion und Thrombusbildung untersuchen, war der Phänotyp von CD84 defizienten Mäusen unverändert gegenüber Wildtyp-Kontrollen. Es wurde die Schlussfolgerung gezogen, dass CD84 in Blutplättchen nicht als Modulator der Thrombusbildung fungiert, sondern eher andere Funktionen hat. Im Einklang damit wurde im zweiten Teil dieser Arbeit ein neuer Regulationsmechanismus entdeckt und aufgeklärt. Infolge von Blutplättchenaktivierung wurde der N-terminale Teil von CD84 ausschließlich von *a disintegrin and metalloproteinase 10* (ADAM10) geschnitten, während der intrazelluläre Anteil durch Calpain prozessiert wurde. Weiterhin wurde die Regulation des Blutplättchen-aktivierenden Kollagenrezeptors Glykoprotein VI (GPVI) untersucht. Es konnte gezeigt werden, dass GPVI, im Gegensatz zu CD84, einer differenziellen Regulation durch ADAM10 und ADAM17 unterliegt. Unter pathophysiologischen Bedingungen wurde eine neue Rolle von CD84 aufgedeckt, da CD84 defiziente Mäuse vor ischämischem Schlaganfall im *transient middle cerebral artery occlusion* Modell geschützt waren. Dieser Schutz beruhte auf dem Fehlen von CD84 auf T Zellen.

Ca^{2+} ist ein wichtiger sekundärer Botenstoff, der die Aktivierung von Blutplättchen ermöglicht sowie diverse Funktionen in verschiedenen eukaryotischen Zellen erfüllt. *Store-operated Ca^{2+} entry* (SOCE) stellt den Hauptmechanismus dar, der zum Anstieg der intrazellulären Ca^{2+} Konzentration in nicht-erregbaren Zellen führt. Der Ca^{2+} Sensor STIM1 (*stromal interaction molecule 1*) und das SOC-Kanal Protein Orai1 sind als Vermittler des SOCE in Blutplättchen bekannt. STIM2 stellt die Hauptisoform der STIM Moleküle in Neuronen dar, jedoch war die Rolle des SOC-Kanal Proteins Orai2 in Blutplättchen und Neuronen weitgehend unbekannt. Im dritten Teil dieser Arbeit wurden Orai2 defiziente Mäuse generiert und analysiert. Orai2 war nicht essentiell für die Funktion von Blutplättchen, jedoch waren

Orai2 defiziente Mäuse vor ischämischer Neurodegeneration geschützt. Dieser Phänotyp wurde auf einen defekten SOCE in Neuronen zurückgeführt.

Table of contents

1	Introduction	1
1.1	Platelets	1
1.2	Thrombus formation	2
1.3	GPVI	4
1.3.1	Structure and signaling of GPVI	4
1.3.2	GPVI as potential antithrombotic target	5
1.4	SLAM family receptors	6
1.5	CD84.....	9
1.5.1	Gene and protein structure.....	9
1.5.2	CD84 in platelets and other cell types	10
1.6	Downregulation of platelet receptor expression	12
1.6.1	Metalloproteinases of the ADAM family	13
1.6.2	Calpain.....	14
1.7	Thrombotic diseases	15
1.8	Store-operated calcium entry (SOCE)	17
1.9	Orai2.....	18
1.10	Aim of the study	19
2	Materials and Methods	21
2.1	Materials	21
2.1.1	Chemicals and reagents.....	21
2.1.2	Kits.....	23
2.1.3	Cell culture material.....	24
2.1.4	Radioactive labeling	24
2.1.5	Buffers and media	24
2.1.6	Oligonucleotides.....	30
2.1.7	Antibodies	32
2.1.8	Other materials.....	33

Table of contents

2.1.9	Plasmids	33
2.1.10	Bacteria.....	33
2.2	Methods	34
2.2.1	Molecular biology	34
2.2.1.1	PCR	34
2.2.1.2	Agarose gel electrophoresis	35
2.2.1.3	DNA extraction from agarose gels.....	35
2.2.1.4	Digestion of plasmid DNA	36
2.2.1.5	Ligation of insert and vector	36
2.2.1.6	TOPO cloning	36
2.2.1.7	Transformation	37
2.2.1.8	Mini Plasmid DNA purification	37
2.2.1.9	Midi Plasmid DNA purification	37
2.2.1.10	Sequencing of DNA.....	38
2.2.2	Stem cell work.....	38
2.2.2.1	Feeder cells	38
2.2.2.2	Electroporation	38
2.2.2.3	Selection of ES cells	39
2.2.2.4	Picking of Geneticin-resistant ES cell clones.....	39
2.2.2.5	Freezing of picked stem cells	40
2.2.2.6	Lysis of stem cells	40
2.2.2.7	Precipitation of stem cell DNA	40
2.2.2.8	Analysis of stem cell DNA by Southern blot.....	40
2.2.2.9	Reculturing of positive stem cells	41
2.2.3	Isolation of DNA	42
2.2.4	Genotyping of <i>Cd84^{-/-}</i> mice by PCR.....	42
2.2.5	Genotyping of <i>Orai2^{-/-}</i> mice by PCR	43
2.2.6	RNA isolation and RT-PCR	45
2.2.7	Adoptive transfer of T cells.....	45

Table of contents

2.2.8	Preparation of lysates from different organs	46
2.2.9	Biochemistry	46
2.2.9.1	Western blotting (Immunoblotting).....	46
2.2.9.2	HRP-labeling of antibodies.....	47
2.2.9.3	FITC-labeling of antibodies	47
2.2.9.4	Biotinylation of antibodies.....	47
2.2.9.5	sCD84 ELISA.....	47
2.2.9.6	sGPVI ELISA	48
2.2.10	Generation of bone marrow chimeric mice	48
2.2.11	Isolation and analysis of immune cells	48
2.2.12	<i>In vitro</i> analysis of platelets	49
2.2.12.1	Platelet preparation and washing	49
2.2.12.2	Platelet counting.....	49
2.2.12.3	Flow cytometry	49
2.2.12.4	Aggregometry	50
2.2.12.5	Spreading assay	51
2.2.12.6	Adhesion under flow.....	51
2.2.12.7	Clot retraction.....	51
2.2.12.8	Shedding of glycoproteins from the platelet surface	52
2.2.13	<i>In vivo</i> studies	52
2.2.13.1	Platelet life span.....	52
2.2.13.2	Intravital microscopy of FeCl ₃ -injured mesenteric arterioles	52
2.2.13.3	Mechanical injury of the abdominal aorta	53
2.2.13.4	Bleeding time assay	53
2.2.13.5	Transient middle cerebral artery occlusion (tMCAO) model.....	53
2.2.14	Isolation and culture of neurons, Ca ²⁺ imaging	54
2.3	Data analysis.....	54
3	Results.....	56
3.1	Generation CD84 deficient mice.....	56

Table of contents

3.1.1	Targeting strategy and electroporation of murine ES cells.....	56
3.1.2	Screening of recombinant stem cell clones and generation of chimeric mice ..	57
3.1.3	Breeding of homozygous <i>Cd84</i> ^{-/-} mice.....	59
3.2	Basal analysis of CD84 deficient mice.....	60
3.2.1	CD84 deficient mice are born in Mendelian ratio and develop normally.....	60
3.2.2	Proof of CD84 deficiency at cellular level	61
3.2.3	Unaltered lymphocyte populations in CD84 deficient mice	62
3.3	Platelet function and thrombus formation in CD84 deficient mice	64
3.3.1	Platelet production	64
3.3.2	Agonist induced activation and degranulation <i>in vitro</i>	65
3.3.3	Aggregation, spreading on fibrinogen and clot retraction.....	66
3.3.4	Procoagulant responses and thrombus formation under flow	68
3.3.5	Thrombus formation <i>in vivo</i>	70
3.3.6	Normal hemostasis in <i>Cd84</i> ^{-/-} mice.....	72
3.4	Regulation of CD84 receptor levels in platelets	73
3.4.1	Ectodomain shedding of CD84 by metalloproteinases in human and murine platelets	73
3.4.2	Calpain and metalloproteinases cleave CD84	76
3.4.3	ADAM10 is the principal sheddase for CD84 in murine platelets.....	78
3.4.4	ADAM10 and calpain regulate surface expression of CD84 in response to agonist receptor stimulation.....	80
3.4.5	High concentrations of sCD84 in plasma of wild-type mice.....	82
3.5	Regulation of GPVI receptor levels in platelets mechanistically differs from CD84 regulation.....	83
3.5.1	GPVI is differentially regulated by ADAM10 and ADAM17 <i>in vitro</i>	83
3.5.2	GPVI shedding <i>in vivo</i> is unaltered in <i>Adam10</i> ^{-/-} and <i>Adam17</i> ^{ex/ex} mice	85
3.5.3	Abrogated GPVI shedding in <i>Adam10</i> ^{-/-} / <i>Adam17</i> ^{ex/ex} double-mutant platelets <i>in vitro</i>	86
3.5.4	Unaltered JAQ1-induced GPVI shedding in <i>Adam10</i> ^{-/-} / <i>Adam17</i> ^{ex/ex} mice.....	86

Table of contents

3.5.5	Differential effects of JER1 antibody administration compared to JAQ1 <i>in vivo</i> ..	87
3.6	CD84 deficient mice are protected from ischemic stroke	89
3.7	Generation of Orai2 deficient mice	92
3.7.1	Cloning of a targeting vector for disrupting the <i>Orai2</i> gene	93
3.7.2	Electroporation of <i>Orai2</i> targeting vector and analysis of recombinant clones ..	94
3.7.3	Breeding of homozygous <i>Orai2</i> ^{-/-} mice.....	95
3.8	Analysis of Orai2 deficient mice.....	96
3.8.1	Orai2 deficient mice are born in Mendelian ratio and develop normally	96
3.8.2	Normal platelet function and hemostasis in Orai2 deficient mice	97
3.8.3	Orai2 deficient mice are protected from ischemic stroke and show reduced SOCE in neurons	100
4	Discussion.....	103
4.1	Analysis of CD84 deficient mice	104
4.1.1	CD84 is dispensable for platelet function in thrombosis and hemostasis	104
4.1.2	Loss of CD84 provides protection from ischemic stroke	107
4.2	Regulation of CD84 in platelets by ADAM10 and calpain	109
4.3	Regulation of GPVI by ADAM10 and ADAM17.....	112
4.4	Orai2 deficiency protects from ischemia-induced neuronal damage.....	115
4.5	Concluding remarks and future plans	118
5	References.....	120
6	Appendix	133
6.1	Abbreviations	133
6.2	Curriculum Vitae.....	136
6.3	Publications.....	137
6.4	Acknowledgements	139
6.5	Affidavit	140

1 Introduction

1.1 Platelets

Blood platelets are discoid-shaped anucleate cell fragments that are produced by megakaryocytes (MKs) in the bone marrow. Thrombopoietin (TPO) is the primary regulator of MK differentiation and platelet production.¹ The exact mechanism of platelet formation from MKs is not fully understood. According to a current model, protrusions, called proplatelets, are released from the MK body into microvessels, where they are further fragmented into platelets,² and this concept is also supported by recent findings from *in vivo* studies in bone marrow.³ Platelets are the smallest cellular components circulating in the blood stream, with a diameter of 1-2 μm in mice and 3-4 μm in humans.⁴ Normal platelet counts range between 150,000-400,000 per μL blood in humans, whereas mice have platelet counts that are on average around 1,000,000 per μL . Mouse platelets have a short lifespan of about 4.5–5.5 days,⁵ whereas human platelet life span reaches 10 days. Due to the lack of a nucleus, platelets are only to a limited extent capable of *de novo* protein synthesis, using MK-derived mRNA and translational machinery.⁶ The bilamellar plasma membrane of platelets extends through interconnected channels of the open canalicular system (OCS), representing a source of membrane for surface increase after platelet activation and shape change.⁷ The dense tubular system derives from the endoplasmic reticulum of the parent MK. Mitochondria, glycogen stores and three different major types of granules (α -granules, dense granules and lysosomes) are found in platelets.⁸ Dense granules contain small molecules such as serotonin, adenosine di- or triphosphate (ADP, ATP), playing a role as amplifiers of platelet aggregation. α -granules store adhesion molecules and coagulation factors such as fibronectin, von Willebrand factor (vWF), thrombospondin-1, P-selectin, fibrinogen, plasminogen, factors V, VII, XI and XIII as well as mitogenic factors like platelet derived growth factor (PDGF) and vascular endothelial growth factor (VEGF). Throughout their life, most platelets never undergo activation and are finally removed from the blood stream by the reticuloendothelial system in the spleen and liver. The pivotal primary hemostatic function of platelets is only retrieved upon injury, when platelets in the flowing blood come into contact with the exposed subendothelial extracellular matrix (ECM), which leads to their rapid activation and the formation of a hemostatic plug. This lifesaving function of platelets limits blood loss following injury. On the other hand, under pathological conditions, like rupture of an atherosclerotic plaque, platelet aggregation may lead to formation of occlusive thrombi resulting in vessel occlusion and infarction of vital organs.⁹ Therefore, platelet activation has to be tightly regulated, which requires a complex interplay of adhesion and activation receptors,¹⁰ release of soluble mediators, inhibitory receptors,¹¹ as well as cleavage and

inactivation of receptors,¹² in order to facilitate stable aggregate formation to seal lesions, while preventing excessive thrombus formation.

1.2 Thrombus formation

Platelet adhesion and subsequent thrombus formation are multistep processes which can be divided into three main steps: adhesion/tethering, activation and aggregation (Figure 1). The first step requires interactions of platelet surface receptors with the exposed ECM, which comprises macromolecules such as fibronectin, collagens and laminins. Upon injury of the vessel wall, initial adhesion of platelets is facilitated by the GPIb-V-IX complex, which functions irrespective of cellular activation. Interaction of GPIb α on circulating platelets tethers platelets to the damaged vessel wall under high shear conditions, such as found in arterioles, by interacting with collagen-bound von Willebrand Factor (vWF).^{13,14} These interactions are only transient and do not mediate firm adhesion, but facilitate the contact between GPVI and collagen. The GPVI-collagen interaction induces intracellular signaling cascades, leading to platelet activation, followed by a conformational change of integrins (most importantly $\alpha 2\beta 1$ and $\alpha \text{IIb}\beta 3$) to a high affinity state, and the release of second-wave mediators like ADP and thromboxane A₂ (TxA₂).¹⁵ These soluble agonists along with locally produced thrombin contribute to full platelet activation through G protein coupled receptors (GPCRs).¹⁶ Consequently, platelet activation is amplified, resulting in thrombus growth by recruiting and activating more platelets from flowing blood.¹⁷

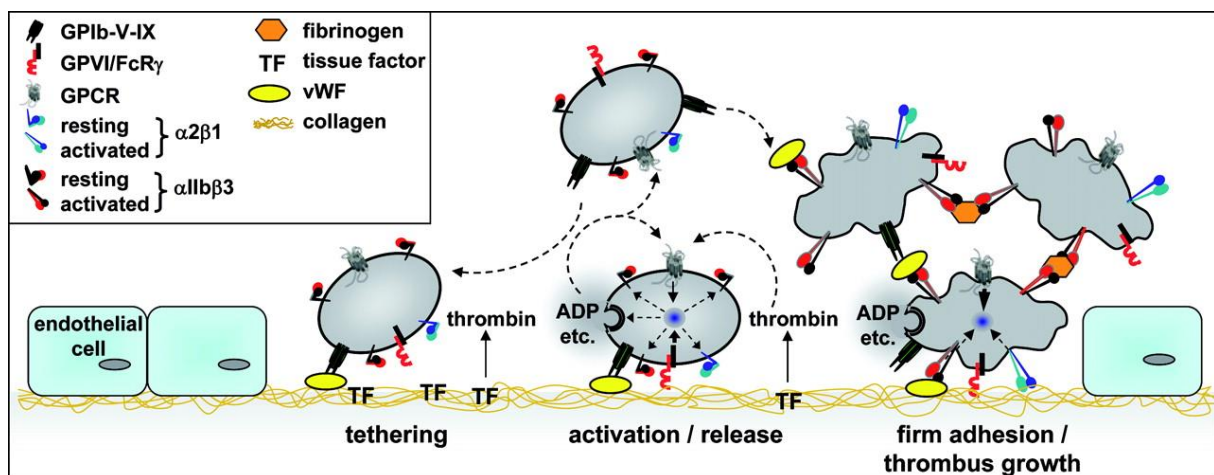


Figure 1. Steps of platelet adhesion, activation, and aggregation at the site of vascular wall injury. The GPIb α -vWF interaction mediates platelet deceleration and tethering on the exposed ECM thus allowing the interaction of GPVI with exposed collagen. This subsequently triggers the shift of integrins (notably $\alpha \text{IIb}\beta 3$) from a low affinity state to a high affinity state and to the release of secondary mediators such as ADP and TxA₂. Together with the locally produced tissue factor (TF) - induced thrombin generation, soluble mediators enhance platelet activation and contribute to the recruitment of further platelets into a growing thrombus. (Taken from: Varga-Szabo *et al.*, *ATVB*, 2008)¹⁰

Activated integrin $\alpha 2\beta 1$ mediates direct adhesion to collagen and $\alpha \text{IIb}\beta 3$ binds to collagen indirectly via vWF. Importantly, activated $\alpha \text{IIb}\beta 3$ also facilitates the formation of platelet aggregates by binding to fibrinogen or vWF, which cross-links newly activated platelets and leads to incorporation of activated platelets into the growing thrombus. Only under conditions of extremely high shear ($>10,000 \text{ s}^{-1}$), conditions comparable to those occurring in stenotic coronary arteries, platelets have been shown to adhere and aggregate irrespectively of cellular activation and GPIb-vWF interaction is sufficient to trigger formation of large but unstable aggregates.^{18,19} Under lower shear conditions, platelet responses like inside-out activation of integrins or coagulant activity, are determined by rise of the intracellular calcium level $[\text{Ca}^{2+}]_i$. Elevations in $[\text{Ca}^{2+}]_i$ can originate from two major sources: the release of compartmentalized Ca^{2+} and the entry of extracellular Ca^{2+} through the plasma membrane (PM). The major Ca^{2+} entry pathway across the PM in platelets is store-operated calcium entry (SOCE). This process involves receptor mediated release of Ca^{2+} from intracellular stores, which then triggers Ca^{2+} influx across the PM via store-operated calcium (SOC) channels.²⁰ SOCE can be initiated by activation of two major platelet signaling pathways - Phospholipase (PL)C β , activated by soluble agonists like thrombin, ADP or TxA₂, which stimulate receptors coupled to the heterotrimeric G-protein G_q, and PLC $\gamma 2$, which is activated downstream of GPVI or CLEC-2.²¹ Activated PLC isoforms hydrolyze the membrane phospholipid phosphatidylinositol-4,5-biphosphate (PIP₂) to inositol-1,4,5-trisphosphate (IP₃) and diacylglycerol (DAG). DAG activates protein kinase C (PKC), and IP₃ directly induces Ca^{2+} release from the intracellular stores. This leads to moderate elevation of $[\text{Ca}^{2+}]_i$. The reduced store content is sensed by the calcium sensor protein STIM1,²² which then triggers profound Ca^{2+} influx across the plasma membrane through SOC channels. Orai1 was recently identified as the major SOC channel in platelets.²³

Together, these mechanisms lead to thrombus formation and growth. Platelet-platelet contacts in thrombi need to be stabilized by further mechanisms, like integrin outside-in signaling²⁴ and other contact dependent signaling. The concept of the "platelet synapse" is based on the assumption that boundaries between adjacent platelets are populated by signaling and adhesion molecules, thereby creating a prothrombotic environment.^{25,26} Among these molecules is CD40L, which was identified as a ligand for $\alpha \text{IIb}\beta 3$, supporting stable formation of arterial thrombi.²⁷ Additionally, Gas6 (stored in α -granules and secreted following activation) binds to the receptor tyrosine kinases Tyro3, Axl, and Mer, thereby stimulating tyrosine phosphorylation of the $\beta 3$ integrin, and thus amplifying outside-in signaling via $\alpha \text{IIb}\beta 3$.²⁸ Interactions of ephrins and Eph kinases on adjacent platelet surfaces in platelet aggregates contribute to high-affinity platelet-platelet contacts.²⁹ SLAM (CD150)

and CD84, two members belonging to the CD2 family of homophilic adhesion molecules, are expressed on the surface of platelets and may contribute to stabilization of thrombi.³⁰

1.3 GPVI

1.3.1 Structure and signaling of GPVI

GPVI is a type I transmembrane receptor of 62 kDa belonging to the immunoglobulin (Ig) superfamily that is exclusively expressed in platelets and MKs.^{31,32} Two Ig domains are followed by a mucin like stalk that contains O-glycosylation sites, a transmembrane region and a 51 amino acid cytoplasmic tail. Mouse GPVI contains only 27 amino acids in its cytoplasmic tail, because it is lacking the C-terminal region downstream of the proline-rich region. The positively charged arginine residue in the transmembrane region of GPVI interacts with the FcR γ chain via a salt bridge³³ (Figure 2). GPVI expression on the platelet surface was demonstrated to strictly depend on its association with the FcR γ chain.³⁴

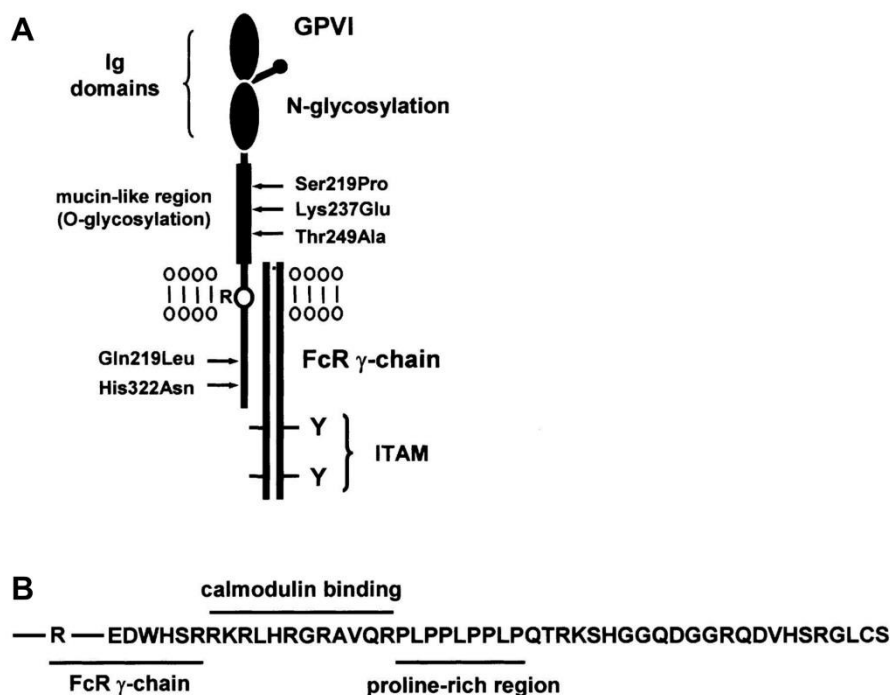


Figure 2. The GPVI/Fc receptor γ -chain complex. (A) GPVI contains 2 extracellular Ig domains, followed by a mucin-rich region containing O-glycosylation sites. The transmembrane domain has an arginine (R) group that is required for the association with the FcR γ -chain through a salt bridge. The FcR γ -chain is present as a disulphide-linked homodimer and has 2 tyrosines in a conserved sequence known as an ITAM. Tyrosine residues (Y) in the ITAM are indicated. (B) Amino acid sequence of the cytosolic tail of GPVI showing the sites that interact with FcR γ -chain, calmodulin, and SH3 recognition domain (proline-rich region). (Adapted from Nieswandt and Watson, *Blood*, 2003)¹⁵

The FcR γ chain contains an immunoreceptor tyrosine based activation motif (ITAM) sequence which represents the signaling subunit of the receptor complex.³⁵ Further, GPVI dimerization on platelets was shown to be operative in the process of ligand binding.^{36,37} Collagen is the most important physiological ligand for GPVI. Many collagen isoforms are expressed in the vessel wall, with fibrillar type I and III being the major constituents of the ECM of blood vessels. Approximately 10% of the collagen amino acid composition consists of GPO (glycine-proline-hydroxyproline) repeats, which are essential for GPVI binding.¹⁵ Powerful GPVI activation can also be triggered by non-physiological ligands: the GPO-rich synthetic peptide CRP (collagen-related peptide) or by the snake venom toxin convulxin.³⁸

In response to ligand binding to the extracellular domain of GPVI, the conserved ITAM motif tyrosine residues located in the consensus sequence Yxx(L/I)₆₋₈Yxx(L/I) in the FcR γ chain are phosphorylated by the Src family kinases Fyn and Lyn, which are constitutively bound to the proline-rich region in the GPVI cytosolic tail.³³ The phosphorylated ITAM tyrosine residues in the FcR γ chain then serve as binding site for the two SH2 domains of the tyrosine kinase Syk.³⁹ Activation of Syk leads to formation of the linker of activated T cells (LAT) signalosome, comprising multiple adaptor and signaling proteins, finally resulting in activation of PLC γ 2. Activated PLC γ 2 hydrolyzes PIP₂ into the secondary messengers, IP₃ and DAG, which lead to Ca²⁺ release from intracellular stores and activation of PKC, respectively. This elicits the physiologic responses essential for platelet activation, like integrin activation, platelet degranulation and aggregation.⁴⁰ Since GPVI is critically involved in pathological thrombus formation upon exposure to thrombogenic surfaces, therapeutical downregulation of GPVI may provide a novel therapeutic strategy.

1.3.2 GPVI as potential antithrombotic target

Treatment of mice with the monoclonal anti-GPVI antibody JAQ1 results in specific depletion of the receptor from circulating platelets. JAQ1-treated mice were completely protected for at least two weeks in a model of lethal thromboembolism, but tail bleeding times in JAQ1-treated mice were only moderately increased.⁴¹ Another study showed that “therapeutical” downregulation of GPVI was independent of targeting of the collagen binding site of the receptor, because other antibodies (JAQ2 and JAQ3), which bind to different epitopes on GPVI, were also effectively depleting GPVI from the platelet surface.⁴² JAQ1-treated mice were also protected in models of arterial thrombosis^{43,44} and ischemic stroke.⁴⁵ These findings suggested that targeting of GPVI by antibodies might be a safe future option to prevent or treat thrombotic diseases.

Observations made in patients support this idea. Already in 1989, Moroi *et al.* described a patient deficient in GPVI. This patient showed only a mild bleeding time prolongation.⁴⁶ Boylan *et al.* found that plasma of another patient contained an autoantibody that bound specifically to GPVI.⁴⁷ Importantly, also in this patient only a mild bleeding disorder and a moderately reduced platelet count occurred, and platelets failed to become activated in response to collagen or CRP and inefficiently adhered to immobilized collagen under conditions of arterial shear. The amount of GPVI platelet mRNA and the nucleotide sequence of the GPVI gene were found to be normal but surface expression of GPVI and the FcR γ chain was dramatically reduced. Collectively, this argues for antibody-mediated GPVI depletion in this patient.

As antibody-induced GPVI loss was demonstrated in both humans and mice, and these findings might serve as basis for the development of safe antithrombotic therapeutics, a better understanding of the molecular mechanisms of GPVI downregulation is desirable. In mice, downregulation of GPVI in response to JAQ1 antibody injection has been shown to be mediated by two independent mechanisms: internalization and metalloproteinase-dependent ectodomain shedding.⁴⁸ However, no *in vivo* evidence was available at that time, which could determine the GPVI-cleaving enzyme(s).

1.4 SLAM family receptors

Signaling lymphocyte activation molecule (SLAM) family members are recognized as important immunomodulatory receptors, regulating both innate and adaptive immune responses.⁴⁹ The SLAM family of cell surface receptors belongs to the CD2 subset of the Ig superfamily of molecules.⁵⁰ Most studies carried out on SLAM family receptors were performed on immune cells.

Interestingly, expression of two members of the SLAM family has been demonstrated in platelets: CD150 and CD84.⁵¹ Both receptors were tyrosine phosphorylated in response to platelet aggregation. Further, CD150 deficient mice displayed a defect in platelet aggregation *in vitro* and a delayed arterial thrombotic process *in vivo*.⁵¹ Thus, these two SLAM family members were proposed as novel targets for antithrombotic drug discovery.²⁶

The SLAM family comprises nine members, SLAMF1-SLAMF9: CD150 (SLAM(F1)), CD48 (SLAMF2), Ly9 (SLAMF3), 2B4 (SLAMF4), CD84 (SLAMF5), NTB-A (SLAMF6, Ly108), CRACC (SLAMF7), BLAME (SLAMF8), and SF2001 (SLAMF9).⁵² All genes encoding SLAM related receptors are located in humans on chromosome 1. Seven genes cluster in a contiguous genomic region (*NTB-A, CD84, CD150, CD48, CRACC, Ly9 and 2B4*). *BLAME* and *SF2001* are located outside this region.⁵³ In mice, all genes encoding SLAM related

receptors are likewise located on chromosome 1H3.⁵⁴ Figure 3 illustrates the organization of mouse and human SLAM family gene clusters. The location of *SLAM* related genes in a genomic segment on chromosome 1 in humans and mice implies that they evolved by serial gene duplication.⁵⁵

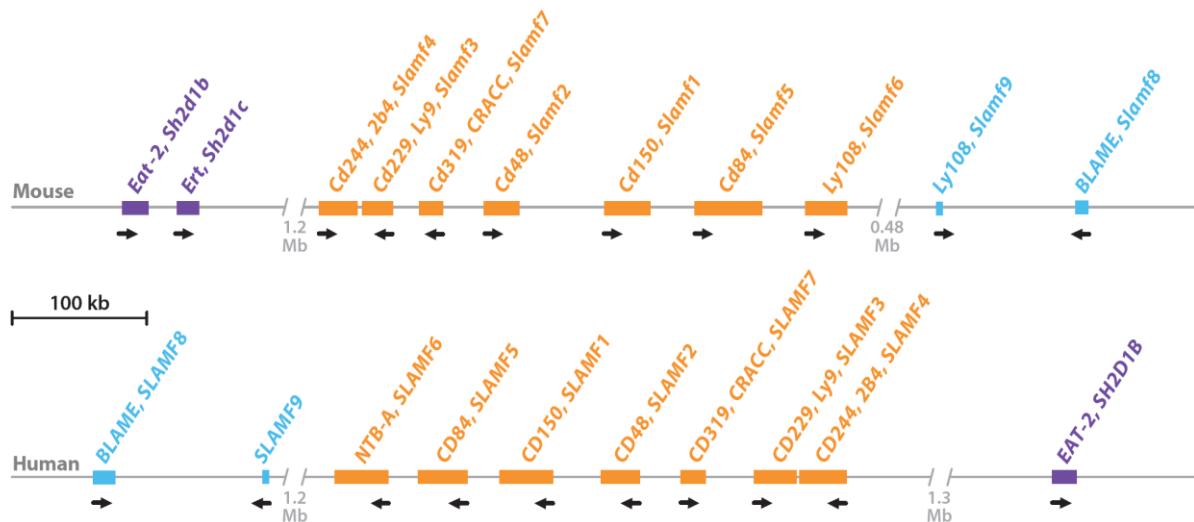


Figure 3. Genomic organization of the mouse and human SLAM family cluster. The genes encoding members of the SLAM receptor family (SLAM locus) are located in human and mouse on chromosome 1, clustered in a genomic segment of 359 kb in humans and 392 kb in mice. *SLAMF8* and *SLAMF9* are located in the same chromosome region, but outside of the SLAM locus. Human *SH2D1B* (*EAT2*) as well as mouse *Sh2d1b* (*Eat2a*) and *Sh2d1c* (*Eat2b*) are also located close to the SLAM locus. The arrangement of the SLAM gene family is identical in mouse and human genomes with the exception of the gene orientation relative to the centromere. Black arrows signify the transcriptional direction of these genes. (Adapted from Cannons *et al.*, *Annu. Rev. Immunol* 2011)⁴⁹

SLAM related receptors exhibit a common N-terminal ectodomain structure with a membrane-distal immunoglobulin variable domain (V) lacking an Ig disulfide bond, and a membrane-proximal immunoglobulin constant-2 domain (C2), stabilized by disulfide bonds. An exception is CD229 (Ly9), which contains a tandem repeat of the IgV-IgC2 motif. The extracellular region is followed by a transmembrane domain, and an intracellular tyrosine-rich region. Several alternatively spliced isoforms of SLAM, CD84, CRACC, Ly108, Ly9 and 2B4 have been identified that differ in the length of their cytoplasmic domain.⁴⁹ SLAM family receptors are capable of homotypic association, mediated by their external Ig-like domains.⁵⁶ Heterotypic interaction occurs between CD244 and CD48.⁵⁷ The intracellular regions of the receptors differ in length and amino acid composition. Six members contain one or more copies of the immunoreceptor tyrosine-based switch motif (ITSM).⁴⁹ The ITSM bearing the consensus sequence TxYxxI/V differs from the ITAM, which contains two YxxI/L motifs. The ITSM motif shows similarities to the immunoreceptor tyrosine-based inhibition motif (ITIM),

(I/V)xYxx(L/V).⁵⁸ Both motifs contain tyrosines that can be phosphorylated by protein tyrosine kinases, such as Src family members, following activation of corresponding receptors by ligand-binding or antibody-induced receptor clustering.⁵⁹ A phosphorylated ITSM can recruit Src homology 2 (SH2) domain-containing proteins, such as the phosphotyrosine phosphatase 2 (SHP-2) or the inositol phosphatase SHIP, depending on receptor type and cellular context.⁶⁰ Furthermore, the adaptor proteins SAP (SLAM-associated protein, encoded by *SH2D1A* gene), EAT-2 (Ewing's sarcoma activated transcript 2, encoded by *SH2D1B* gene), ERT (Eat-2-related transducer) and the p85 subunit of phosphatidylinositol-3 kinase are able to bind to an ITSM.^{61,62} While the interaction of SLAM (CD150) and the adaptor protein SAP is constitutive, the interactions between SAP and other receptors require tyrosine phosphorylation.^{63,64} The ITSM transduces activating or inhibiting signals, depending on the particular cell type.⁵⁸ In natural killer (NK) cells, for instance, SAP appears to enhance, whereas EAT-2 has been shown to suppress cytotoxicity and IFN- γ secretion.⁶⁵ SAP binds directly to both Src-like kinases FynT and Lck, and this was shown to be required for SLAM and Ly9 phosphorylation in thymocytes and peripheral T cells.⁶⁶

SLAM family members are differentially expressed in a variety of cell types.⁶⁷ SLAM is expressed in double-positive thymocytes, activated T cells, B cells, platelets, and mature dendritic cells (DCs). Ly-9, CD84 and CRACC are expressed in macrophages.⁵⁵ NTBA is expressed in NK, T and B cells.⁶⁸ CD48, Ly-9, CD84, NTBA, CRACC and SF2001 are present on the surface of T and B cells. Expression profiles of the SLAM family members led to their establishment as markers of hematopoietic stem cells among progenitor cells.⁶⁹ Differential expression of SLAM family receptors has been detected in human hematopoietic stem and progenitor cells.⁷⁰ SLAM proteins are supposed to be critical for fine-tuning of lymphocyte responses.⁷¹

During the last years, critical roles of the SLAM family of receptors and the SAP family of adaptor molecules have been established in lymphocyte development, differentiation, and effector functions.⁵⁰ Severe immune disorders result from disturbance or alteration of SLAM related receptor function. X-linked lymphoproliferative (XLP) disease, a human immunodeficiency characterized by an extreme sensitivity and inadequate immune response to Epstein-Barr virus (EBV) infection, is the most prominent example.⁷² XLP patients carry a mutated *SH2D1A* gene, resulting in inactivated SAP adaptor molecule. Studies in SAP deficient mice showed immunoglobulin E (IgE) deficiency and low serum IgG levels before and after viral infections, which were associated with impaired CD4⁺ T-helper function.⁷³ Another example is systemic lupus erythematosus (SLE), an antibody-mediated chronic autoimmune disease. Loss of B cell tolerance is characteristic of SLE. In mice, the susceptibility locus *Sle1z/Sle1bz* for this autoimmune disease is located on chromosome 1

and associated with production of autoantibody to chromatin. The main candidate for Sle1bz is the Ly108.1 isoform of the Ly108 gene, which is highly expressed in immature B cells from lupus-prone Sle1z mice. The normal Ly108.2 allele, but not the lupus-associated Ly108.1 allele, was found to sensitize immature B cells to deletion.⁷⁴ SLAM molecules may function as regulators that shape the stringency with which self-reactive B cells are suppressed during early development, which in the end protects from autoimmunity. So far, the understanding of the contribution of individual SLAM family members to complex processes like immune responses and other biological processes is still limited.

1.5 CD84

1.5.1 Gene and protein structure

As illustrated above in Figure 3, the *CD84* gene is located in the SLAM locus in humans on chromosome 1q24, and in mice on chromosome 1H3 at 93.3 cM. It was originally discovered in 1997 by isolation of cDNA from a Raji human Burkitt lymphoma cell line library.⁷⁵ A genomic characterization published by Palou *et al.* revealed five isoforms of CD84 that differ only in the length of the predicted cytoplasmic tail. These isoforms arise from alternative splicing of different exons, and use of a cryptic splice site.⁷⁶ According to recent genome browser data (<http://www.ensembl.org>), human *CD84* comprises 7 exons, which are translated into a 328 amino acid protein, whereas mouse *Cd84* contains 9 exons, which give rise to a 329 amino acids. In addition, protein database analysis (<http://www.uniprot.org>) reveals two mouse CD84 protein isoforms that differ from the canonical sequence, which is due to the existence of alternatively spliced transcripts. For human CD84, six additional isoforms are listed in the database. Mouse CD84 shares 58% amino acid identity with human according to sequence alignment using BLAST (<http://blast.ncbi.nlm.nih.gov>) and similar domain organization (Uniprot accession no. Q9UIB8 and Q18PI6). Figure 4 schematically depicts the murine *Cd84* exon structure, and the corresponding protein domains.

Like other SLAM family members, CD84 is a type-I transmembrane glycoprotein. In both human and mice, the 21 amino acid (aa) signal peptide is cleaved before integration of the mature protein into the plasma membrane. The extracellular domain containing an IgV and an IgC2 domain comprises 199 aa in mice. The extracellular N-terminus is followed by a 25 aa transmembrane region and an 83 aa C-terminal intracellular region.⁷⁵ CD84 has a calculated mass of 39 kDa but shows a higher apparent molecular weight in SDS page, as it is highly glycosylated.^{75,77} Crystal structure analysis recently revealed orthogonal homophilic interaction of CD84 mediated by the IgV domains.⁵⁶ Figure 5A depicts the model of CD84 homophilic interaction.

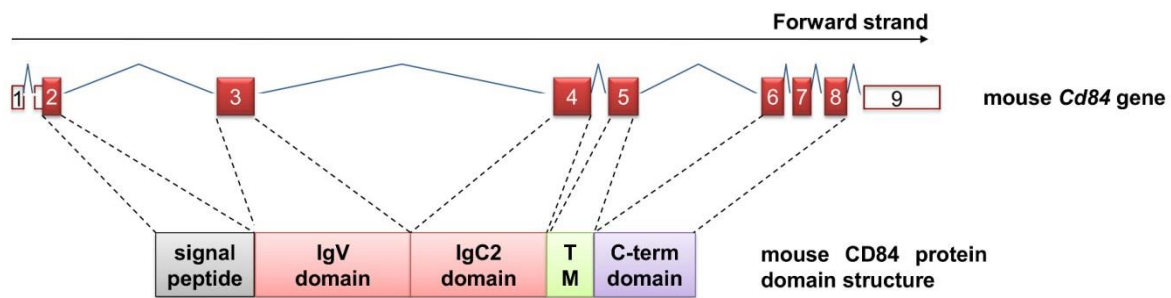


Figure 4. Genomic structure of mouse *Cd84* and corresponding protein domains. Exon-intron structure was drawn according to sequence information from the Ensembl genome browser. Filled red boxes represent translated exons. Protein domains were derived from the canonical sequence published in the UniProt protein database. Exon 1 and part of exon 2 are nontranslated regions (5' UTR), exon 2 encodes the signal peptide, exon 3 the V (variable) Ig-like domain, exon 4 the C2 (constant) Ig-like domain, exon 5 the transmembrane domain and exons 6, 7, 8 encode the cytoplasmic domain with at least 2 ITSMs.

1.5.2 CD84 in platelets and other cell types

CD84 is expressed in platelets and different immune cell populations, including T and B cells, monocytes/macrophages, granulocytes, DCs and mast cells.^{26,67,75,78} The expression of CD84 is upregulated during differentiation from pluripotent stem cells to committed progenitor cells, suggesting that it may be used as a marker of hematopoietic cell differentiation.⁷⁸ CD84 was found at higher levels on memory than naive B cells, but its expression was downregulated on memory B cells following activation *in vitro*, and falls progressively with each cell cycle.⁷⁹ CD84 was found to function as a homophilic adhesion molecule. Cross-linking of CD84 on anti-CD3 mAb-stimulated T cells increases proliferation,⁸⁰ and another study showed that this treatment results in enhanced IFN- γ secretion in human leukocytes.⁸¹ This was not achieved by solely crosslinking CD84, suggesting that CD84 acts as a costimulatory molecule. An earlier study revealed a role of another SLAM family member, CD150, in IFN- γ production by T cells.⁸² Recently, a role for CD84 in LPS-induced cytokine secretion by macrophages was discovered.⁸³

The signaling cascade downstream of CD84 is only partly understood. Crosslinking of CD84 by antibodies leads to phosphorylation of ITSMs and recruitment of the intracellular adaptor protein SAP in T cells and platelets.^{51,80} Phosphorylation is thought to be facilitated by Src kinases, such as Lck and Fyn. In T cells, FynT was shown to be indispensable for SLAM tyrosine phosphorylation, which was drastically enhanced by SAP. A dual functional role for SAP was revealed in SLAM signaling, by acting both as an adaptor for FynT and an inhibitor to SHP-2 binding.⁶⁰ CD84 phosphorylation in activated T cells involves the Src-family kinase Lck.⁸⁰ However, phosphorylation of CD84 can also occur in SAP-deficient cell lines and T

cells from XLP patients, where SAP is mutated,^{79,80} raising the possibility that CD84 does not require SAP mediated Fyn recruitment for receptor tyrosine phosphorylation, while still requiring SAP for downstream signal transduction.⁸⁴ Tyrosine phosphorylation has been detected in B cells after crosslinking with antibodies, even though they do not express SAP, and therefore EAT-2 was proposed to serve as a functional homolog of SAP.^{79,85} The SH2 domain containing adaptor EAT-2 was shown to be expressed in macrophages and B lymphocytes, to bind to phosphorylated CD84, and to interfere with recruitment of the tyrosine phosphatase SHP-2.⁸⁵ Figure 5B shows a model of signal transduction by CD84.

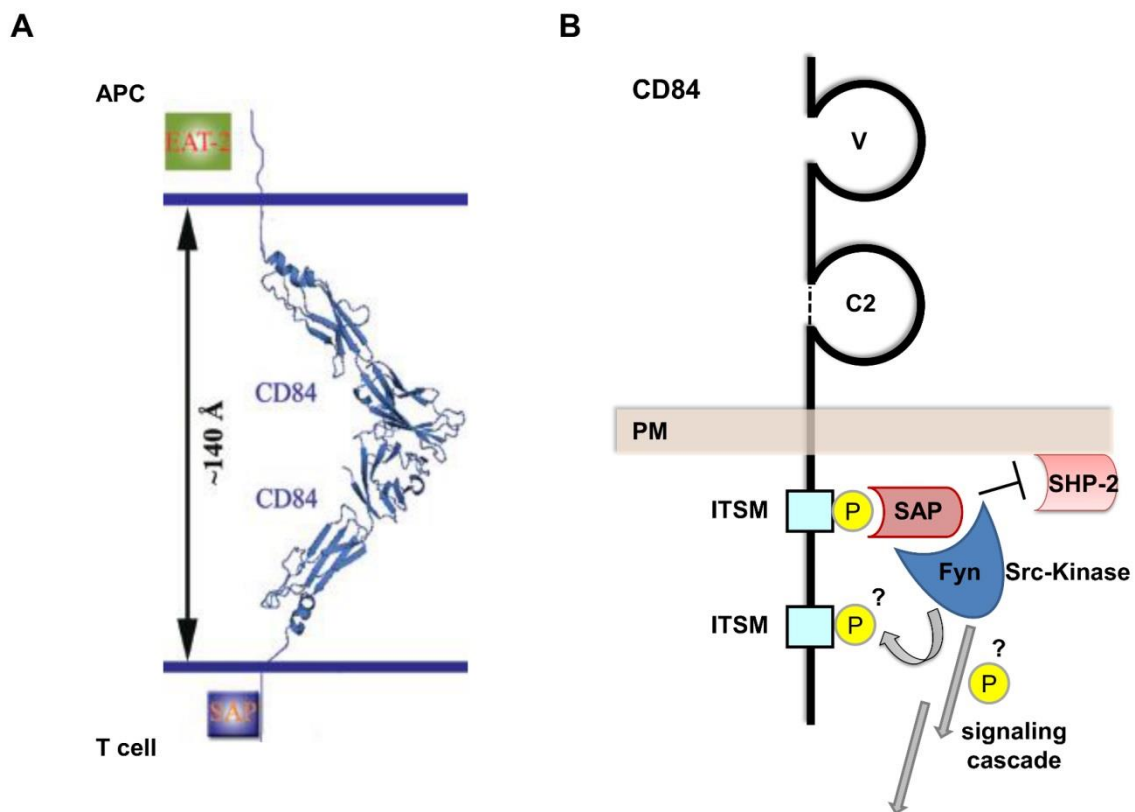


Figure 5. CD84 structure and signaling. (A) Model of CD84 homophilic interaction, adapted from Yan *et al.*⁵⁶ (B) CD84 signaling (hypothetic model): Tyr phosphorylation of the membrane proximal ITSM of CD84 is essential for recruitment of adaptors like SAP. SAP in turn binds to the tyrosine kinase Fyn and/or other protein tyrosine kinases leading to downstream signal transduction.⁵² Binding of SAP to phosphorylated ITSM inhibits SHP-2 binding.⁶⁰ Phosphorylation of CD84 also occurs in SAP deficient T cells. Phosphorylation is mediated by Src kinase Lck,⁸⁰ but Fyn is required for downstream signaling.

In resting platelets, CD84 is in a nonphosphorylated state.⁵¹ Phosphorylation of Y290 and Y310 occurs upon platelet aggregation in response to collagen, thrombin and thrombin receptor activating peptide (TRAP) but can be inhibited by α IIb β 3 antagonists (platelet aggregation blocker). Only Y310 lies within an ITSM motif, but not Y290. Platelet spreading

on the immobilized CD84 extracellular domain was shown to be dependent on SAP. EAT-2 was also found in murine platelets, but its functional relevance remained unclear.⁵¹ These findings pointed towards a role of CD84 as a receptor on the platelet surface that signals via tyrosine phosphorylation induced by platelet aggregation. This occurs subsequently to integrin-mediated platelet-platelet contacts, possibly enhancing platelet aggregate formation and stability.

The first mice deficient in CD84, which were recently described, show no overt phenotype, but display a specific defect in germinal center formation and T cell:B cell interactions.⁸⁴ Early T cell:B cell interactions were found to be dependent on integrins, and sustained interaction required SAP and CD84. Platelets of these mice have not been studied. Even though CD84 is highly expressed in platelets⁷⁷ and tyrosine phosphorylation of the cytoplasmic tail in response to aggregation has been demonstrated, the role of this receptor in platelet function is unclear. Nanda *et al.*⁵¹ suggested a role for CD84 in thrombus stabilization, based on the observation that CD84 is tyrosine phosphorylated in response to platelet aggregation, like CD150. However, in this study, only CD150 deficient mice were studied and thus CD84 function in platelets remained elusive. The model of the immune synapse was proposed to be applicable to platelets. According to this model, primary cell-cell interactions are mediated by integrins, but secondary signaling by additional receptors is initiated by cell proximity.²⁶ CD84 might be a novel receptor that exerts its function at the “platelet synapse” or “gap” between platelets in a growing thrombus.^{26,30} Theoretically, also a negative role of CD84 in platelets is conceivable. In human mast cells for example, CD84 was shown to dampen FcεRI-mediated Ca²⁺ signaling, and this process involved the inhibitory kinase Fes and the phosphatase SHP-1.⁸⁶ Nevertheless, no platelet activation studies on CD84 deficient mice have been reported in the literature yet.

1.6 Downregulation of platelet receptor expression

Platelet receptors can be downregulated from the platelet surface by internalization,^{48,87} or intracellular, or extracellular proteolytic cleavage. The latter mechanism, termed ectodomain shedding, has been described for a number of major receptors, including GPIIbα,⁸⁸ GPVI,^{89,90} GPV,^{91,92} Semaphorin 4D,⁹³ P-Selectin,⁸⁷ JAM-A,⁹⁴ or CD40L.⁹⁵ A mass spectrometric study recently provided evidence that many more surface proteins, including CD84, might be proteolytically downregulated in activated platelets, but the underlying mechanisms were not addressed in detail in that study.⁹⁶ Members of the a disintegrin and metalloproteinase (ADAM) family have been identified to be involved in the proteolysis of some prominent platelet receptors with ADAM17 mediating the cleavage of GPIIbα,⁸⁸ whereas shedding of

GPV can occur through either ADAM10 or ADAM17.⁹⁷ A role for both metalloproteinases was also shown for JAM-A shedding.⁹⁴ ADAM10 was implicated in cleavage of a GPVI-based synthetic peptide,⁹⁷ but it was unclear whether other metalloproteinases are also capable of GPVI cleavage.

To study platelet receptor regulation, ectodomain shedding can be induced *in vitro* by treatment of platelets with carbonyl cyanide m-chlorophenylhydrazone (CCCP),⁸⁹ which induces mitochondrial injury by uncoupling oxidative phosphorylation, or by the calmodulin inhibitor W7, which blocks the interaction of receptors and calmodulin.⁹⁰ N-ethylmaleimide (NEM) treatment provides a mechanism for directly inducing shedding without accompanying platelet activation¹² (see also 1.6.1). Treatment of platelets with physiological agonists may also lead to metalloproteinase-dependent shedding. Stimulation of human platelets *in vitro* with different GPVI agonists led to loss of GPVI from the platelet surface, but the identity of the metalloproteinase that cleaves GPVI has been unclear.⁹⁰ In contrast to human platelets, mouse platelets did not lose GPVI from their surface after stimulation with physiological agonists *in vitro*.⁸⁹ However, the same study showed that CCCP induced shedding of GPVI from the platelet surface by a metalloproteinase-dependent mechanism. As illustrated above in Figure 2, calmodulin binds the basic region of GPVI.⁹⁸ Metalloproteinase-dependent GPVI shedding *in vitro* was also demonstrated in response to platelet treatment with the calmodulin inhibitor W7. GPVI can be experimentally downregulated *in vivo* in mice by injection of the monoclonal antibody JAQ1.⁴¹ This occurs by two independent mechanisms: internalization and ectodomain shedding,⁴⁸ but detailed studies on the identity of the GPVI sheddase(s) were lacking.

1.6.1 Metalloproteinases of the ADAM family

The ADAM family has been implicated in diverse biological processes like control of membrane fusion, cytokine, growth factor and receptor shedding, cell migration, as well as processes such as fertilization and cell fate determination.⁹⁹ ADAM17 (TNF- α -converting enzyme, TACE) and ADAM10 are the best characterized members of that family.¹⁰⁰ Both are expressed in platelets and one or both have been shown to act as sheddases of platelet receptors, most notably GPIb α ,⁸⁸ GPV,⁹¹ or GPVI.⁸⁹ ADAM10 and ADAM17 share a modular domain structure: a propeptide domain, a catalytic metalloproteinase domain containing a metal ion-coordination motif, a disintegrin domain, a cysteine-rich domain, a transmembrane domain, and a cytoplasmic tail (Figure 6). Removal of the propeptide domain produces the active form of the enzyme. The prodomain of ADAM10 and ADAM17 contains a cysteine switch, a free sulfhydryl maintaining the metalloproteinase in an inactive form. Activation of the

enzyme occurs after proteolytic removal of the prodomain or upon modification by the thiol-modifying reagent NEM.^{12,101}

Proteins of the TIMP (tissue inhibitor of metalloproteinases) family are established as endogenous ADAM inhibitors.¹⁰² Tight regulation of ADAM function appears to be essential, illustrated by the observation that for example TIMP3 deficient mice exhibit increased TNF- α levels and chronic hepatic inflammation.¹⁰³ The fact that ADAMs exert critical functions during embryonic development is emphasized by the observations that *Adam10*^{-/-} mice die during embryonic development¹⁰⁴ and ADAM17 deficiency leads to perinatal lethality.¹⁰⁵ Minimal expression of ADAM17 appears to be sufficient for survival, as recently shown in *Adam17*^{ex/ex} mice by Chalaris *et al.*¹⁰⁶

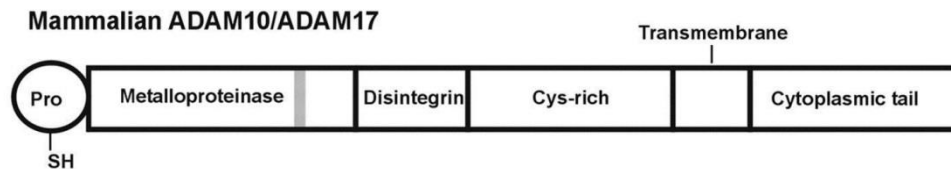


Figure 6. Domain structure of ADAM10/ADAM17. The modular organization consist of a propeptide (Pro) domain, a metalloproteinase catalytic domain containing the Zn²⁺-coordination motif (grey bar), a disintegrin domain, and a Cys-rich domain. The free thiol (Cysteine-switch) within the prodomain regulates catalytic activity. (Adapted from Andrews *et al.*, *ATVB*, 2007)¹²

Shedding of platelet receptors through metalloproteinases probably represents a negative feedback loop to limit platelet activation and thrombus growth. It provides a mechanism for downregulating surface expression resulting in loss of ligand binding, decreasing signaling and generation of proteolytic fragments that may be functional or provide platelet-specific biomarkers.¹⁰⁷ Therefore, a more detailed understanding of platelet receptor cleavage is not only required for insights into the complex biological functions of this regulatory process, but may be relevant with respect to development of potential antithrombotic therapies.

1.6.2 Calpain

Another mechanism to regulate platelet receptor signaling is proteolytic cleavage of the receptor by intracellular proteases like calpain.¹⁰⁸ Calpain is a cysteinyl protease that is in part regulated by intracellular Ca²⁺ levels and cleaves a number of proteins, many of them involved in the regulation of the cytoskeleton.¹⁰⁹ Several studies have demonstrated that calpain cleaves the intracellular part of β 3 integrin,¹¹⁰ Fc γ RIIa,¹¹¹ and PECAM-1.¹¹² Platelets express calpain-1, which accounts for ~80% of calpain protease activity in these cells, and

calpain-2, mediating ~20% calpain protease activity.¹¹³ Deficiency of calpain-1 in platelets resulted in impaired platelet aggregation and clot retraction, which could be attributed to enhanced PTP1B activity, but tail bleeding times of calpain-1 deficient mice were unaltered.^{113,114} More recently, Kuchay *et al.* discovered that calpain-1 regulates platelet spreading on collagen and fibrinogen through Rho GTPases.¹¹⁵ Importantly, calpain activity can be induced under the same conditions that activate metalloproteinases in platelets (e.g. in response to calmodulin inhibitors),^{12,111} suggesting that intra- and extracellular cleavage events might be simultaneously operative in the downregulation of receptor signaling in platelets.

1.7 Thrombotic diseases

Venous thromboembolism constitutes a leading cause of cardiovascular death and consists of deep vein thrombosis (DVT), and its complication, pulmonary embolism.¹¹⁶ A recent study in mice underscored the role of platelets in DVT, as they initiate and propagate venous thrombosis, by interaction with monocytes and neutrophils, supporting neutrophil extracellular trap (NET) formation, which in turn triggers FXII-dependent thrombus propagation.¹¹⁷ Novel oral anticoagulants like Rivaroxaban are in clinical use for treatment of DVT.¹¹⁸ On the other hand, platelets are established as central players in arterial thrombosis.^{119,120} Undesired platelet activation and thrombus formation, e.g. upon exposure of thrombogenic surfaces after rupture of an atherosclerotic plaque, can lead to stenosis or complete occlusion of vessels and infarction of organs distal from the occlusion site.¹²¹ If coronary arteries are affected, this can result in myocardial infarction, a leading cause of death in industrialized countries.¹²² Thrombi might also embolize and block blood flow in smaller arteries, leading to infarction of various organs. Ischemic stroke, resulting from blockade of cerebral arteries is a major cause of disability and the second leading cause of death worldwide.¹²³ Several antiplatelet drugs are currently applied to prevent stroke or myocardial infarction in high risk patients. Aspirin, a cyclooxygenase inhibitor, or clopidogrel, an antagonist of the P2Y₁₂ ADP receptor are among the established oral antiplatelet drugs in clinical use.¹²⁴ Despite the common use of platelet inhibitors, ischemic stroke is still among the most devastating cardiovascular events, due to the high risk of disability or death. Thus, there is a strong need to discover novel molecular targets in order to develop new drugs for safe therapeutic intervention.

Around 80% of strokes are caused by cerebral ischemia as a result of arterial occlusion, whereas the remaining 20% are due to intracerebral hemorrhages.¹²⁵ Thromboembolism in the brain might originate from atherosclerotic plaque rupture or from the heart, especially in patients with atrial fibrillation. Occlusion of major or multiple smaller intracerebral arteries by

embolized thrombi leads to focal impairment of the blood flow and to secondary thrombus formation within the cerebral microvasculature.¹²⁵ Treatment options are limited to early thrombolysis using recombinant tissue plasminogen activator (t-PA).¹²⁶

In the acute phase of ischemic stroke, oxygen and glucose deprivation leads to energy failure, consequently ion gradients cannot be maintained in neurons within the ischemic territory.¹²⁷ The membrane potential is lost, thus neurons and glia depolarize. The excitatory amino acid glutamate accumulates and leads to activation of N-methyl-D-aspartate (NMDA) receptors and metabotropic glutamate receptors, resulting in Ca^{2+} overload, leading to glutamate excitotoxicity.¹²⁷ Prolonged elevation of intracellular Ca^{2+} induced by cerebral ischemia leads to activation of Ca^{2+} -dependent enzymes, mitochondrial damage, activation of prooxidant pathways, and finally to neuronal death by either necrosis or apoptosis.¹²⁸

Paradoxically, despite successful vessel recanalization, many patients show secondary infarct growth, a phenomenon referred to as reperfusion injury.¹²⁹ Breakdown of the endothelial cell permeability barrier, edema formation, expression of endothelial cell-leukocyte adhesion receptors and the resulting microvascular obstruction by platelet-leukocyte and platelet-fibrin aggregates, as well activation of coagulation foster this process.¹³⁰ Considerable knowledge of the contribution of platelets and immune cells has been obtained through studies in mice, using the stroke model of transient middle cerebral artery occlusion (tMCAO).¹³¹ Inhibition of platelet adhesion and activation receptors, GPIIb/IIIa and GPVI, respectively, resulted in protection of mice from infarct progression in that model.⁴⁵ In contrast, blockade of $\alpha\text{IIb}\beta\text{3}$ -mediated platelet aggregation was not protective and increased intracerebral hemorrhage. These studies indicated that inhibition of early steps of platelet adhesion to the ischemic endothelium and the subendothelial matrix may offer a safe treatment strategy in acute stroke.⁴⁵ Platelets contribute to activation of the coagulation cascade by phosphatidylserine exposure, thereby binding coagulation factors and facilitating assembly of tenase and prothrombinase complexes.¹³² In addition, platelets release negatively charged polyphosphates, which activate coagulation factor XII (FXII).¹³³ Activated FXII also triggers inflammation by activation of the kallikrein-kinin system, which results in production of the proinflammatory mediator bradykinin.¹³⁴ Furthermore, it is well known that ischemic stroke induces inflammatory responses, including recruitment of granulocytes, as well as T cells and macrophages.¹³⁵ These findings revealed the relationship between platelets and inflammation in ischemic stroke and led to the novel concept of ischemic stroke as a “thrombo-inflammatory disease”.¹²⁹ The infiltration of different immune cell types into the ischemic regions follows distinct temporal and spatial dynamics.¹³⁶ Proinflammatory cytokines like TNF are produced by mast cells, microglia, perivascular macrophages or T cells during early phases of brain ischemia.¹³⁷ During the last

years, especially T cells received attention. Mice lacking T cells were protected from infarct progression following tMCAO.¹³⁸ Reconstitution of T cell deficient mice with normal T cells restored susceptibility to cerebral ischemia, and these effects were antigen-independent.¹³⁹ A very recent study revealed that among T cells also regulatory T cells lead to impaired tissue reperfusion by interaction with endothelium and platelets in the early course of tMCAO.¹⁴⁰

In light of the complex processes acting in concert to promote infarct development in ischemic stroke, it appears conceivable that targeting receptors or signaling pathways in diverse cell types may represent promising options for future treatment. These may include antiplatelet strategies, as well as immune cell- or neuron-specific pharmacological intervention. Therefore, there is a strong need to identify potential novel molecular targets in either of these cell types.

1.8 Store-operated calcium entry (SOCE)

Ca^{2+} is an ubiquitous messenger in eukaryotic cells, controlling diverse cellular functions such as contraction, secretion, gene transcription, cell growth, or cell death.¹⁴¹ Activation of PLC isoforms can lead to increased Ca^{2+} entry from the extracellular space by receptor-operated channels (ROC).¹⁴² More importantly, the store-operated Ca^{2+} entry (SOCE, also called capacitive calcium entry) pathway has been established as the major Ca^{2+} influx mechanism in mammalian cells.¹⁴³ SOCE comprises the IP_3 -induced release of Ca^{2+} from intracellular stores and concomitant activation of Ca^{2+} entry through store operated Ca^{2+} (SOC) channels in the PM. For many years, the identity of the SOC channels remained unknown. Also the mechanism that senses the store depletion and communicates store depletion to the SOC channels in the PM was elusive. Only a few years ago, the EF hand containing protein STIM1^{144,145} was found to be the calcium sensor residing in the ER that activates Orai1, the pore forming subunit of the SOC channel.^{146,147} According to current models, STIM1 proteins sense the depletion of Ca^{2+} from the ER, cluster rapidly, and translocate to junctions adjacent to the PM, where they organize Orai channels into clusters and open these channels to achieve SOC entry.¹⁴⁸

In platelets, SOCE is the major Ca^{2+} entry pathway across the PM. Upon agonist stimulation, activated PLC β and PLC γ 2 isoforms hydrolyze the membrane phospholipid PIP_2 to IP_3 and DAG. IP_3 directly induces Ca^{2+} release from the intracellular stores. This leads to moderate elevation of $[\text{Ca}^{2+}]_i$. The reduced store content is sensed by the Ca^{2+} sensor protein STIM1,²² which then triggers profound Ca^{2+} influx across the PM through Orai1.²³ SOCE is also known as the major Ca^{2+} influx mechanism in lymphocytes,¹⁴⁹ essential for the activation of and cytokine gene expression by T and B cells. A mutation in *ORAI1* was identified as genetic

defect responsible for one form of hereditary severe combined immune deficiency (SCID) syndrome in human patients.¹⁴⁶

The Orai protein family comprises three homologs: Orai1, Orai2 and Orai3. The active pore consists of four Orai molecules¹⁵⁰ and it is likely that the three Orai homologs can form heteromeric channels with distinct properties¹⁵¹.

The role of another Ca^{2+} sensor protein, STIM2, is less clear. Besides activating SOCE upon smaller decreases of ER Ca^{2+} , STIM2 was shown to regulate basal cytosolic and ER calcium levels in eukaryotic cells.¹⁵² Until recently, no clear data have been available on the presence and functional role of SOC channels in neurons, which are activated in response to Ca^{2+} store depletion to allow capacitive Ca^{2+} entry and store replenishment. In 2009, Berna-Erro *et al.* could show that SOCE plays a critical role in neurons, since mice deficient in the Ca^{2+} sensor STIM2 were protected from ischemia-induced neuronal damage.¹⁵³ However, the identity of the major SOC channel in neurons remained unknown.

1.9 Orai2

The human *ORAI2* gene is located on chromosome 7, whereas in mice *Orai2* is located on chromosome 5. Genome browser data (<http://www.ensembl.org>) revealed 4 exons for human and 3 exons for the mouse gene. In both species, only two of these exons are protein coding exons. The human Orai2 protein consists of 254 amino acids (28.6 kDa), whereas the murine Orai2 protein contains 250 amino acids (28.2 kDa) (Uniprot accession no. Q96SN7 and Q8BH10). Figure 7 illustrates the murine *Orai2* genomic and protein domain organization. Sequence alignment (<http://blast.ncbi.nlm.nih.gov>) revealed 95% identity between the human and the murine amino acid sequences. Orai2 is a membrane protein containing 4 transmembrane protein domains. The N- and C- termini face the cytoplasm.¹⁵¹

The current knowledge of Orai2 function is still limited. Orai2 can form heteromultimers with Orai1, but in contrast to Orai1, it is not glycosylated.¹⁵⁴ Like other Orai homologs, Orai2 contains conserved acidic residues located in the extracellular loop between the first and second transmembrane domains, which are associated with Ca^{2+} binding.¹⁵¹ Overexpression of Orai2 together with STIM1 in HEK293 cells enhanced SOCE, but to a lesser extent than Orai1.¹⁵⁵ Differences between SOC channels formed by Orai1 and Orai2 reside in their sensitivity to inactivation by internal Ca^{2+} and their functional expression seems to be cell type dependent.¹⁵⁶

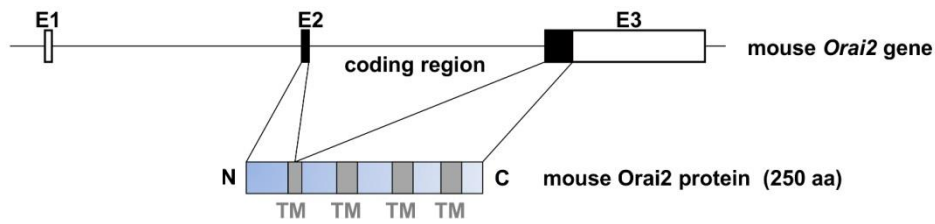


Figure 7. Genomic structure of mouse *Orai2* and corresponding protein domains. Sequence information was obtained from the Ensembl genome browser. Filled black boxes represent translated exon sequences (coding region). Protein domains were derived from the sequence published in the UniProt protein database. Exon 3 codes for the major part of the 250 amino acid *Orai2* protein. The *Orai2* protein contains 4 transmembrane (TM) domains.

Mouse thymocytes and T cells were found to express more *Orai2* than *Orai1* and *Orai3*, thus suggesting that murine T cell SOC channels might use *Orai2*, whereas human T cells require *Orai1*.¹⁵⁷ In mouse dendritic cells, *Orai2* was recently shown to interact selectively with STIM2 upon store depletion.¹⁵⁸ Northern blot studies have shown prominent *Orai2* expression in several organs of mice, whereas *Orai1* and *Orai3* appeared to be more broadly expressed.¹⁵⁶ Nothing is known about the functional relevance of *Orai2* in platelets and neurons. Low expression was found in platelets,²³ whereas in brain tissue high expression of *Orai2* has been detected.¹⁵⁹

1.10 Aim of the study

Given the key role of platelets in normal hemostasis as well as in thrombotic events, progress in understanding of platelet receptor function is required in order to find potential new targets for antithrombotic therapy. The SLAM family member CD84 is expressed in platelets and immune cells. This receptor has been proposed to stabilize thrombi, but no experimental data to support this hypothesis have been available so far. Studying CD84 also appeared interesting in the context of ischemic stroke, where platelets and immune cells play critical pathogenic roles in infarct progression. The first aim of this thesis was to generate a CD84 deficient mouse line and analyze the role of CD84 in platelet function *in vitro* and *in vivo*, and in addition, in “thrombo-inflammatory” disease states like ischemic stroke.

For several platelet surface receptors including GPVI, tight regulation by (metallo-) proteinases has been described, but it was completely unclear whether and if yes, how CD84 levels in platelets are regulated. Therefore, the second aim of this study was to identify potential mechanisms of CD84 receptor regulation, and in addition, to study detailed regulation mechanisms for the platelet collagen receptor GPVI *in vitro* and *in vivo*.

Store operated Ca^{2+} entry (SOCE) is an essential mechanism to allow Ca^{2+} entry and full activation of platelets. The Ca^{2+} sensor STIM1 and the SOC channel subunit protein Orai1 are critically involved in this process in platelets. STIM2 is the major STIM isoform in neurons, but the role of the SOC channel subunit protein Orai2 in platelets and neurons has remained elusive. The third aim of this study was to generate and analyze Orai2 deficient mice to reveal the physiological relevance of Orai2 in platelets and neurons.

2 Materials and Methods

2.1 Materials

2.1.1 Chemicals and reagents

3,3',5,5'-tetramethylbenzidine (TMB)	Becton Dickinson (Heidelberg, Germany)
6x Loading Dye Solution	Fermentas (St. Leon-Rot, Germany)
Acetic acid	Roth (Karlsruhe, Germany)
ADP	Sigma (Schnelldorf, Germany)
Agar	Roth (Karlsruhe, Germany)
Agarose	Roth (Karlsruhe, Germany)
Alexa Fluor 488 reactive dye	Molecular Probes (Karlsruhe, Germany)
ALLN	Calbiochem (Bad Soden, Germany)
Ammonium peroxodisulphate (APS)	Roth (Karlsruhe, Germany)
Ampicillin	Roth (Karlsruhe, Germany)
Apyrase	Sigma (Schnelldorf, Germany)
Atipamezole	Pfizer (Karlsruhe, Germany)
Avertin® (2,2,2-tribromoethanol)	Sigma (Deisenhofen, Germany)
β-mercaptoethanol	Roth (Karlsruhe, Germany)
Bovine serum albumin (BSA)	AppliChem (Darmstadt, Germany)
Calcium chloride	Roth (Karlsruhe, Germany)
Carbonyl cyanide m-chlorophenylhydrazone	Sigma (Schnelldorf, Germany)
Chloramphenicol	Roth (Karlsruhe, Germany)
Collagen related peptide (CRP)	prepared in our laboratory
Complete Mini protease inhibitors (+EDTA)	Roche Diagnostics (Mannheim, Germany)
Convulxin (CVX)	Enzo (Lörrach, Germany)
Disodiumhydrogenphosphate	Roth (Karlsruhe, Germany)
dNTP mix	Fermentas (St. Leon-Rot, Germany)
ECL solution	GE Healthcare (Freiburg, Germany)
EDTA	AppliChem (Darmstadt, Germany)
Ethanol	Roth (Karlsruhe, Germany)
Ethidium bromide	Roth (Karlsruhe, Germany)
EZ-Link sulfo-NHS-LC-biotin	Pierce (Rockford, IL, USA)
Fat-free dry milk	AppliChem (Darmstadt, Germany)
Fentanyl	Janssen-Cilag (Neuss, Germany)

Fibrillar type I collagen (Horm)	Nycomed (Munich, Germany)
Flumazenil	Delta Select (Dreieich, Germany)
Fluoresceine-5-isothiocyanate (FITC)	Molecular Probes (Karlsruhe, Germany)
Forene® (isoflurane)	Abbott (Wiesbaden, Germany)
GeneRuler 1kb DNA Ladder	Fermentas (St. Leon-Rot, Germany)
Glucose	Roth (Karlsruhe, Germany)
Glycerol	Roth (Karlsruhe, Germany)
Glycine	AppliChem (Darmstadt, Germany)
GM6001	Calbiochem (Bad Soden, Germany)
Hematoxylin	Sigma (Schnelldorf, Germany)
High molecular weight heparin	Sigma (Schnelldorf, Germany)
horseradish peroxidase-conjugated streptavidin	Dianova (Hamburg, Germany)
Human fibrinogen	Sigma (Schnelldorf, Germany)
Igepal CA-630	Sigma (Schnelldorf, Germany)
Immobilon-P transfer membrane	Millipore (Schwalbach, Germany)
Indomethacin	Calbiochem (Bad Soden, Germany)
Isopropanol	Roth (Karlsruhe, Germany)
Kanamycin sulfate	Roth (Karlsruhe, Germany)
Magnesium sulfate	Roth (Karlsruhe, Germany)
MDL28170	Calbiochem (Bad Soden, Germany)
Medetomidine (Dormitor)	Pfizer (Karlsruhe, Germany)
Midazolam (Dormicum)	Roche (Grenzach-Wyhlen, Germany)
Naloxon	Delta Select (Dreieich, Germany)
N-ethylmaleimide (NEM)	Calbiochem (Bad Soden, Germany)
Nonidet P-40	Roche (Mannheim, Germany)
PageRuler Prestained Protein Ladder	Fermentas (St. Leon-Rot, Germany)
PD-10 column	GE Healthcare (Freiburg, Germany)
Peptone (pancreatic digested)	Roth (Karlsruhe, Germany)
Phenol/chloroform/isoamylalcohol	AppliChem (Darmstadt, Germany)
Potassium chloride	Roth (Karlsruhe, Germany)
Prostacyclin (PGI ₂)	Sigma (Schnelldorf, Germany)
Protease-Inhibitor cocktail tabs	Roche Diagnostics (Mannheim, Germany)
Protein G sepharose	GE Healthcare (Freiburg, Germany)
Rotiphorese Gel 30 Acrylamide	Roth (Karlsruhe, Germany)
Salmon sperm DNA	Sigma (Schnelldorf, Germany)
Sodium azide	Roth (Karlsruhe, Germany)

Sodium chloride	AppliChem (Darmstadt, Germany)
Sodium hydroxide	AppliChem (Darmstadt, Germany)
Sodium Orthovanadate	Sigma (Schnelldorf, Germany)
Sodiumdihydrogenphosphate	Roth (Karlsruhe, Germany)
TEMED	Roth (Karlsruhe, Germany)
Thrombin	Roche Diagnostics (Mannheim)
TRIS ultra	Roth (Karlsruhe, Germany)
Tris/HCL	Roth (Karlsruhe, Germany)
Trizol reagent	Invitrogen (Karlsruhe, Germany)
Tween 20	Roth (Karlsruhe, Germany)
U46619	Alexis Biochemicals (San Diego, USA)
Western Lightning Chemiluminescence (ECL)	PerkinElmer LAS (Boston, USA)
Yeast extract	AppliChem (Darmstadt, Germany)

Restriction endonucleases were purchased from Fermentas (St. Leon-Rot, Germany). Highly concentrated *Bam*HI and *Eco*RV were obtained from New England Biolabs (Frankfurt am Main, Germany). Rhodocytin was a generous gift from J. Eble (University Hospital Frankfurt, Germany). All other non-listed chemicals were obtained from AppliChem (Darmstadt, Germany), Sigma (Schnelldorf, Germany) or Roth (Karlsruhe, Germany).

2.1.2 Kits

○ DNA Purification :	
PureYield Plasmid Midiprep System	Promega (Mannheim, Germany)
NucleoSpin Extract II Kit	Macherey-Nagel (Düren, Germany)
○ Electrophoresis	
<i>NuPAGE[®] Pre-cast gel system</i>	
NuPAGE [®] MOPS SDS Running Buffer (20X)	Invitrogen (Karlsruhe, Germany)
NuPAGE [®] Bis-Tris 10% Gel, 1.0mm	Invitrogen (Karlsruhe, Germany)
NuPAGE [®] LDS Sample Buffer (4X)	Invitrogen (Karlsruhe, Germany)
SeeBlue [®] Plus2 Pre-Stained Standard	Invitrogen (Karlsruhe, Germany)
○ PCR:	
PCR Extender System	5 PRIME (Hamburg, Germany)
GeneAmp XL PCR Kit	Applied Biosystems (New Jersey, US)
VenorGeM Mycoplasma Detection Kit	Sigma (Schnelldorf, Germany)
○ Proteinbiochemistry	
Peroxidase Labeling Kit	Roche (Mannheim, Germany)

Pierce BCA Protein Assay Kit Thermo (Schwerte, Germany)

2.1.3 Cell culture material

70 µm or 40 µm nylon cell strainer	BD Falcon (Heidelberg, Germany)
Cryotubes	Roth (Karlsruhe, Germany)
DMEM + GlutaMAX-I	Gibco (Karlsruhe, Germany)
D-PBS	Gibco (Karlsruhe, Germany)
Dimethylsulfoxide (DMSO)	AppliChem (Darmstadt, Germany)
Fetal Calf Serum (FCS)	Gibco (Karlsruhe, Germany)
Ganciclovir	Invitrogen (Karlsruhe, Germany)
Geneticin G-418 sulphate	Gibco (Karlsruhe, Germany)
Leukaemia Inhibitory Factor (LIF)	Chemicon (Hampshire, UK)
Nonessential amino acids	Gibco (Karlsruhe, Germany)
Penicillin-Streptomycin	Gibco (Karlsruhe, Germany)
Stem cells R1 male 129/Sv	kindly provided by Nagy A. ¹⁶⁰
Steritop Bottle Top Filter 0.22 µm	Millipore (Schwalbach, Germany)
Tissue culture dishes (100x20 mm)	BD Falcon (Bedford, USA)
Tissue culture flasks (25 or 175 cm ²)	BD Falcon (Bedford, USA)
Trypsin-EDTA	Gibco (Karlsruhe, Germany)
Well plates (6-well, 24-well or 96-well)	BD Falcon (Bedford, USA)

2.1.4 Radioactive labeling

Probequant G 50 Microcolumns	GE Healthcare (Freiburg, Germany)
Rediprime DNA Labelling Kit	GE Healthcare (Freiburg, Germany)
Redivue-α ³² P-dCTP; 250 µCi	GE Healthcare (Freiburg, Germany)

2.1.5 Buffers and media

All buffers were prepared in deionized water obtained from a MilliQ Water Purification System (Millipore, Schwalbach, Germany). pH was adjusted with HCl or NaOH.

- Biotinylation buffer, pH 9.0

NaHCO ₃	50 mM
NaCl	0.9%

Materials and Methods

- Blocking solution for immunoblotting
 - BSA or fat-free dry milk 5% in TBS or TBS-T

- Blotting buffer A for immunoblotting
 - TRIS, pH 10.4 0.3 M
 - Methanol 20%

- Blotting buffer B for immunoblotting
 - TRIS, pH 10.4 25 mM
 - Methanol 20%

- Blotting buffer C for immunoblotting
 - ϵ -amino-n-caproic acid, pH 7.6 4 mM
 - Methanol 20%

- Church buffer for Southern blot
 - Phosphate buffer (0.5 M; pH 7.2) 50%
 - SDS (20%) 33%
 - EDTA (0.5 M, pH 8.0) 0.1%
 - Salmon sperm DNA 1%
 - BSA 10 g/l

- Church wash buffer for Southern blot
 - Phosphate buffer (0.5 M; pH 7.2) 4%
 - SDS (20%) 5%

- Coating buffer, pH 9.5
 - NaHCO_3 100 mM

- Coomassie staining solution
 - Acetic acid 10%
 - Methanol 40%
 - Coomassie Brilliant blue 1 g

- Coomassie destaining solution
 - Acetic acid 10%
 - Methanol 40%

Materials and Methods

- Coupling buffer, pH 8.3
 - NaHCO₃ 0.2 M
 - NaCl 0.5 M

- Denaturation buffer for Southern blot
 - NaCl 1.5 M
 - NaOH 0.5 M

- EF medium
 - DMEM
 - FCS 10%

- ES medium
 - DMEM
 - FCS 20%
 - Nonessential amino acids 1%
 - β-mercaptoethanol 3.5 μL
 - LIF 1,000 U/mL

- ES+G-418 medium
 - DMEM
 - FCS 20%
 - Nonessential amino acids 1%
 - β-mercaptoethanol 3.5 μL
 - LIF 1,000 U/mL
 - Geneticin (G-418) 400 μg/mL

- FACS buffer
 - PBS (1x)
 - FCS 1%
 - NaN₃ 0.02%

- Freezing medium
 - DMEM
 - FCS 50%
 - DMSO 10%

- IP buffer
 - TRIS/HCl (pH 8.0) 15 mM
 - NaCl 155 mM
 - EDTA 1 mM
 - NaN₃ 0.005%

- Laemmli buffer for SDS-PAGE
 - TRIS 40 mM
 - Glycine 0.95 M
 - SDS 0.5%

- LB medium
 - Peptone (pancreatic digested) 10 g/l
 - Yeast extract 5 g/l
 - NaCl 10 g/l
 - Agar 15 g/l

- Lysis buffer for DNA sample preparation from mouse tissue
 - TRIS base 100 mM
 - EDTA (0.5 M) 5 mM
 - NaCl 200 mM
 - SDS 0.2%
 - add Proteinase K (20 mg/ mL) 100 µg/mL

- Neutralisation buffer for Southern blot
 - NaCl 1.5 M
 - TRIS base 0.5 M
 - HCl (37%) until pH 7.2

- Phosphate buffer (0.5 M; pH 7.2)
 - 68.4% Solution A (1 M)
 - Na₂HPO₄ x 2 H₂O 1 M
 - 31.6% Solution B (1 M)
 - NaH₂PO₄ x 2 H₂O 1 M

- Phosphate buffered saline (PBS), pH 7.14

Materials and Methods

NaCl	137 mM (0.9%)
KCl	2.7 mM
KH ₂ PO ₄	1.5 mM
Na ₂ HPO ₄ x 2H ₂ O	8 mM
○ RIPA lysisbuffer pH 8	
Tris-HCl	50 mM
NaCl	150 mM
SDS	0.1%
Natriumdoxycholot	1%
TritonX-100	1%
○ SDS sample buffer, 2x	
β-mercaptoethanol (for reduced conditions)	10%
TRIS buffer (1.25 M), pH 6.8	10%
Glycerine	20%
SDS	4%
Bromophenolblue	0.02%
○ Separating gel buffer	
TRIS/ HCl (pH 8.8)	1.5 M
add H ₂ O	
○ Solution I for Mini Plasmid DNA purification	
Glucose	50 mM
TRIS base	25 mM
EDTA	10 mM
○ Solution II for Mini Plasmid DNA purification	
NaOH	0.2 M
SDS	1%
○ Solution III for Mini Plasmid DNA purification (pH 4.8)	
Potassium acetate	3 M
○ Stacking gel buffer	
TRIS/HCl (pH 6.8)	0.5 M

- Storage buffer, pH 7.0
 - Tris 20 mM
 - NaCl 0.9%
 - BSA 0.5%
 - NaN₃ 0.09%

- Stripping buffer, pH 2.0
 - PBS (1x)
 - glycine 25 mM
 - SDS 1%

- 10x SSC for Southern blot
 - NaCl 1.5 M
 - Na-citrate 0.25 M

- 50x TAE
 - TRIS base 0.2 M
 - Acetic acid 5.7%
 - EDTA (0.5 M, pH 8) 10%

- TE buffer (pH 8)
 - TRIS base 10 mM
 - EDTA 1 mM

- Tyrodes buffer pH 7.3
 - NaCl 137 mM (0.9%)
 - KCl 2.7 mM
 - NaHCO₃ 12 mM
 - NaH₂PO₄ 0.43 mM
 - Glucose 0.1%
 - Hepes 5 mM
 - BSA 0.35%
 - CaCl₂ 2 mM
 - MgCl₂ 1 mM

- Washing buffer for Western blot (PBS-T)

Tween 20

0.1% in PBS

2.1.6 Oligonucleotides

All primer sequences presented in 5' → 3' direction:

CD84 external probe amplification

Cd84-Extp-for1: GGA GAA CTG ATA TTG AGA TA

Cd84-Extp-rev1: GGA TCC CTG ACA AAA TGA GT

CD84 mouse genotyping

CD84intr1.4f: CAG AGT GGG TCT TGG GGT GCT CA

CD84intr1.4r: CAG TGT GGT GTT TCC GGA GCT GGA G

GentrapF: TTA TCG ATG AGC GTG GTG GTT ATG C

GentrapR: GCG CGT ACA TCG GGC AAA TAA TAT C

Orai2 external probe amplification

Orai2Extp3F: 5' ATGCCCCAGCCTCATCATAC 3'

Orai2Extp3R: 5' GTAGCTGAAGACCGGCTACA 3'

Orai2 5' arm amplification

Orai2/5F1: AAGCGGCCGCACTTCTGATAGACTGTCTTGA

Orai2/5R1: AAGCGGCCGCGAGGTGACTGTAGATCACTGA

Orai2 5' arm sequencing

Orai2/5fSeq1: TGCAGACTATGTTTACCACT

Orai2/5fSeq2: GTGCCTGAGAAGGGTGG AAC

Orai2/5fSeq3: CCT CAT GAT TGC ATA GCA GA

Orai2/5fSeq4: CCACAAGTGTGCTCAGTTGT

Orai2/5fSeq5 :GCACGAGGCATGATGTCACA

Orai2/5fSeq6: GGATCCTGGCCTTGAGACCA

Orai2 3' arm amplification

Orai2/3F1: AAGTCGACGGGAGGCCGTTGCGATTTGCT

Orai2/3R1: AACTCGAGCTTCGCCAAGGTGGTACAGCT

Orai2 3' arm sequencing

Orai2/3fSeq1: GCTGCTTGAGTGTGCAGAGG
Orai2/3fSeq2: CATGCATACTGTGCTATAACC
Orai2/3fSeq3: CAAGCCTGGAGACCTGAGTT
Orai2/3fSeq4: CATCCCACAGCTTTGTCAGGA
Orai2/3fSeq5: GAGAAGTGTGTACCATGGTT
Orai2/3fSeq6: GCTCAGGAAGTAGCACTATT
Orai2/3fSeq7: GCTAAGCAGTGACTIONGTCTGG
Orai2/3fSeq8: CGCATGCAGATGAAGCATCT

Orai2 mouse genotyping

O2GenF: CAG GCT ACC ATT CAG AC
O2GenR: CCT AGT ATG TCC ATG GAT CT
PGKrev2: TGTGCGAGGCCAGAGGCCACT

RT-PCR

mOrai2RTf: CTTCGCCATGGTGGCCATGG
mOrai2RTTr: ACCAGGGAACGGTAGAAGTG
mActinf: GTGGCCGCTCTAGGCACCAA
mActinr: CTCTTTGATGTCACGCACGATTTC

2.1.7 Antibodies

Monoclonal antibodies were either generated and modified in our laboratory or purchased:

Antibody	Clone	Isotype	Antigen	Source/description
p0p4	15E2	IgG2b	GPIb α	¹⁶¹
p0p6	56F8	IgG2b	GPIX	¹⁶¹
DOM2	89H11	IgG2a	GPV	¹⁶¹
ULF1	96H10	IgG2a	CD9	¹⁶¹
JAQ1	98A3	IgG2a	GPVI	⁴¹
JAQ3	0E3	IgG2a	GPVI	⁴²
JON6	14A3	IgG2b	α IIb β 3	unpublished
LEN1	12C6	IgG2b	α 2	¹⁶²
Anti-integrin β 1 chain (CD29)	9EG7	IgG2a	β 1	BD Pharmingen
INU1	11E9	IgG1	CLEC-2	¹⁶³
JER1	10B6	IgG2a	CD84	¹⁶⁴
Anti-CD16/32	2.4G2	IgG2b	Fc γ RII, IIIa	¹⁶⁵
JON/A	4H5	IgG2b	α IIb β 3	¹⁶⁶
WUG 1.9	5C8	IgG1	P-Selectin	unpublished
EDL-1	57B10	IgG2a	β 3 integrin	¹⁶¹
Anti-CD4-PE	RM4-5	IgG2a	CD4	BD Pharmingen
Anti-CD8-PE-Cy5	53-6.7	IgG2a	CD8	BD Pharmingen
Anti-B220 (CD45R)- Alexa 647	RA3-6B2	IgG2a	B220	BD Pharmingen
Anti-MAC1 (CD11b)-PE	M1/70	IgG2b	CD11b	BD Pharmingen
Anti-F4/80-PE-Cy5	BM8	IgG2a	F4/80	eBioscience
Biotin anti-mouse CD84	mCD84.7	IgG	CD84	Biologend
Anti-human CD84- Biotin	2G7	IgG1	human CD84	eBioscience
Anti-human CD84- FITC	MZ18- 21F6	IgG1	human Cd84	Miltenyi
Anti-human CD84	Max.3	IgG1	human Cd84	⁷⁷

Table 1. Monoclonal antibodies used in this thesis, including clone names and sources.

Polyclonal antibodies and secondary reagents were purchased:

M130 (rabbit anti-mouse CD84)	Santa Cruz Biotech (Heidelberg, Germany)
Donkey anti-rat IgG (-HRP)	Dianova (Hamburg, Germany)
Goat anti-rabbit IgG (-HRP)	Cell Signaling (Frankfurt/Main, Germany)
Goat anti-rat IgG/M (H+L)	Dianova (Hamburg, Germany)
Rabbit anti-mouse IgG (-HRP)	DAKO (Hamburg, Germany)
Rabbit anti-rat IgG-FITC	DAKO (Hamburg, Germany)
Streptavidin-FITC	DAKO (Hamburg, Germany)
Streptavidin-horseradish peroxidase	DAKO (Hamburg, Germany)

2.1.8 Other materials

Vivaspin 6 centrifugal concentrators	Sartorius stedim (Aubagne, France)
Micra D1 homogenizing drive	ART Labortechn. (Mülheim, Germany)

2.1.9 Plasmids

TOPO XL	Invitrogen (Karlsruhe, Germany)
pBluescriptKS	Stratagene (La Jolla, CA, USA)
pSP72	Promega (Mannheim, Germany)

2.1.10 Bacteria

XL10-Gold	Stratagene (La Jolla, CA, USA)
DH5 α	Invitrogen (Karlsruhe, Germany)

2.2 Methods

2.2.1 Molecular biology

2.2.1.1 PCR

- Standard PCR with Taq-Polymerase (Fermentas)

100 ng	forward primer
100 ng	reverse primer
1 µL	10 mM dNTP
5 µL	10x Taq-buffer (+ KCl, - MgCl ₂)
20 ng	DNA template
1-5 U	Taq-Polymerase
5 µL	25 mM MgCl ₂

H₂O was added to a final volume of 50 µL.

Program: (product < 2 kb)

96°C	3 min	
94°C	30 s	} 35 cycles
60°C	30 s	
72°C	30 s	
72°C	10 min	
4°C	Stop	

- Gradient PCR with Extender Kit (5 PRIME)

PCR cycler: Mastercycler gradient (Eppendorf)

100 ng	Primer forward
100 ng	Primer reverse
20 ng	DNA template
5 µL	Extender buffer
1 µL	10 mM dNTP
0.5 µL	Enzyme TH

H₂O was added to a final volume of 50 µL.

Program 1: (product < 2 kb)

96°C	3 min	
94°C	30 s	} 35 cycles
x°C	30 s	
68°C	45 s	

68°C 10 min
4°C Stop

Program 2: (product > 2 kb)

96°C	3 min	} 35 cycles
94°C	30 s	
x°C	30 s	
68°C	2-5 min	
68°C	10 min	
4°C	Stop	

x°C: PCR reaction was performed with increasing annealing temperatures:

sample 1: 50°C; sample 2: 50.3°C; sample 3: 51.4°C; sample 4: 53.2°C; sample 5: 55.5°C;
sample 6: 58°C; sample 7: 60.8°C; sample 8: 63.5°C

2.2.1.2 Agarose gel electrophoresis

Agarose was dissolved in 1x TAE buffer. Depending on the length of DNA fragments to be separated, different amounts of agarose were used (0.8-1.5%). Subsequently, the agarose in TAE buffer was heated in a microwave. When the temperature had decreased to approx. 60°C, 5 µL ethidiumbromide (2 mg/mL) per 100 mL were added, and the fluid was poured into a tray with a comb. This tray was positioned in an electrophoresis chamber containing 1x TAE buffer. DNA samples were diluted in 6x loading buffer and loaded into the slots of the gel. For size-separation according to their electrophoretic mobility, DNA samples were run at about 120 kV. In one slot a 1 kb ladder was loaded to determine the size of the DNA bands under UV light later on.

2.2.1.3 DNA extraction from agarose gels

DNA extraction was performed using the NucleoSpin Extract II Kit (Macherey-Nagel, Düren, Germany). Under UV light, DNA bands were excised from an agarose gel. 700 µL NT buffer was added to the isolated agarose piece and shaken at 55°C for several min until the gel was completely dissolved. The DNA solution was applied onto the column and centrifuged at 11,000 x g for 30 s. Next, the column was washed twice with 750 µL NT3 buffer containing ethanol at 11,000 x g for 1 min. To dry the membrane the empty column was centrifuged at 11,000 x g for 2 min. Ethanol was removed by air-drying the tube with open lid for 3-5 min. Finally, 30 µL H₂O were added onto the membrane and incubated for 2-4 min. DNA was eluted by centrifugation at 11,000 x g for 2 min.

2.2.1.4 Digestion of plasmid DNA

All samples were digested for at least 45 min at 37°C.

1-10 U restriction enzyme per sample

2 µL 10x enzyme buffer

0.5-2 µg DNA

H₂O was added to a final volume of 20 µL.

To perform a double digestion, additional 2-10 U of a second enzyme were added, if the reaction was possible under same buffer and temperature conditions.

2.2.1.5 Ligation of insert and vector

The target vector was digested with the desired enzyme for 1.5 h at 37°C. Then the reaction was stopped at 60°C for 10 min. After cooling of the sample, 1µL CIAP (calf intestinal alkaline phosphatase) was added and incubated at 37°C for 30 min to prevent religation of the vector. This step was repeated. Gel electrophoresis was performed, bands were cut and DNA was purified as described above.

Purified insert and vector were mixed in a ratio of 2:1 and ligated using Ready-to-go T4 DNA ligase (GE Healthcare):

5 µL vector, 10 µL insert, and 5 µL H₂O were mixed in 1 vial of T4 Ligase by pipetting up and down. Then samples were incubated for 45 min at 16 °C and then inactivated for 10 min at 70 °C. Then 1 µL was used to transform 50 µL (one vial) of One Shot® TOP10 bacteria (Invitrogen).

2.2.1.6 TOPO cloning

For cloning of long PCR products, ligation into TOPO XL vectors (Invitrogen) was performed according to the manufacturer's protocol.

The PCR product was run on an agarose gel. Then the gel was stained with Crystal Violet and purified using the supplied columns of the TOPO XL kit. For ligation, 2-4 µL of purified PCR product and 1 µL pCR-XL-TOPO vector were mixed. After 10 min at room temperature (RT) the reaction was stopped with 1 µL 6x TOPO Cloning Stop. Transformations were performed with competent cells provided with the kit. Therefore, 2 µL of the TOPO Cloning reaction were added to one vial of chemically competent cells and incubated on ice for 30 min. The cells were heat-shocked at 42°C for 30 seconds. The tubes were transferred on ice for 2 min. Following addition of 250 µL S.O.C. medium, the samples were shaken at 37°C for one h. 150 µL were plated on an LB plate containing 50 µg/mL kanamycin and incubated at 37°C o/n.

2.2.1.7 Transformation

1 µL plasmid DNA (approx. 20-50 ng) was added to 100 µL chemically competent *E. coli* cells (DH5α or XL10Gold) and incubated on ice for 45 min. Heat shock was performed for 90 s at 42°C. Then, cells were incubated on ice for 2 min. 1 mL LB medium without antibiotics was applied to the cells and incubated for 30 min at 37°C. After centrifugation for 2 min at 5,000 x g, the cells were plated onto a LB plate containing 50 µg/ mL ampicillin or 25 µg/ mL kanamycin. The plate was incubated at 37°C o/n.

2.2.1.8 Mini Plasmid DNA purification

3 mL LB medium containing the selective antibiotic (50 µg/mL ampicillin or kanamycin) and a picked single colony were shaken for 12-16 h at 37°C. The cells were spun down at 11,000 rpm for 30 seconds and the pellet was resuspended in 200 µL solution I. 300 µL of solution II were used to lyse the cells for about 5 min at RT. Then, 300 µL of solution III were added and the sample was incubated for 5 min at RT. Subsequently, the tube was centrifuged at 11,000 rpm for 5 min. The supernatant was transferred into a new tube and mixed with 700 µL isopropanol and incubated on ice for 5 min. After centrifugation at 14,000 rpm for 10 min at 4°C, the pellet was washed with 500 µL 70% ethanol and incubated for 8 min at RT. The sample was centrifuged at 14,000 rpm for 8 min at 4°C and finally the dried DNA pellet was dissolved in 30 µL TE buffer containing 0.1 µg/µL RNaseA.

2.2.1.9 Midi Plasmid DNA purification

DNA purification was performed using the PureYield Plasmid Midiprep System from Promega (Mannheim, Germany).

A picked single colony was added to 100 mL LB medium containing the selective antibiotic (50 µg/mL ampicillin or 25 µg/mL kanamycin). The medium was shaken at 37°C o/n. Bacterial cells were pelleted by centrifugation at 6,000 x g for 10 min at RT. The bacterial pellet was resuspended in 3 mL cell suspension solution. Then, 3 mL cell lysis solution were added, the tube was inverted 4-6 times and incubated for 3 min at RT. 5 mL neutralization solution were poured to the sample, inverted and incubated for 3 min at RT. Next, the sample was centrifuged at 15,000 rpm for 8 min in a Multifuge 3 S-R (Heraeus). The supernatant was poured onto the blue PureYield Clearing Column, soaked through onto the white PureYield Binding Column and was removed by vacuum. Next, 5 mL endotoxin removal wash were added onto the white column and removed by vacuum. Then 20 mL column wash solution was added to the binding column, holding up the vacuum for 60 s after flow through. The column tip was tapped onto a paper towel to remove the remaining solution. The binding column was put into an empty 50 mL tube, loaded with 600 µL nuclease free water and

incubated for 5 min at RT. The DNA was eluted by centrifugation at 2,000 x g for 5 min and DNA concentration was measured at OD₂₆₀.

2.2.1.10 Sequencing of DNA

Sequencing of DNA (PCR product or plasmid DNA) was performed by MWG Biotech (Ebersberg, Germany). 3 µg DNA was diluted in TE buffer to a final volume of 20 µL. Either standard primers from the company were chosen or own primers were sent with the template. 1 µg of the respective primer was diluted in TE buffer to a final volume of 13 µL.

An NCBI online search tool was used to analyze the sequencing results:

<http://www.ncbi.nlm.nih.gov/blast/bl2seq/wblast2.cgi>

2.2.2 Stem cell work

2.2.2.1 Feeder cells

For culturing of murine embryonic stem cells, irradiated feeder cells containing a neomycin resistance gene were used. Feeder cells were obtained from E18 embryos heterozygous for a collagen IX null allele which contains a neomycin-resistant cassette¹⁶⁷. Feeder cells were prepared in our laboratory.

2.2.2.2 Electroporation

Five to seven days prior to starting the electroporation, stem cells (R1 clone, 129/Sv, passage number 17)¹⁶⁰ were cultured. Therefore, half a pellet of one cryotube with feeder cells and 0.5 mL stem cells were cultured in a 25 cm² tissue culture flask containing 5 mL ES medium. Every day medium was changed. After the second day, stem cells were trypsinized and transferred into a 175 cm² tissue culture flask. In each 175 cm² flask a new feeder cell layer was required. Thus, 2 mL feeder cells were centrifuged and the pellet was resuspended in 2.5 mL ES medium. The feeder cells and the trypsinized stem cells resuspended in 5 mL ES medium were transferred into a 175 cm² flask and diluted with additional 25 mL ES medium. Cells were electroporated when an optimal density was reached.

For electroporation, either 100 µg DNA of the *Cd84* targeting vector plasmid DNA were linearized by digestion with *NotI*, or 100 µg DNA of the *Orai2* targeting vector plasmid DNA were linearized by digestion with *XhoI*, at 37 °C for 2 h.

100 µg DNA

10x enzyme buffer

200 U enzyme (*NotI* or *XhoI*)

add H₂O to a final volume of 300 µL

To confirm linearization of the vector, same DNA amounts of digested and undigested vector were compared on a 0.7% agarose gel. To precipitate the digested DNA, phenol/chloroform was added to the sample in the ratio 1:1 and inverted several times. After centrifugation at 14,000 x g for 10 min at RT, the upper phase was transferred into a new 1.5 mL tube. Then, chloroform was added in a ratio of 1:1 and the sample was shaken and spun down. 10% 3 M sodium acetate pH 5.2 and three volumes 100% ethanol were added to the supernatant and DNA was precipitated. In a sterile reaction tube the DNA was washed twice with 800 μ L of 70% ethanol. The pelleted DNA was dried under sterile conditions, resuspended in 700 μ L sterile 1x PBS and mixed well.

Stem cells in the 175 cm² tissue culture flask were trypsinized and diluted in 10 mL ES medium. Next, cells were centrifuged and resuspended in 10 mL sterile 1x PBS. Then cells were spun down again and supernatant was removed. The linearized plasmid DNA in PBS was added to the stem cells, resuspended, and electroporated in a cuvette (Bio-Rad, Munich, Germany) with 0.8 kV (Gene Pulser II from Bio-Rad). The electroporated stem cells were diluted with 8 mL ES medium and distributed to eight beforehand prepared 10 cm tissue culture dishes. Therefore, 0.75 mL feeder cells per dish were suspended in ES medium and pelleted. After discarding the supernatant, cells were diluted in ES medium. 1 mL feeder cells in ES medium and additional 10 mL ES medium were used for each tissue culture dish. Cells were cultured at 37°C and 5% CO₂.

2.2.2.3 Selection of ES cells

On the first day after electroporation the selection was started by treatment with the antibiotic Geneticin (G418). Therefore, the ES-Medium was removed and 10 mL ES-Medium with Geneticin was added. This change of medium was done daily for 5-7 days depending on the cell growth. Every day each tissue culture dish was checked for contamination with bacteria or yeast.

2.2.2.4 Picking of Geneticin-resistant ES cell clones

1 mL feeder cells were used for one 24 well plate. Therefore, ES+G418 Medium was added to the feeder cells and spun down. Afterwards, the pellet of feeder cells was diluted with 24 mL ES+G418 Medium and evenly distributed to each well of a 24 well plate and stored at 37°C until use.

The picking of stem cell clones with a pipette was performed under a LEICA MS5 microscope (setting: 0.63x magnification). Surviving clones which had the appropriate size and shape were picked. Cells looking differentiated or necrotic were not picked. The picked

clones were transferred into a well of a 96 well plate containing three drops of trypsin. After incubation for three min at 37°C and 5% CO₂ each clone was resuspended in the well with trypsin and added to one well of the beforehand prepared 24 well plate. The cells were incubated at 37°C o/n and then the ES+G418 Medium was changed. After this treatment the cells grew 2-4 days without changing medium. Every day each well plate was checked on contamination with bacteria or yeast.

2.2.2.5 Freezing of picked stem cells

The cells in the 24 well plates were trypsinized and then 1 mL freezing medium was added to each well. After resuspension, 600 µL of the sample were transferred to a labeled cryotube and immediately stored at –80°C. According to the cryotube the well was labeled with the same number. The remaining 400 µL were filled up with ES+G418 Medium and incubated for 12-16 h at 37°C. Then, the medium was replaced by new ES+G418 Medium.

2.2.2.6 Lysis of stem cells

Under normal cell growth usually after 3-4 days of culturing, the color of medium turned yellow, indicating cell growth by a shift in pH. The medium was removed from the wells and cells were lysed. Therefore, 0.5 mL lysis buffer containing Proteinase K was added per well and the ES cells were lysed for at least 24 h and not longer than five days at 37°C and 5% CO₂.

2.2.2.7 Precipitation of stem cell DNA

Following lysis of the ES cells, DNA was precipitated by adding one mL isopropanol per well. Thereby, sterile conditions were not required anymore. To enhance the precipitation of genomic DNA, the samples were slightly agitated on a shaker for 6 h at RT. Meanwhile, 1.5 mL reaction tubes were labeled with the corresponding numbers to the 24-well plate and filled with 150 µL TE buffer. Precipitated DNA fibers were transferred by a stick into the corresponding tube. The samples were mixed for 1 min and DNA was incubated for 12-16 h at 55°C. Then, the samples were mixed again and were ready for analysis.

2.2.2.8 Analysis of stem cell DNA by Southern blot

- Digestion of the stem cell DNA

Each sample of stem cell DNA was digested in order to distinguish a positive clone that integrated the electroporated DNA via homologous recombination and a negative clone that

could not integrate the electroporated DNA homologously. The genomic stem cell DNA was digested o/n at 37°C:

20 µL stem cell DNA

4 µL 10x *Bam*HI buffer (for CD84) / 4 µL *Eco*RV buffer (for *Orai2*)

25 U *Bam*HI enzyme (High conc., for CD84) / 25 U *Eco*RV enzyme (High conc., for *Orai2*)

add H₂O to a final volume of 40 µL

- Southern blot

The digested DNA samples were run on a 1% agarose gel for at least 2-3 h at 150 kV. Then a photo was taken from the gel with a ruler to estimate the size of the bands after development. The gel was incubated two times in denaturation buffer for 20 min and two times in neutralization buffer for 20 min. Afterwards, the DNA was blotted from the agarose gel on a membrane o/n at room temperature. DNA transfer was performed by capillary forces in 20 x SSC buffer on Hybond-XL membranes (GE Healthcare). Membranes were air-dried. Gel slots were labeled on the membrane. Then DNA was crosslinked with the membrane with 120 mJ/cm² (HL-2000 HybriLinker from UVP).

For probe labeling and hybridization the following steps were performed in an isotope lab:

The external probe (10–100 ng) was diluted in 35 µL TE buffer and incubated for three min at 96°C. When the DNA was resuspended in the Rediprime DNA Labeling Kit, α ³²P-dCTP was added to the DNA and incubated for 20 min at 37°C. In the meantime, buffer of the Probequant G 50 Microcolumns was removed via centrifugation and the membrane was briefly preincubated in Church wash buffer. The DNA with the radioactive substance was loaded on the column and centrifuged for 1 min at 2,000 rpm (Biofuge A from Haereus). The flow-through containing the radioactive-labeled DNA was incubated for 3 min at 96°C and then added to the membrane in Church buffer. The membrane was shaken in Church buffer o/n at 68°C. Then the membrane was washed twice with Church wash buffer for 20 min at 68°C. Subsequently, a film was placed on the membrane and stored at –80°C. The film was developed after 4-7 days.

2.2.2.9 Reculturing of positive stem cells

According to the southern blotting, positive frozen clones (cryotube) were thawed and added to one well of a 6-well plate containing feeder cells and ES medium supplemented with 50 U/mL penicillin and 50 µg/mL streptomycin (P/S). After one or two days growing at 37°C and 5% CO₂ the cells were trypsinized and cultured in a 25 cm² flask. Two days later the cells were trypsinized again and transferred into a 175 cm² tissue culturing flask.

Supernatants were tested for contamination with Mycoplasma (VenorGeM Mycoplasma Detection Kit). Cells were trypsinized when grown to 90% confluence, washed, and then freezing medium was added to the stem cell pellet and separated into 4 cryotubes. Four cryotubes were stored at -80°C .

A small amount of each positive clone was further cultured and tested again by Southern blot for homologous recombination. Afterwards, one tube with ES cells was sent to “Transgenic Service” at the Max Planck Institute of Neurobiology (Munich, Germany), where blastocyst injection was performed.

2.2.3 Isolation of DNA

5 mm² of ear tissue was digested in 500 μL DNA lysis buffer with Proteinase K at 56°C overnight under shaking conditions. Samples were mixed (1:1 vol) with phenol/chloroform, and centrifuged at 14,000 rpm for 10 min. The upper phase containing the DNA was transferred to a fresh tube containing isopropanol (1:1 vol) and mixed. After centrifugation at 14,000 rpm for 10 min, the DNA pellet was washed with 70% ethanol. The DNA pellet was left to dry at 37°C and finally resuspended in 50 μL of H₂O.

2.2.4 Genotyping of *Cd84*^{-/-} mice by PCR

wt PCR:

1 μL genomic DNA (50 – 100 ng)
1 μL CD84intr1.4f 1:10 (100 ng)
1 μL CD84intr1.4r 1:10 (100 ng)
1 μL dNTPs (10 mM each)
5 μL Taq-buffer (10x)
4 μL MgCl₂
0.2 μL Taq-Polymerase (Fermentas)
add H₂O

50 μL

Program “CD84wt”:

Temp ($^{\circ}\text{C}$)	Time
96	3 min
94	30 s
63,5	30 s
72	1 min

GOTO 2 REP 37

72 5 min

HOLD 22°C

Cd84 ko-PCR:

1 µL genomic DNA (50 – 100 ng)

1 µL GentrapiF (100 ng)

1 µL GentrapiR (100 ng)

1 µL dNTPs (10 mM each)

5 µL Taq-buffer (10x)

5 µL MgCl₂

0.2 µL Taq-Polymerase

add H₂O

50 µL

Program

Temp (°C)	Time
-----------	------

96	3 min
----	-------

94	30 s
----	------

51,4	30 s
------	------

72	45 s
----	------

GOTO 2 REP 35

72 5 min

HOLD 22°C

Result (expected band sizes):

wt/wt: 672 bp

wt/ko: 672 bp and 750 bp

ko/ko: 750 bp

2.2.5 Genotyping of *Orai2*^{-/-} mice by PCR

wt PCR:

1 µL genomic DNA (50 – 100 ng)

1 µL O2genF 1:10 (100 ng)

1 µL O2genR 1:10 (100 ng)

1 µL dNTP's (10 mM each)

Materials and Methods

5 μ L Taq-buffer (10x)
4 μ L MgCl₂
0,2 μ L Taq-Polymerase
add H₂O

50 μ L

Program "Or2" (for both wild-type and ko PCR)

Temp (°C)	Time
96	3 min
94	30 s
51	30 s
72	1 min
GOTO 2 REP 37	
72	5 min
HOLD 22°C	

Orai2 ko PCR:

1 μ L genomic DNA (50 – 100 ng)
1 μ L O2genF: 1:10 (100 ng)
1 μ L PGKrev2: 1:10 (100 ng)
1 μ L dNTP's (10 mM each)
5 μ L Taq-buffer (10x)
4 μ L MgCl₂
0,2 μ L Taq-Polymerase
add H₂O

50 μ L

Result (expected band sizes):

wt/wt: 400 bp

wt/ko: 400 bp and 500 bp

ko/ko: 500 bp

2.2.6 RNA isolation and RT-PCR

For platelet RNA isolation, platelets from 3 mice per group were washed in PBS/EDTA and the pellet was resuspended in 250 μ L IP buffer with 1% NP-40. 800 μ L of Trizol reagent was added, samples were vortexed and incubated for 60 min at 4°C.

Alternatively, tissue samples of different organs were cut into small pieces and homogenized in 1 mL Trizol reagent, using a Miccra D1 homogenizing drive (ART Labortechnik, Mülheim, Germany). Samples were incubated for 60 min at 4°C.

After incubation, 250 μ L of chloroform was added and samples were incubated again for 15 min at 4°C. Samples were then centrifuged at 10,000 rpm for 10 min and the upper phase was incubated with three volumes of 70% ethanol with 10% sodium acetate (pH 5.2) for 1 h at -20°C. After centrifugation at maximal speed for 15 min, the pellet was washed with 70% ethanol, then centrifuged again and dried at 37°C. The pellet was resuspended in 20-40 μ L of RNase free water and concentration was determined by absorbance readings at 260 nm, whereas the ratio of absorbance at 260/280 and 260/230 was used to assess purity. Samples with 260/280 readings of >1.8 and 260/230 readings of >1.9 were subsequently used to prepare cDNA. 1 μ g RNA was incubated with 2 μ L Oligo dT primers (0.5 μ g/ μ L) in a total volume of 20 μ L at 70°C for 10 min and afterwards transferred on ice. 2 μ L DTT (0.1 M), 1 μ L dNTPs (10 mM), 0.1 μ L RNasin, 4 μ L 5x first strand buffer and 1 μ L Super Script Reverse Transcriptase (Invitrogen) were added. The total volume was adjusted to 40 μ L by adding RNase free water and the samples were incubated at 42°C for 1 h. Then, the reaction was stopped by incubation at 70°C for 10 min.

A gradient PCR was performed with Taq polymerase to determine the correct annealing temperature. Following this, a Polymerase chain reaction (PCR) with the appropriate annealing temperature was performed. For *Orai2* RT-PCRs, annealing temperature of 56°C and 40 cycles with 30s reaction time were appropriate. The following primers were used:

mOrai2RTf: CTTCGCCATGGTGGCCATGG

mOrai2RTr: ACCAGGGAACGGTAGAAGTG

mActinf: GTGGGCCGCTCTAGGCACCAA

mActinr: CTCTTTGATGTACGCACGATTTC

2.2.7 Adoptive transfer of T cells

Single-cell suspensions of spleens and lymph nodes of wt or *Cd84^{-/-}* donor mice were generated by mashing the organs through a 40 μ m cell strainer (Becton Dickinson). Red blood cells were lysed with ACK buffer (0.15 M NH₄Cl, 10 mM KHCO₃, 0.1 mM EDTA). Isolated myeloid immune cells and lymphocytes were washed in MACS buffer (1xPBS, PAA Laboratories, supplemented with 0.5% BSA and 2 mM EDTA, Sigma Aldrich). CD4⁺ T cells

were magnetically separated (CD4⁺ T cell Isolation Kit II, Miltenyi Biotec). Cells were resuspended to 750,000 cells in 100 µl 1 x PBS and intravenously injected in *Rag1*^{-/-} or *Cd84*^{-/-} recipient mice 24 h before tMCAO. These transfer experiments were performed at the Department of Neurology, Würzburg, in the group of Prof. Dr. Guido Stoll.

2.2.8 Preparation of lysates from different organs

50 µg tissue from the desired organ was homogenized in 1 mL ice cold RIPA lysisbuffer using a Micra D1 homogenizing drive (ART Labortechnik, Mülheim, Germany). The lysate was incubated at 4°C on a rotor for 1 h, followed by centrifugation at 14,000 rpm for 30 min at 4°C. Supernatants were frozen at -80°C. For Western Blot analysis, lysates were incubated with reducing or nonreducing sample buffer and boiled for 5 min at 95°C.

2.2.9 Biochemistry

2.2.9.1 Western blotting (Immunoblotting)

Platelets were washed twice in Tyrodes buffer and solubilized in IP buffer containing 1% NP-40. For the separation of proteins by SDS-PAGE, polyacrylamide gels were prepared with either a 10% or a 12% separating part and a 4% stacking part. 5-20 µL of protein samples per lane were loaded on the gel, previously assembled in a chamber filled with Laemmli buffer. The gel ran at 15 mA until the bands reached the separating part. Then the current was raised to 25 mA. After separation, gels were removed from the chamber and subjected to immunoblotting.

For semidry immunoblotting the stacking part of the gel was removed and the gel was put into blotting buffer B to soak. A polyvinylidene difluoride (PVDF) membrane (Millipore, Schwalbach, Germany) was soaked first in methanol and then in blotting buffer B. The transfer was achieved as follows: Whatman paper was soaked in blotting buffers A and B (3 sheets each) and placed on the blotting apparatus, followed by the PVDF membrane, the gel and another three sheets of paper soaked in blotting buffer C. Blotting was performed for 1 h with 65 mA per gel. The membrane was blocked in blocking solution for 1 h at RT, or o/n at 4°C. The membrane was incubated with the primary antibody, diluted in blocking solution for 1 h at RT, followed by washing 4 x 15 min in washing buffer and incubated with the secondary antibody for 1 h. After this, membranes were washed 4 x 15 min in washing buffer and proteins were visualized using ECL.

2.2.9.2 HRP-labeling of antibodies

HRP-labeling of monoclonal antibodies was performed with the Peroxidase labeling Kit (Roche, Mannheim, Germany) according to the manufacturer's manual.

2.2.9.3 FITC-labeling of antibodies

4 mg of antibody was dialyzed against coupling buffer overnight at 4°C. FITC was dissolved in anhydrous DMSO to a final concentration of 1 mg/mL. 50 µL of this solution was added to the antibody and left to incubate at RT for 4 h and then o/n at 4°C on a rotor. The reaction was stopped by addition of 100 µL of 1 M NH₄Cl. FITC-labeled antibody was separated from unbound FITC by gel filtration on a PD-10 column. The antibody was diluted in storage buffer to the desired concentration.

2.2.9.4 Biotinylation of antibodies

3 mg of antibody was dialyzed against coupling buffer over night at 4°C. Then EZ-link sulfo-NHS-LC-biotin was added to a final concentration of 300 µg/mL for 30 min at RT with rotation. The reaction was stopped by addition of 100 µL of 1 M NH₄Cl and the antibody was finally dialyzed against PBS over night at 4°C. To check the efficiency of the biotinylation, washed platelets were incubated with the biotinylated antibody (2, 5 and 10 µg/mL) for 10 min at RT, then centrifuged (2,800 rpm, 5 min) to remove unbound antibody, and subsequently incubated with FITC-labeled streptavidin (1.5 µg/mL; 10 min, RT). Samples were analyzed by flow cytometry.

2.2.9.5 sCD84 ELISA

Soluble mouse CD84. Washed platelets were resuspended at a concentration of 3×10^8 platelets/mL in Tyrodes-HEPES buffer containing 2 mM CaCl₂ and 0.02 U/mL apyrase. To induce CD84 shedding, platelets were treated in the presence or absence of the broad range metalloproteinase inhibitor GM6001 (100 µM, 15 min, 37°C) for 1 h with CCCP (100 µM), W7 (150 µM), or for 20 min with NEM (2 mM) at 37°C. Alternatively, platelets were treated for 1 h with convulxin (1 µg/mL), CRP (40 µg/mL), rhodocytin (2 µg/mL), thrombin (0.5 U/mL) or PAR4 peptide (NH₂-AYPGKF; 1-4 mM). Platelets were centrifuged (2800 rpm) and supernatants were incubated on JER1-coated (10 µg/mL) ELISA plates for 2 h at RT. After extensive washing, plates were incubated with biotinylated antibody mCD84.7 (10 µg/mL) for 1 h at RT. After extensive washing, plates were incubated with HRP-labeled streptavidin for 45 min at RT and developed using 3,3',5,5'-tetramethylbenzidine (TMB). The reaction was stopped by addition of 2N H₂SO₄ and absorbance at 450 nm was recorded on a Multiskan

Ascent (Thermo Scientific). Alternatively, plasma or serum samples were applied to JER1-coated ELISA plates.

Soluble human CD84. Human platelet samples were treated as described above for mouse platelets. MAX.3 (10 µg/mL) was used as coating antibody and biotinylated 2G7 (5 µg/mL) as secondary antibody.

2.2.9.6 sGPVI ELISA

In vitro GPVI ELISA. Washed platelets were resuspended in Tyrodes-HEPES buffer without CaCl₂ containing PGI₂ (0.1 µg/mL) and apyrase (0.02 U/mL). Biotinylated JAQ1 antibody (10 µg/mL) was added and incubated for 5 min at RT. After centrifugation, platelets were resuspended in Tyrodes-HEPES buffer containing 2 mM CaCl₂ and 0.02 U/mL apyrase. To induce GPVI shedding, the cells were treated with CCCP (100 µM) or W7 (150 µM) for 1 h at 37°C. Platelets were centrifuged and supernatants were incubated on JAQ3-coated (10 µg/mL) ELISA plates for 1 h at 37°C. After extensive washing, plates were incubated with HRP-labeled streptavidin for 45 min at 37°C and developed using 3,3',5,5'-tetramethylbenzidine (TMB). The reaction was stopped by addition of 2 N H₂SO₄ and absorbance at 450 nm was recorded on a Multiskan (Thermo Scientific).

Ex vivo GPVI ELISA. Plasma of mice treated with 100 µg biotinylated JAQ1 or vehicle was incubated on JAQ3-coated (10 µg/mL) plates for 1 h at 37°C and further processed as described above.

2.2.10 Generation of bone marrow chimeric mice

For the generation of bone marrow chimeric mice, 5-6 week old mice were irradiated with a single dose of 10 Gy, and bone marrow cells from donor mice of the desired genotype were injected intravenously into the irradiated mice (4 x 10⁶ cells diluted in 150 µL DMEM/mouse). Water supplemented with 2 g/l neomycin was provided to the mice for 6 weeks.

2.2.11 Isolation and analysis of immune cells

Peritoneal macrophages were flushed out of the peritoneal cavity of mice with 10 mL PBS without Ca²⁺, centrifuged at 480 g for 5 min and resuspended in FACS buffer. Cells from thymus, spleen and lymph nodes were isolated from 8 week-old mice as follows. Organs were isolated, placed inside a 70 µm cell strainer with ice-cold PBS/1% FCS and gently smashed with a piston from a 10 mL syringe. Spleen cell suspensions were further subjected to hypo-osmotic shock for red blood cell depletion using ACK buffer. The suspensions were then centrifuged at 480 g for 5 min. Cells were resuspended in FACS buffer for counting.

Cells counts were determined using a Sysmex KX-21N automated hematology analyzer (Sysmex, Norderstedt, Germany).

For FACS analysis, stainings were performed with 1×10^6 cells in a v-bottom 96 well plate. Fc γ Rs were blocked with 25 μ L FACS buffer supplemented with 10 μ g/mL 2.4G2 antibody at 4°C. Cells were stained with appropriately diluted antibodies in 25 μ L FACS buffer in the dark for 15 min at 4°C. Cells were washed again in FACS buffer, resuspended, transferred into FACS tubes and analyzed. Measurements were performed on a FACSCalibur flow cytometer using Cell Quest software (BD Biosciences, Heidelberg, Germany). Data were analyzed using FlowJo v7 (TreeStar, Ashland, OR, USA).

2.2.12 *In vitro* analysis of platelets

2.2.12.1 Platelet preparation and washing

Mice were bled under isofluran anesthesia from the retroorbital plexus. Blood was collected in a tube containing 20 U/mL heparin in TBS, and platelet rich plasma (prp) was obtained by centrifugation twice at 300 *g* for 6 min at room temperature. For preparation of washed platelets, prp was washed twice at 1000 *g* for 5 min at RT and the pellet was resuspended in Tyrodes-HEPES buffer in the presence of prostacyclin (0.1 μ g/mL) and apyrase (0.02 U/mL). Platelets were then resuspended in Tyrodes-HEPES buffer containing 2 mM CaCl₂ and 0.02 U/mL apyrase.

Human platelets. Blood (9 volumes) from healthy volunteers was collected in sodium citrate (1 volume) and PRP was obtained by centrifugation at 300 *g* for 20 min. PRP was centrifuged at 380 *g* in the presence of prostacyclin (0.1 μ g/mL), apyrase (0.02 U/mL) and 2 mM EDTA (ethylenediaminetetraacetic acid) for 20 min at RT. After two washing steps, pelleted platelets were resuspended in Tyrode-HEPES buffer containing 2 mM CaCl₂ and 0.02 U/mL apyrase.

2.2.12.2 Platelet counting

For determination of platelet counts, blood (50 μ L) was drawn from the retroorbital plexus of anesthetized mice using heparinized microcapillaries and diluted 1:20 in PBS and analyzed in a Sysmex cell counter.

2.2.12.3 Flow cytometry

For determination of basal glycoprotein expression levels, washed platelets (1×10^6) or diluted blood was stained for 10 min at RT with saturating amounts of fluorophore-conjugated antibodies. The reaction was stopped by addition of 500 μ L PBS, and samples were

analyzed directly on a FACSCalibur instrument (BD, Heidelberg, Germany). For activation studies, platelets were activated with the indicated agonists or reagents for 15 min at RT in the presence of saturating amounts of *phycoerythrin* (PE)-coupled JON/A and *fluorescein isothiocyanate* (FITC)-coupled α -P-selectin antibody. The reaction was stopped by addition of 500 μ l PBS and samples were analyzed. For a two-color staining, the following settings were used:

Detectors/Amps:

Parameter	Detector	Voltage
P1	FSC	E01
P2	SSC	380
P3	FI1	650
P4	FI2	580
P5	FI3	150

Threshold:

Value	Parameter
253	FSC-H
52	SSC-H
52	FI1-H
52	FI2-H
52	FI3-H

Compensation:

Detector	Setting
FI1	-2.4% of FI2
FI2	-7.0% of FI1
FI2	-0% of FI3
FI3	-0% of FI2

2.2.12.4 Aggregometry

To determine platelet aggregation, light transmission was measured using washed platelets in Tyrode's buffer without Ca^{2+} adjusted to a concentration of 0.16×10^8 platelets/mL. Alternatively, heparinized prp was used and diluted 1:3 in Tyrode's buffer. For determination of aggregation, agonists or reagents (100-fold concentrated) were added and light transmission was recorded over 10 min on a FibrinTimer 4 channel aggregometer (Apact 4-

channel optical aggregation system, APACT, Hamburg, Germany). For calibration, Tyrode's buffer (for washed platelets) or 1:3-diluted plasma (for prp) was set as 100% aggregation and washed platelet suspension or prp was set as 0% aggregation. For activation with thrombin, washed platelets were diluted in Tyrode's buffer containing 2 mM Ca^{2+} , for all other agonists platelets were diluted in the same buffer in presence of 70 $\mu\text{g}/\text{mL}$ human fibrinogen.

2.2.12.5 Spreading assay

Washed platelets were resuspended in Tyrode's buffer and adjusted to a concentration of 0.2×10^6 platelets/ μL . 60 μL of the platelet suspension was stimulated with 0.01 U/mL thrombin and immediately placed on coverslips (24 x 60 mm) that had been coated overnight with 100 $\mu\text{g}/\text{mL}$ human fibrinogen and blocked for 1 h with 1% BSA. For statistical analysis, bound platelets were fixed with 4% PFA in Tyrode's buffer at the indicated time points and counted using an inverted microscope Zeiss HBO 100 (Zeiss, Germany). Images were recorded with a 100x objective and analyzed using MetaVue® software and ImageJ (NIH).

2.2.12.6 Adhesion under flow

Rectangular coverslips (24 x 60 mm) were coated with 0.2 mg/mL fibrillar type I collagen (Horm, Nycomed) o/n at 37°C and blocked for 1 h with 1% BSA in H_2O . Blood (700 μL) was collected into 300 μL heparin (20 U/mL in TBS, pH 7.3) or ACD-buffer (for studies under non-anticoagulated conditions). Platelets were labeled with a Dylight-488 conjugated anti-GPIX Ig derivative (0.2 $\mu\text{g}/\text{mL}$) for 5 min at 37°C. Whole blood was diluted 2:1 in Tyrode's buffer containing Ca^{2+} and filled into a 1 mL syringe. Transparent flow chambers with a slit depth of 50 μm , equipped with the coated coverslips, were connected to the syringe filled with diluted whole blood. Perfusion was performed using a pulse-free pump under high shear stress equivalent to a shear rate of $1,000 \text{ sec}^{-1}$ or $1,700 \text{ sec}^{-1}$ (for 4 min). Thereafter, coverslips were washed for 1 min by perfusion with Tyrode's buffer at the same shear stress and phase-contrast and fluorescent images were recorded from at least five different microscopic fields (40x objective). Image analysis was performed off-line using MetaVue® software. Thrombus formation was expressed as the mean percentage of total area covered by thrombi and as the mean integrated fluorescence intensity per mm^2 .

2.2.12.7 Clot retraction

For clot retraction studies, platelets were adjusted to a concentration of 3×10^8 platelets/mL in platelet poor plasma (ppp). 250 μL of the platelet suspension was mixed with 1 μL erythrocyte suspension (to contrast the clot), obtained during platelet isolation from whole blood, and 20 mM CaCl_2 . Clotting was induced by addition of high thrombin concentrations (3 U/mL).

Subsequent clot retraction was monitored at 37°C under non-stirring conditions and documented with a digital camera at different time points.

2.2.12.8 Shedding of glycoproteins from the platelet surface

Washed platelets resuspended at a concentration of 3×10^8 platelets/mL in Tyrodes-HEPES buffer containing 2 mM CaCl_2 and 0.02 U/mL apyrase were treated in the presence or absence of the broad range metalloproteinase inhibitor GM6001 (100 μM , 15 min, 37°C) for 1 h with CCCP (100 μM), W7 (150 μM) or for 20 min with NEM (2 mM) at 37°C and immediately analyzed on a FACSCalibur. Where indicated, platelets were pretreated with the calpain inhibitors calpeptin (5 $\mu\text{g}/\text{mL}$), ALLN (50 μM) or MDL28170 (50 μM) for 15 min at 37°C. Alternatively, platelets were treated for 1 h with convulxin (1 $\mu\text{g}/\text{mL}$), CRP (40 $\mu\text{g}/\text{mL}$), rhodocytin (2 $\mu\text{g}/\text{mL}$), thrombin (0.5 U/mL) or PAR4 peptide (NH_2 -AYPGKF; 1-4 mM). Where indicated, aggregation of mouse platelets was inhibited with saturating concentrations of the integrin $\alpha\text{IIb}\beta 3$ blocking antibody JON/A F(ab)₂¹⁶⁶.

For Western blot analysis, platelets were lysed in 4x Laemmli buffer containing 1% Nonidet P-40. Proteins were separated by SDS-PAGE and blotted onto polyvinylidene difluoride membranes. After blocking with 5% fat free milk in TBS-T, the membrane was incubated with either polyclonal anti-CD84 antibody M-130 over night at 4°C or peroxidase-conjugated monoclonal antibody JER1 (or peroxidase conjugated JAQ-1 for GPVI detection). As secondary antibody for polyclonal M-130, goat anti-rabbit IgG HRP (1 h at room temperature) was used. Bound antibodies were visualized by ECL.

2.2.13 *In vivo* studies

2.2.13.1 Platelet life span

Circulating platelets were labeled *in vivo* by intravenous injection in the retro-orbital plexus of 5 μg Dylight-488-anti-GPIX Ig derivative in 200 μL PBS. 30 min after antibody injection (and every 24 h for 5 days) 50 μL blood was taken from the retro-orbital plexus of treated mice and as the percentage of the positive population was determined by flow cytometry.

2.2.13.2 Intravital microscopy of FeCl_3 -injured mesenteric arterioles

Mice (4-5 weeks of age, weight 15-18 g) were anesthetized with 2.5% avertin and the mesentery was exteriorized through a midline abdominal incision. Arterioles (35-60 μm in diameter) were visualized with a Zeiss Axiovert 200 inverted microscope (10x objective) equipped with a 100-W HBO fluorescent lamp source, and a CoolSNAP-EZ camera (Visitron, Munich, Germany). Digital images were recorded and analyzed off-line using MetaVue®

software. Injury was induced by topical application of a 3 mm² filter paper saturated with FeCl₃ (20%). Adhesion and aggregation of fluorescently labeled platelets (Dylight-488 conjugated anti-GPIX Ig derivative) in arterioles was monitored for 40 min or until complete occlusion occurred (blood flow stopped for >1 min). This experiment was performed by Martina Morowski in the group of Prof. Dr. Bernhard Nieswandt.

2.2.13.3 Mechanical injury of the abdominal aorta

The abdominal cavity of anesthetized mice (~6 weeks of age) was opened by a longitudinal incision and the abdominal aorta was exposed. A Doppler ultrasonic flow probe (Transonic Systems, New York, USA) was placed around the aorta and thrombosis was induced by mechanical injury with a single firm compression with forceps upstream of the flow probe. Blood flow was monitored until complete occlusion occurred or up to 30 min. This experiment was performed by Martina Morowski in the group of Prof. Dr. Bernhard Nieswandt.

2.2.13.4 Bleeding time assay

Mice were anesthetized with a triple anesthesia (medetomidine 0.5 µg/g, midazolam 5 µg/g, and fentanyl 0.05 µg/g body weight) and a 1 mm segment of the tail tip was removed with a scalpel. Tail bleeding was monitored by gently absorbing the drop of blood with a filter paper in 20 sec intervals without directly contacting the wound site. When no blood was observed on the paper, bleeding was determined to have ceased. The experiment was manually stopped after 20 min by cauterization. Alternatively, tail bleeding times were determined in 37°C warm saline (0.9% NaCl). Upon ablation, the tail tip was placed in a plastic tube containing 4 mL saline, bleeding was observed and determined to have ceased when stopped for >1 min.

2.2.13.5 Transient middle cerebral artery occlusion (tMCAO) model

Experiments were conducted in 6-8 week old male mice according to published recommendations for research in mechanism-driven basic stroke studies.¹⁶⁸ Transient middle cerebral artery occlusion (tMCAO) was induced under inhalation anesthesia using the intraluminal filament (6021PK10; Doccol, Redlands, CA) technique.⁴⁵ After 60 min, the filament was withdrawn to allow reperfusion. For measurements of ischemic brain (infarct) volume, animals were sacrificed 24 h after induction of tMCAO and brain sections were stained with 2% 2,3,5-triphenyltetrazolium chloride (TTC; Sigma-Aldrich, Germany). Brain infarct volumes were calculated and corrected for edema. Neurological function and motor function were assessed 24 h after tMCAO using Bederson score¹⁶⁹ and the grip test.¹⁷⁰ This

work was performed by Dr. Peter Kraft in the group of Prof. Dr. Guido Stoll, Department of Neurology, University Hospital, Würzburg.

2.2.14 Isolation and culture of neurons, Ca²⁺ imaging

For Ca²⁺ measurements, primary neuronal cultures were obtained from newborns at postnatal day 0. Tissue was collected from whole cortices and cells were cultured in Neurobasal-A medium (Gibco, Invitrogen, Germany) containing 2% B27 supplement, 1% GlutaMAX-I and 1% penicillin/streptomycin (Gibco, Germany). Cells were plated in a density of 50.000 cells/cm² on poly-L-lysine coated coverslips in 24-well plates (Sarstedt, USA) and cultured for up to 24 days.

Measurements of [Ca²⁺]_i in single cortical neurons were carried out using the fluorescent indicator fura-2 AM in combination with a monochromator-based imaging system (T.I.L.L. Photonics, Germany) attached to an inverted microscope (BX51WI, Olympus, Germany). Emitted fluorescence was collected by a CCD camera. Cells were loaded with 5 μM fura-2-AM (Molecular Probes, The Netherlands) supplemented with 0.01% Pluronic F127 for 35 min at 20-22°C in a standard bath solution containing: 140 mM NaCl, 5 mM KCl, 1 mM MgCl₂, 2 mM CaCl₂, 10 mM glucose and 10 HEPES, adjusted to pH 7.4 with NaOH. For measurements of [Ca²⁺]_i, cells were held in standard bath solution and fluorescence was excited at 340 and 380 nm. Fluorescence intensities of single cells were acquired in intervals of 2s or 20s. After correction for the individual background fluorescence, the fluorescence ratio $R = F_{340}/F_{380}$ was calculated. Quantities for [Ca²⁺]_i were then calculated by the equation: $[Ca^{2+}]_i = K_D \beta (R - R_{min}) / (R_{max} - R)$, with $K_D = 224$ nM, $\beta = 2.64$, $R_{min} = 0.272$ and $R_{max} = 1.987$ obtained from single dye-loaded cells in the presence of 5 μM ionomycin added to standard bath solution or to a solution containing 10 mM EGTA instead of 2 mM CaCl₂. For oxygen-glucose deprivation (OGD) experiments, cells were immediately transferred to a sealed, N₂-purged (~2 l/min) chamber continuously superfused with a N₂-bubbled solution containing (mM): 140 NaCl, 5 KCl, 1 MgCl₂, 2 CaCl₂ and 10 HEPES, adjusted to pH 7.4. All experiments were carried out at 20-22°C. All chemicals were obtained from Sigma (Germany). These experiments were performed by Dr. Robert Kraft, University of Leipzig.

2.3 Data analysis

If not stated otherwise, the results shown in this thesis are mean ± SD from at least three independent experiments. When parametric conditions were fulfilled, differences between two groups were statistically analyzed using a modified t-test (Welch's test, also applicable for unequal variances). For Bederson score and grip tests analysis, Mann-Whitney-U-test was applied. For analysis of more than two groups, one-way Anova and Bonferroni multiple

comparison post-hoc test was applied. When parametric conditions were not fulfilled, Kruskal Wallis test and the appropriate post-hoc test were applied. Microsoft Excel or IBM SPSS were used for analysis. *P*-values <0.05 were considered as statistically significant (*), $p < 0.01$ (**), and $p < 0.001$ (***)

3 Results

3.1 Generation CD84 deficient mice

To explore the relevance of CD84 in platelet biology and beyond, CD84 deficient mice (*Cd84*^{-/-}) were generated. The cloning of the targeting vector for disruption of the mouse *Cd84* gene has been already described in the thesis “Construction of a targeting vector for the generation of CD84 deficient mice” by Rastislav Pozgaj in our research group. All further steps in the process of *Cd84*^{-/-} mouse generation, starting with the electroporation of embryonic stem cells are described in the following chapters.

3.1.1 Targeting strategy and electroporation of murine ES cells

This chapter illustrates the targeting strategy to disrupt the *Cd84* gene in murine embryonic stem (ES) cells. Since CD84 expression is known to be restricted mainly to the hematopoietic system, the intention was to generate constitutive knockout mice. Parts of exon 1, intron 1, and a critical part exon 2 were replaced by a cassette containing a neomycin resistance gene, allowing for selection of recombinant clones (Figure 8A). In the targeting vector, partially deleted exon 1, the selection cassette, as well as partially deleted exon 2 were fused together (Figure 8B). Homologous arms facilitate site specific recombination. By means of this strategy, the 5' UTR of the mRNAs and the coding sequence of the signal peptide are deleted. Deletion of the 5' UTR of the mRNA causes inhibition of ribosome binding and therefore protein synthesis is abolished. If still alternatively spliced CD84 isoforms were translated from mRNAs, these isoforms without signal peptide could not be transported to the plasma membrane in the cells, inducing a loss of function mutation. Test digestions of the targeting construct with different restriction endonucleases revealed the expected restriction lengths (Figure 8C). The targeting vector was linearized with *NotI*, purified and electroporation of ES cells was performed as described in the methods section.

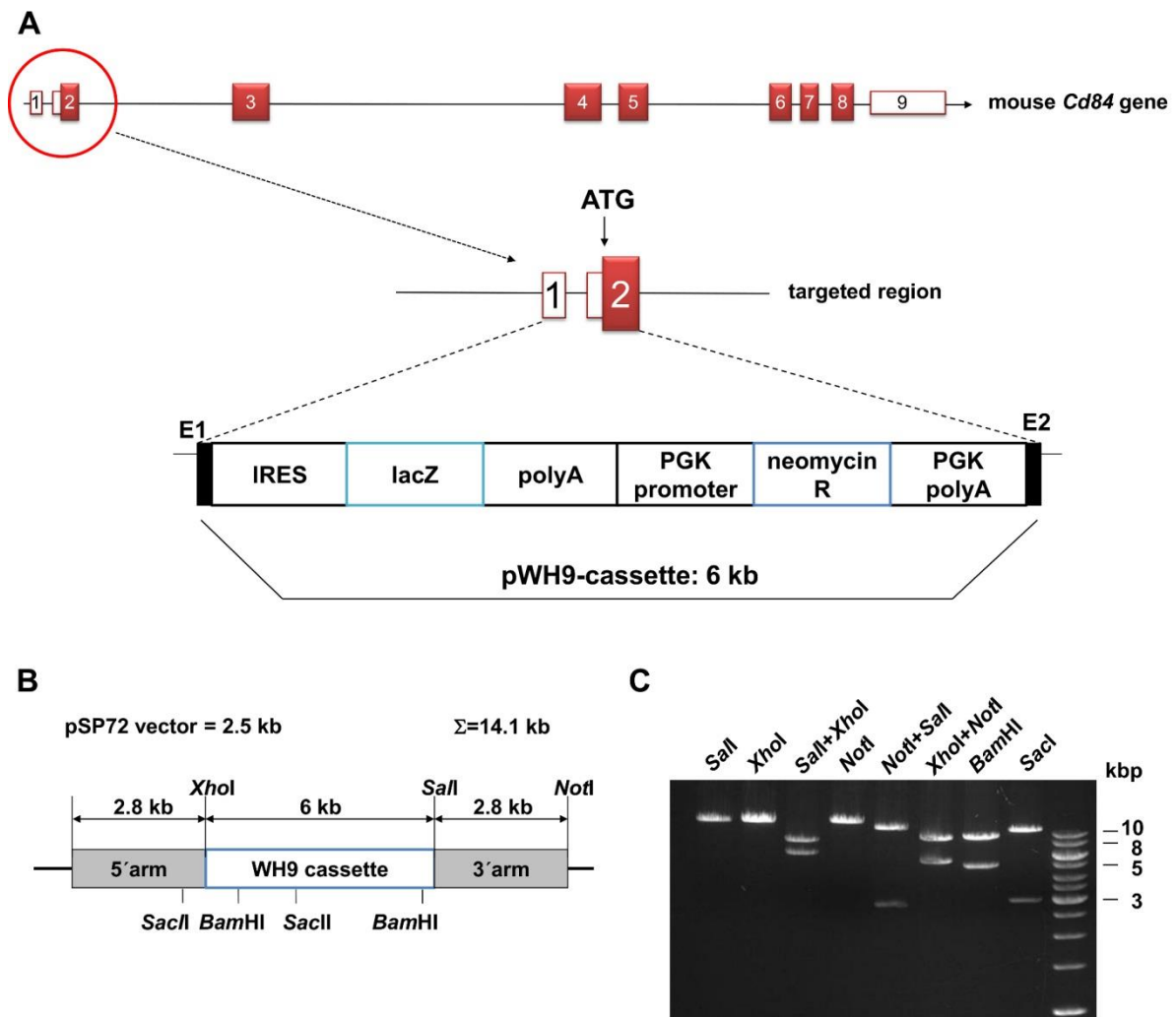


Figure 8. Targeting strategy and test digestion of the final vector. (A) The mouse *Cd84* gene comprises 9 exons. The scheme displays the strategy for the generation of a CD84 knockout allele. A neomycin resistance cassette (WH9 cass) replaces intron 1 of CD84 and fuses together remaining parts of exon 1 and exon 2. The signal peptide (exon 2) was deleted. IRES: Internal ribosomal entry site; R: resistance. (B) Scheme of the final targeting vector containing recognition sites for the indicated restriction endonucleases. (C) Test digestions of the targeting vector showed the expected restriction fragment lengths.

3.1.2 Screening of recombinant stem cell clones and generation of chimeric mice

432 and 443 stem cell clones, which survived the Geneticin selection process, were picked. ES cell DNA was digested with *BamHI* and screened for homologous recombination by Southern blot analysis (see Figure 9A for Southern blot strategy). According to the strategy, the radioactively labeled external probe binds to a sequence in intron 2, located downstream of the 3' arm of the targeting vector. Homologous recombination introduces a new *BamHI* site into the targeted allele, allowing for detection of a 3.5 kb ko allele, whereas the wt allele will appear as a 15 kb fragment. In total, four homologous-recombinant stem cell clones were

detected. These clones ($Cd84^{+/-}$) showed the wt band at 15 kb and the expected knockout band at 3.5 kb (Figure 9B).

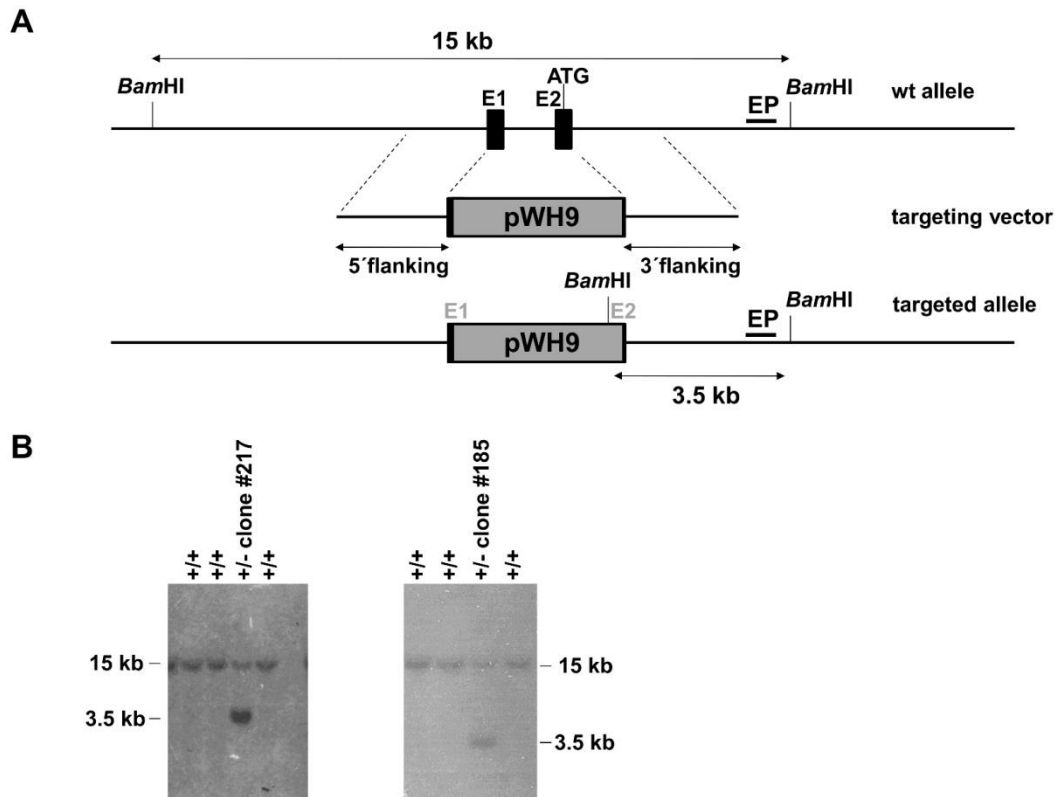


Figure 9 Detection of homologous-recombinant clones. (A) This scheme illustrates the detection of wt and CD84 knockout (targeted) alleles. The external probe (EP) recognizes a sequence downstream of 3' arm in intron 2. The wt band between the two *Bam*HI sites is approximately 15 kb in size. The WH9 cass contains an additional *Bam*HI site. The mutant band is approximately 3.5 kb in size. (B) Representative Southern blot pictures showing each one homologous-recombinant stem cell clone (+/-).

$Cd84^{+/-}$ ES cells were recultured, retested in Southern blot, and injected into C57BL/6 blastocysts in collaboration with Dr. Michael Bösl (Max Planck Institute of Neurobiology, Martinsried), to generate chimeric mice. Three of these ES cell clones gave rise to seven chimeric mice (Table 2).

chimeric mice	derived from ES cell clone #	chimerism (%)	germline transmission
male	185	100	Yes
male	346	95	Yes
male	346	30	Yes
male	346	25	No
female	346	90	No
female	219	80	No
female	346	25	No

Table 2 Chimeric mice obtained after blastocyst injection of *Cd84*^{+/+} ES cells. Germline transmission was obtained where indicated.

3.1.3 Breeding of homozygous *Cd84*^{-/-} mice

The chimerism of mice obtained after blastocyst injection is determined according to their coat color. The injected stem cells were from a 129/Sv ES cell line¹⁶⁰ and the blastocyst was obtained from C57BL/6J mice. Therefore, a high percentage of brown coat color indicates high chimerism, implicating a high chance of germline transmission. Chimeric male mice were backcrossed with female C57BL/6J and chimeric females were backcrossed with male C57BL/6J mice.

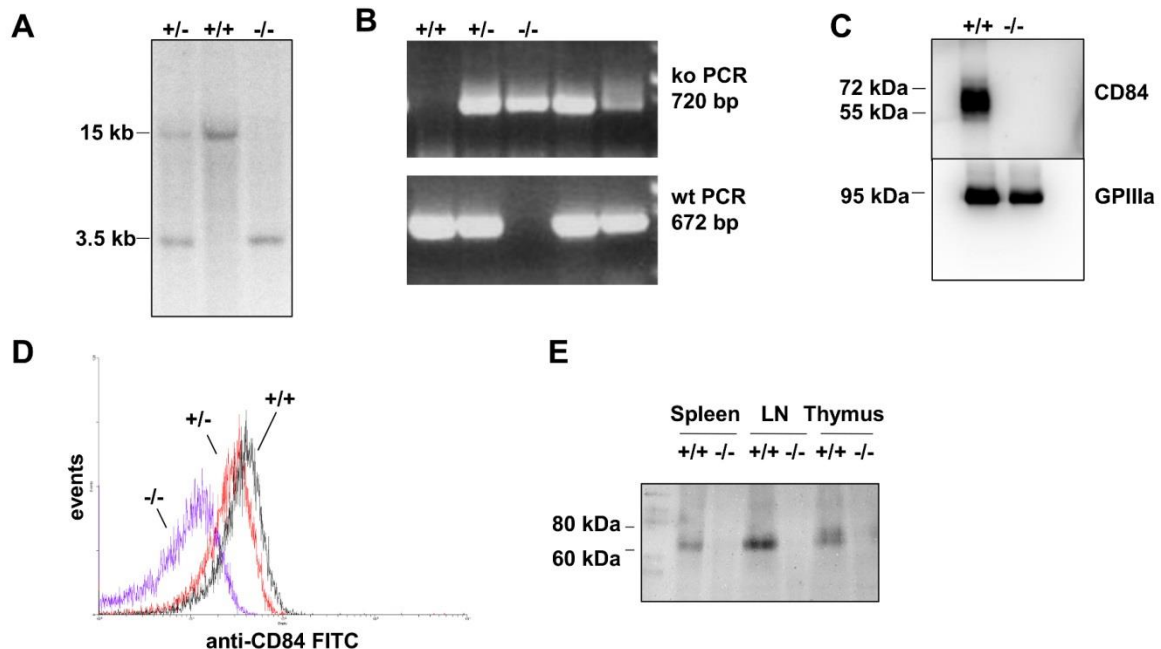


Figure 10. Homozygous *Cd84* ko mice. (A) Southern blot and (B) PCR strategy to detect wt (+/+), heterozygous (+/-) and ko (-/-) mice. (C) Western blot confirming absence of CD84 in platelets of -/- mice. GPIIIa was used as loading control. (D) Flow cytometric measurement of wt, heterozygous, and ko mouse platelets. (E) Western blot detecting absence of CD84 in spleen, lymph nodes and thymus of -/- mice. 40 μ g protein (determined by BCA assay) from organ lysates was loaded per lane.

Germline transmission occurred only in chimeric males. Their heterozygous offspring ($Cd84^{+/-}$) mice were intercrossed to finally obtain $Cd84^{-/-}$ mice (Figure 10A). Mouse genotypes were determined by Southern blot and by PCR (Figure 10B).

3.2 Basal analysis of CD84 deficient mice

To determine whether loss of CD84 caused any obvious deficits in mice, like impairment of reproduction, or alterations at blood cell level, initial data on heterozygous mating statistics and hematologic parameters were assessed.

3.2.1 CD84 deficient mice are born in Mendelian ratio and develop normally

Following heterozygous matings, $Cd84^{-/-}$ (ko) and $Cd84^{+/+}$ (wt) mice were born approximately in Mendelian ratio (Table 3). Therefore, it was concluded that loss of CD84 does not severely affect embryonic development.

Genotype $Cd84$	number of mice	percentage	expected percentage
+/+	34	27.0 %	25 %
+/-	67	53.2 %	50 %
-/-	25	19.8 %	25 %
total	126	100 %	100 %

Table 3 $Cd84^{-/-}$ mice were born in Mendelian ratio after intercrossing of heterozygous animals.

$Cd84^{-/-}$ mice developed normally and were morphologically indistinguishable from wt mice. Intercrossing of ko mice yielded approximately same litter sizes as intercrossing of wt mice. Litters from ko mouse intercrossing also developed normally, indicating that ko females had no deficit in bearing and feeding their offspring. A first analysis of basal hematologic parameters (Table 4) did not show a significant difference between wt and $Cd84^{-/-}$ mice.

Genotype $Cd84$	WBC	RBC	HGB	HCT
+/+	6.30 ± 2.66	8.33 ± 0.85	13.93 ± 1.30	44.03 ± 3.78
-/-	6.58 ± 3.05	7.90 ± 1.56	12.74 ± 2.21	41.37 ± 6.83
p	n.s.	n.s.	n.s.	n.s.

Table 4. Normal hematologic parameters in $Cd84^{-/-}$ mice. White blood cell count (WBC; $\times 10^3/\mu\text{L}$), erythrocytes (RBC; $\times 10^6/\mu\text{L}$), hemoglobin (HGB; g/dl) and hematocrit (HCT; %) as determined by a hematologic analyzer (Sysmex) were unaltered in CD84 deficient mice. n=10. n.s.: not significant.

3.2.2 Proof of CD84 deficiency at cellular level

CD84 expression in humans has been documented on various cell types, including monocytes, macrophages, B cells, T cells, granulocytes and platelets.^{77,78} In addition to the above mentioned proof of CD84 loss by Western blot analysis (Figure 10), different immune cells from spleen, lymph nodes and thymus were analyzed with regard to CD84 expression by flow cytometry. The different cell populations were identified by scatter properties in combination with specific surface markers. In all cell types of wt (*Cd84^{+/+}*) mice, CD84 was clearly detectable by the anti CD84 antibody, JER1-FITC. This is in accordance with published data on human CD84, which is broadly expressed on leukocytes.^{67,78} As expected, the antibody did not bind to the same cell types from *Cd84^{-/-}* mice.

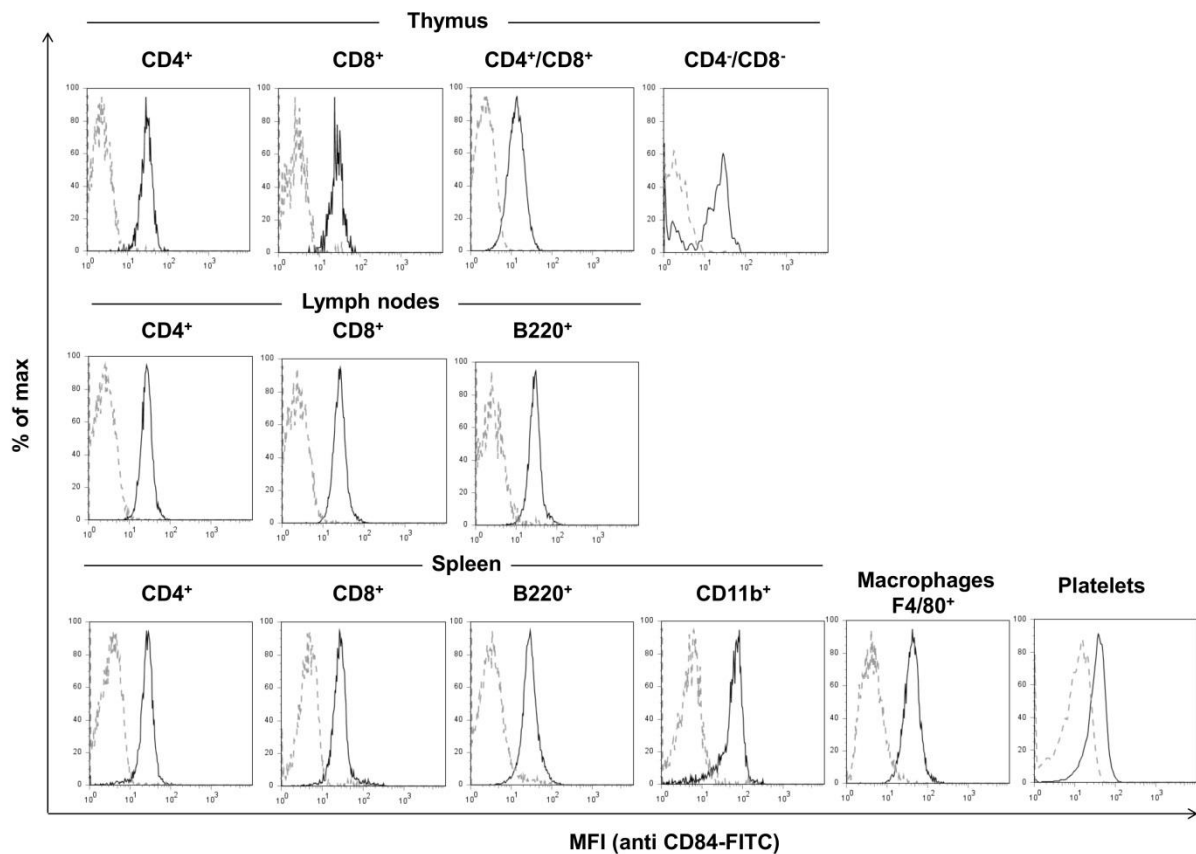


Figure 11. Determination of CD84 expression in leukocytes and platelets by flow cytometry. Histograms represent CD84 levels, as detected by JER1-FITC. In wt mice (solid lines), CD84 was detected in all tested cell types: T cells and thymocytes (CD4⁺, CD8⁺, CD4⁺/CD8⁺, CD4⁻/CD8⁻), B cells (B220⁺), granulocytes and monocytes (CD11b⁺) cells, peritoneal macrophages (F4/80⁺) and platelets. CD84 was absent in ko mice (dashed lines).

The data in Figure 11 clearly demonstrated the lack of CD84 protein in all tested cell types of the *Cd84^{-/-}* mouse line. This confirmed that the strategy for generation of a *Cd84* knockout

was successful. For wt leukocytes, mean fluorescence intensities (MFI) detected with JER1-FITC were between 25 and 43, whereas MFIs for *Cd84*^{-/-} were between 3 and 6 (CD4⁺ lymphocytes: wt: 27.2 ± 2.03; *Cd84*^{-/-}: 3.12 ± 0.31; CD8⁺ lymphocytes: wt: 25.29 ± 1.38; *Cd84*^{-/-}: 3.02 ± 0.47; splenic B-cells: wt: 32.3 ± 0.10; *Cd84*^{-/-}: 4.49 ± 0.26; peritoneal macrophages: wt: 43.41 ± 6.08; *Cd84*^{-/-}: 5.76 ± 0.84). It remains unclear why JER1-FITC signals on *Cd84*^{-/-} platelets were higher than on other cell types (wt: 36.4 ± 0.58; *Cd84*^{-/-}: 12.8 ± 0.31). Elevated background values might be due to a certain degree of unspecific binding, nevertheless residual expression of CD84 on platelets can be excluded because Western blots from platelet lysates clearly demonstrated complete absence of CD84 in ko platelets (Figure 10C).

3.2.3 Unaltered lymphocyte populations in CD84 deficient mice

As shown in 3.2.2, CD84 is broadly expressed in wt mice in cells of primary and secondary lymphoid organs. To clarify whether CD84 deficiency alters lymphocyte subsets, thymocyte subsets in thymus, as well as T and B cell compositions in spleen and lymph nodes were analyzed. Flow cytometric measurements of thymocytes revealed that *Cd84*^{-/-} mice displayed normal subset distributions for CD4⁺ cells (wt: 7.55 ± 1.01 %; *Cd84*^{-/-}: 9.18 ± 3 %; p≥0.05), CD8⁺ cells (wt: 2.25 ± 0.28 %; *Cd84*^{-/-}: 2.54 ± 1.04 %; p≥0.05), CD4⁻CD8⁻ cells (wt: 1.25 ± 0.52 %; *Cd84*^{-/-}: 2.08 ± 0.55 %; p≥0.05), and CD4⁺CD8⁺ cells (wt: 88.57 ± 1.69 %; *Cd84*^{-/-}: 85.3 ± 4.8 %; p≥0.05). These data (Figure 12) indicate unaltered maturation of CD84 deficient T cells in thymus.

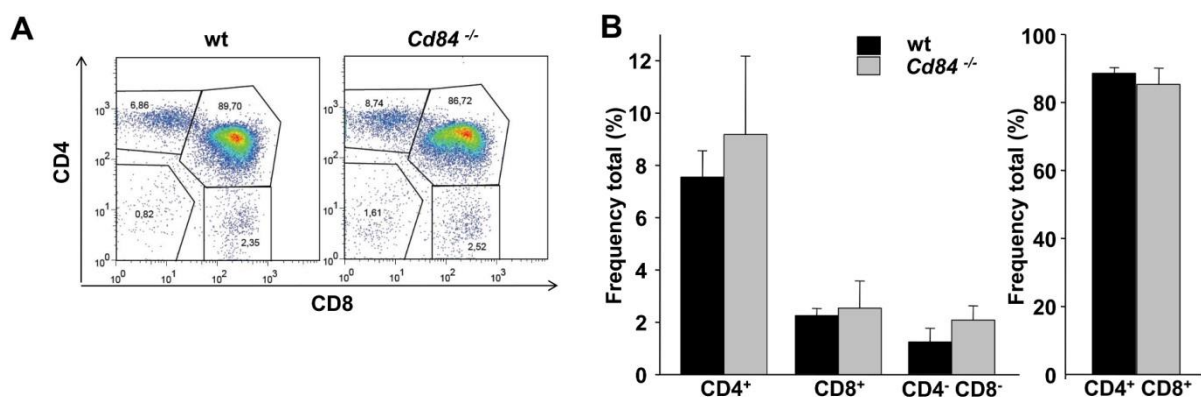


Figure 12. Unaltered distribution of cell populations in thymus. (A) Representative dot plots of CD4 vs CD8 expression in thymocytes of wt (left) or *Cd84*^{-/-} (right) mice as measured by flow cytometry. (B) Frequencies of CD4⁺, CD8⁺, double negative, or double positive thymocytes in wt (black bars) or *Cd84*^{-/-} mice (gray bar). Numbers represent percentages of total thymocyte numbers, 4 mice per group, p≥0.05.

Lymphocyte and splenocyte subset distributions were also studied by flow cytometry, using CD4 and CD8 antibodies for detection of T cells, or B220 antibodies for B cells. No significant differences were found for T and B cells in lymph nodes (CD4⁺ cells: wt: 42.2 ± 3.41 %; *Cd84*^{-/-}: 43.29 ± 1.31 %; p≥0.05. CD8⁺ cells: wt: 24.3 ± 3.9 %; *Cd84*^{-/-}: 29.08 ± 1.95 %; p≥0.05. B220⁺ cells: wt: 23.83 ± 0.12 %; *Cd84*^{-/-}: 19.30 ± 1.82 %; p≥0.05; see Figure 13A). Splenic T and B cell composition was also comparable in wt and CD84 deficient mice (CD4⁺ cells: wt: 19.73 ± 1.45 %; *Cd84*^{-/-}: 17.89 ± 0.96 %; p≥0.05. CD8⁺ cells: wt: 11.9 ± 0.43 %; *Cd84*^{-/-}: 11.47 ± 1.29 %; p≥0.05. B220⁺ cells: wt: 47.2 ± 3.49 %; *Cd84*^{-/-}: 40.99 ± 1.01 %; p≥0.05; see Figure 13B).

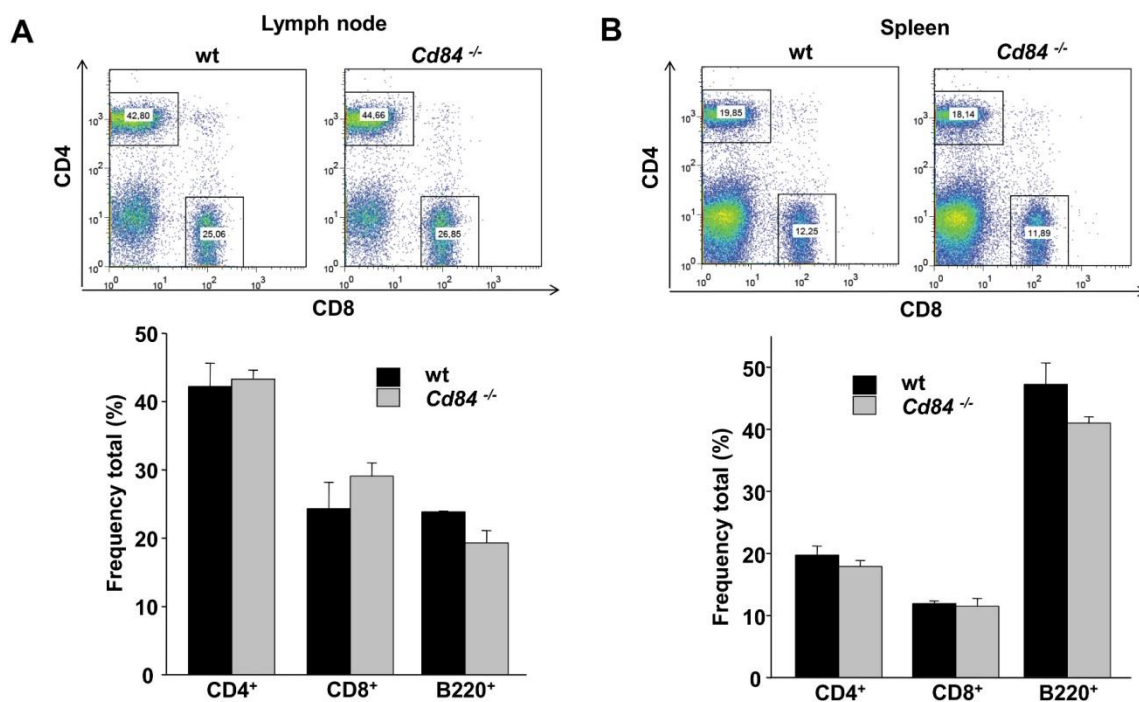


Figure 13. Unaltered distributions of cell populations in lymph nodes and spleen in *Cd84*^{-/-} mice. (A) Representative dot plots of CD4 vs CD8 expression in lymph nodes of the indicated mice as measured by flow cytometry. Bar graphs show frequencies of CD4⁺, CD8⁺, and B cells (B220⁺) in wt or *Cd84*^{-/-} mice. (B) Dot plots and bar graphs showing frequencies of spleen cells, as described in A. Numbers represent percentage of total lymphocyte or splenocyte numbers, 4 mice per group, p≥0.05.

Together, these data suggested normal B and T cell development in *Cd84*^{-/-} mice, which is in line with recently published immunological studies from Cannons *et al.*,⁸⁴ who also reported normal thymic, lymph node and splenic cellularity in their own CD84 deficient mouse line.

3.3 Platelet function and thrombus formation in CD84 deficient mice

3.3.1 Platelet production

Western blot analysis and flow cytometric measurements verified that CD84 is expressed in wt, but not in *Cd84*^{-/-} platelets (Figure 10). To study whether CD84 deficiency had an influence on platelet formation, platelet counts, size and expression of prominent glycoproteins were measured by a hematologic analyzer (Sysmex) and by flow cytometry (Figure 14A-C), respectively.

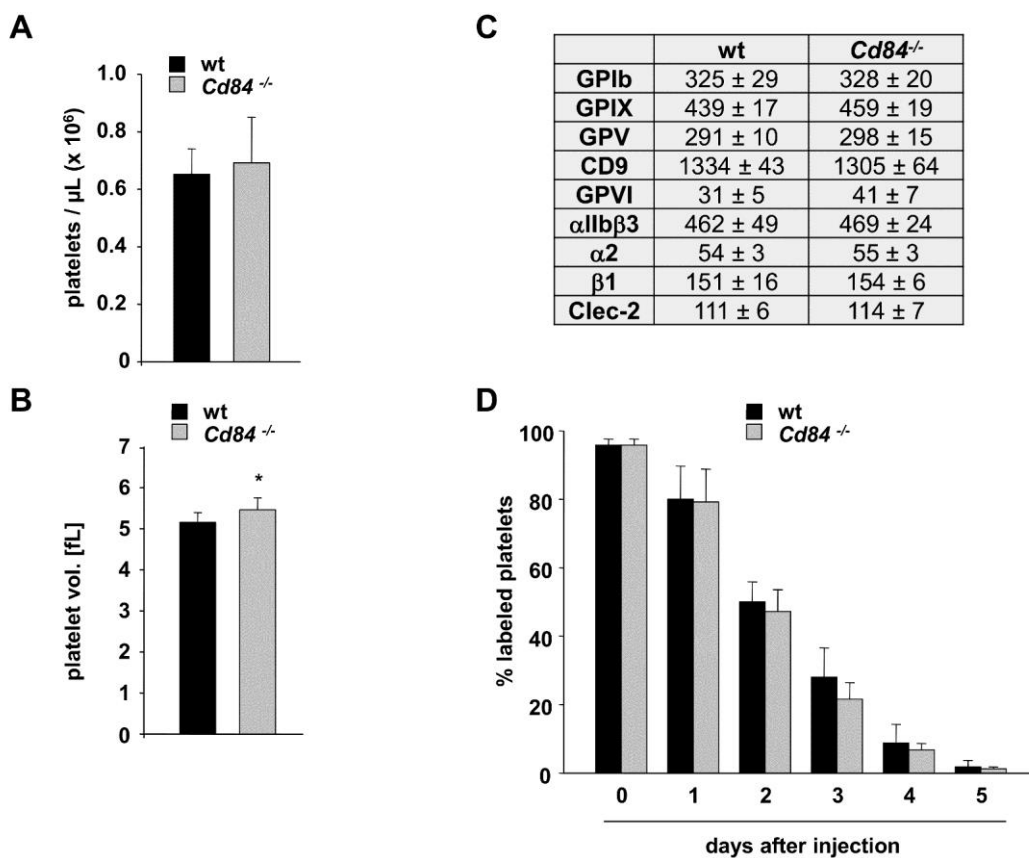


Figure 14. *Cd84*^{-/-} mice display normal platelet production but slightly increased platelet size. (A) Platelet counts (platelets $\times 10^6/\mu\text{L}$) and (B) platelet volumes (femtoliters) were determined by a hematologic analyzer (Sysmex). Values are mean \pm SD, $n \geq 8$ per group, $*p < 0.05$. (C) Expression levels of prominent platelet surface receptors were measured by flow cytometry and expressed as mean fluorescence intensity \pm SD, $n = 5$ per group. (D) wt and *Cd84*^{-/-} mice were injected with a DyLight 488-conjugated anti-GPIX Ig derivative to label platelets *in vivo*. Percentage of fluorescently labeled platelets determined by flow cytometry at the indicated days after injection is illustrated. Values are mean \pm SD of 5 mice per group.

Platelet counts in CD84 deficient mice were unaltered (wt: $653 \pm 87.8 \times 10^3$ plt/ μL blood; *Cd84*^{-/-}: $692 \pm 158 \times 10^3$ plt/ μL blood; $p \geq 0.05$). However, CD84 deficient platelets displayed a slightly increased size (wt: 5.15 ± 0.24 fL; *Cd84*^{-/-}: 5.46 ± 0.29 fL; $p < 0.05$). Expression levels

of prominent platelet receptors were found to be normal. To determine whether the slightly elevated platelet size in CD84 deficient mice was due to altered platelet turnover, platelet life span was determined in *Cd84*^{-/-} and wt mice *in vivo*. For this, circulating platelets were labeled by injecting mice with a fluorescently labeled, non-cytotoxic anti-GPIX antibody derivative and the labeled platelet population was monitored by flow cytometry during the next 5 days. One h after antibody injection, >95% of circulating platelets were labeled in both wt and *Cd84*^{-/-} mice and this platelet population constantly declined over the next 5 days (<2% at day 5) in both groups, without a statistically significant difference (Figure 14D). Taken together, *Cd84*^{-/-} mice display normal platelet production and life span, with a slight increase in platelet size.

3.3.2 Agonist induced activation and degranulation *in vitro*

To study the effect of CD84 deficiency on platelet activation, agonist-induced activation of the major platelet integrin α IIb β 3 and degranulation-dependent P-selectin exposure were measured by flow cytometry. PE-conjugated JON/A antibody specifically detects only the activated form of integrin α IIb β 3.¹⁶⁶ Since P-selectin is stored in α -granules of unactivated platelets and is not present on the platelet surface under resting conditions, detection of P-selectin on the platelet surface after agonist-induced activation is a measure for degranulation. CD84 deficient platelets became fully activated in response to thrombin, ADP/U46619 (stable TxA₂ analogue), collagen related peptide (CRP), convulxin (CVX, a snake venom protein activating GPVI) and rhodocytin (RC, a snake venom protein activating CLEC-2). Therefore, loss of CD84 does not alter integrin activation and degranulation in response to G-protein coupled or ITAM coupled receptor stimulation (Figure 15).

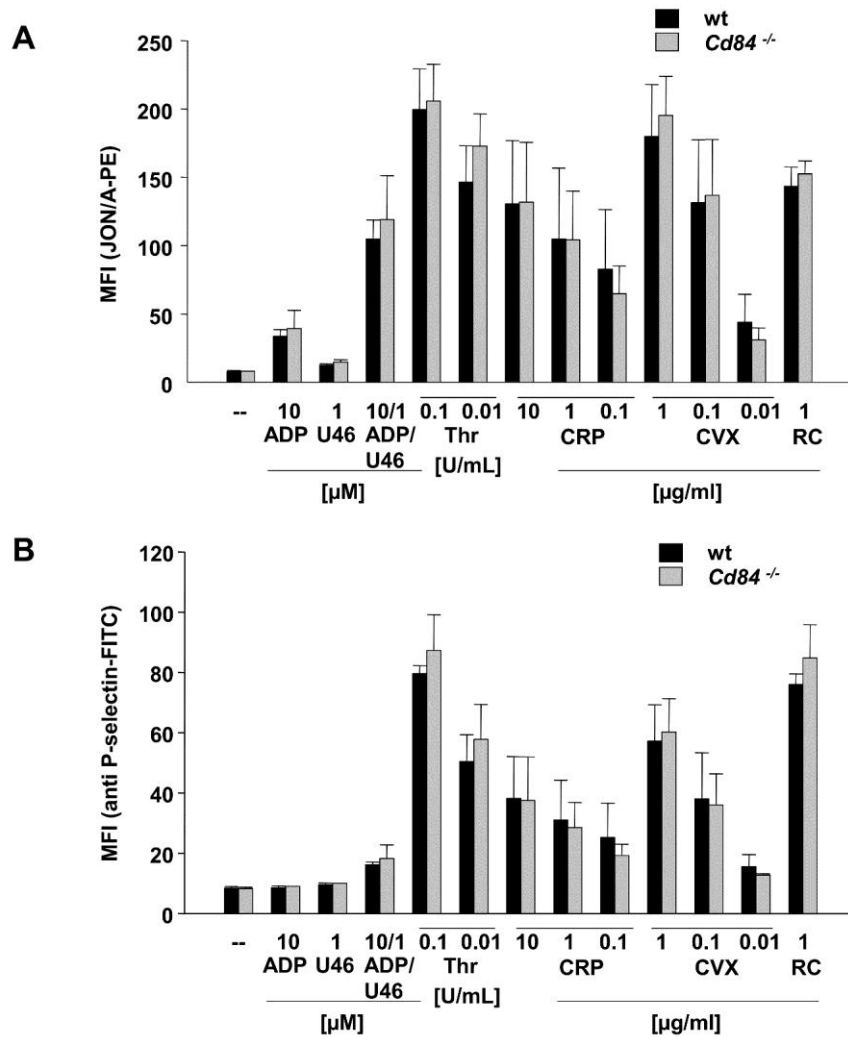


Figure 15. Activation and α -granule release of *Cd84*^{-/-} platelets *in vitro*. Flow cytometric analysis of (A) α IIb β 3 integrin activation (binding of JON/A-PE) and (B) degranulation-dependent P-selectin exposure in response to the indicated agonists. Values are mean fluorescence intensity (MFI) \pm SD; 5 mice per group. U46=U46619, Thr=thrombin.

3.3.3 Aggregation, spreading on fibrinogen and clot retraction

CD84 has been shown to become tyrosine phosphorylated in activated platelets, but only when aggregation was allowed to occur.⁵¹ Therefore, CD84 might act as an aggregation-induced co-receptor supporting stable aggregate formation.²⁶ To test the impact of CD84 loss on platelet aggregate formation *in vitro*, washed platelets from *Cd84*^{-/-} mice and wt mice were stimulated with various agonists in the presence of 2 mM extracellular Ca²⁺. Aggregometry light transmission traces reached similar maximal aggregation rates for *Cd84*^{-/-} as for wt platelets. Also at intermediate and low concentrations of all tested agonists (CVX, collagen, CRP, thrombin, U46619, ADP) no obvious alteration of aggregation was detectable (Figure 16A). Thus, *in vitro* aggregation results indicate that loss of CD84 does not affect aggregate

formation or stability, at least during the typical observation period of 10 min. However, an effect on long term thrombus stability cannot be excluded based on these data.

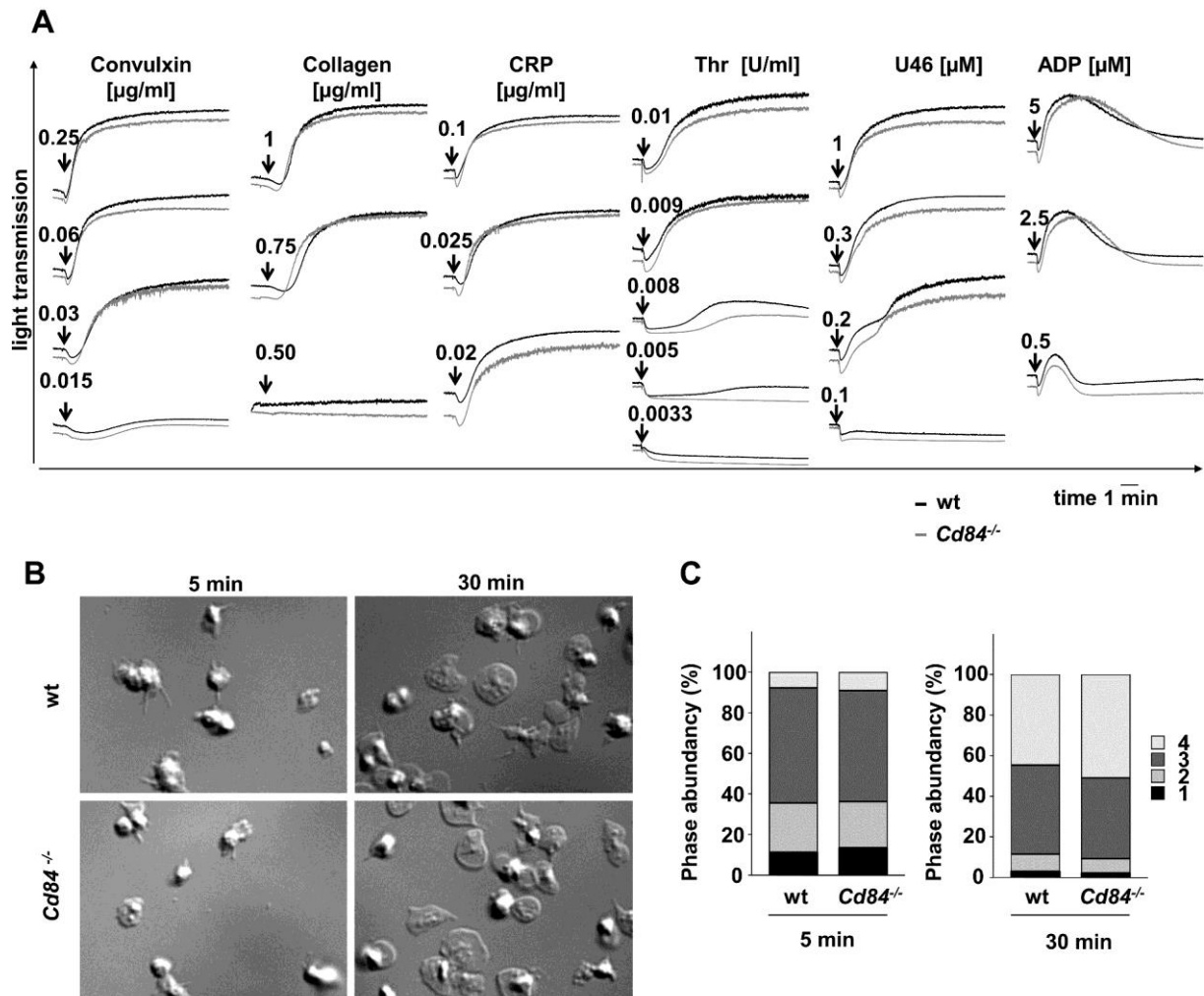


Figure 16. Unaltered aggregation and spreading of $Cd84^{-/-}$ platelets *in vitro*. (A) Washed platelets were stimulated with the indicated agonists and light transmission was recorded in an aggregometer. ADP measurements were performed in prp. Representative aggregation curves for wt (black line) and $Cd84^{-/-}$ platelets (grey line) of 3 independent measurements. Thr=thrombin, U46=U46619. (B) Platelets were allowed to spread on fibrinogen (100 $\mu\text{g/ml}$) after stimulation with 0.01 U/mL thrombin. Representative differential interference contrast (DIC) images of 3 individual experiments from the indicated time points. (C) Statistic evaluation of the percentage of spread platelets at different spreading stages at the indicated time point. 1: roundish, 2: only filopodia, 3: filopodia and lamellipodia, 4: fully spread.

Aggregation of platelets requires inside-out as well as outside-in activation of integrins. Another process requiring integrin mediated adhesion, outside-in signaling, and subsequent rearrangements of the cytoskeleton is spreading of platelets on extracellular matrix proteins, like fibrinogen.¹⁷¹ To study the role of CD84 in this process, washed platelets were allowed to spread on a fibrinogen-coated surface *in vitro*, after prestimulation with 0.01 U/mL thrombin.

Cd84^{-/-} platelets formed filopodia and lamellipodia to the same extent and with kinetics similar to wt platelets, resulting in ~50% fully spread platelets after 30 min in both groups, whereas less than 10% of all platelets were in stages with only adhesion or filopodia formation (Figure 16B, C). Hence, absence of CD84 does not influence the ability of platelets to perform integrin α IIb β 3-mediated adhesion and the reorganization of the actin cytoskeleton to facilitate shape change and spreading.

Upon ligand binding, integrin α IIb β 3 also mediates clot retraction, a process relying on outside-in signaling. Through the process of clot retraction, platelets generate force to contract the fibrin mesh, decrease the clot size, and pull together the edges of damaged tissue to form a mechanically stable clot.¹⁷² To study whether loss of CD84 alters clot retraction, clot formation was induced in prp of *Cd84*^{-/-} and wt mice by addition of a high dose of thrombin (5 U/mL) in presence of 20 mM Ca²⁺ and clot retraction was monitored over time. Clot retraction started as early as 30 min after activation with thrombin and progressed to its maximum at 4 h (Figure 17). The excess fluid extruded during clot retraction was 86.4 \pm 1.53 % for wt and 85.8 \pm 1.80 % for *Cd84*^{-/-} (in % of initial prp volume). These data show that CD84 has no essential role in integrin-dependent clot retraction.

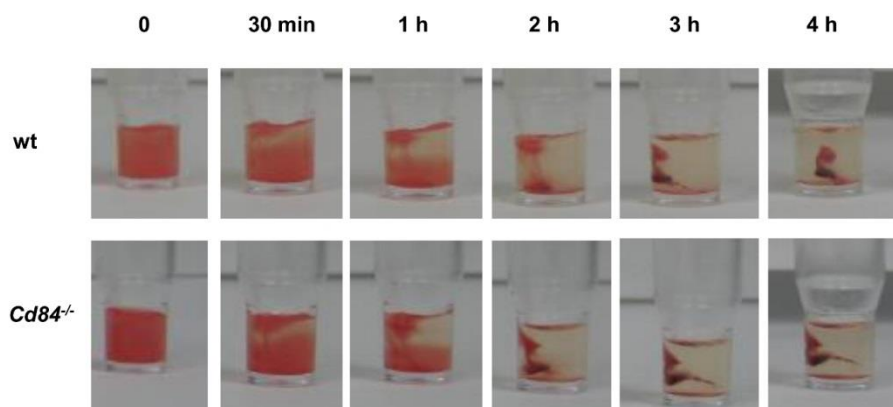


Figure 17. *Cd84*^{-/-} platelets facilitate integrin-dependent clot retraction. Wt and CD84 deficient prp was activated with 5 U/mL thrombin in the presence of 20 mM CaCl₂. Pictures were taken at the indicated time points.

3.3.4 Procoagulant responses and thrombus formation under flow

Elevation in cytosolic [Ca²⁺]_i upon strong platelet activation leads to exposure of phosphatidylserine (PS) at the outer surface of the membrane.¹³² This process contributes to coagulant activity of platelets, supporting blood coagulation at sites of platelet activation. To test whether CD84 is involved in PS exposure, wt and *Cd84*^{-/-} platelets were activated with different agonists and the percentage of Annexin-V-DyLight488 positive platelets was

determined by flow cytometry. Whereas CRP or CVX alone only evoked a submaximal percentage of Annexin-V-DyLight488 positive platelets in both groups, a combined activation with thrombin and CRP led to 77.6 ± 3.21 % positive wt and 77.0 ± 3.74 % positive *Cd84*^{-/-} platelets (Figure 18). Therefore, loss of CD84 does not influence procoagulant activity of platelets.

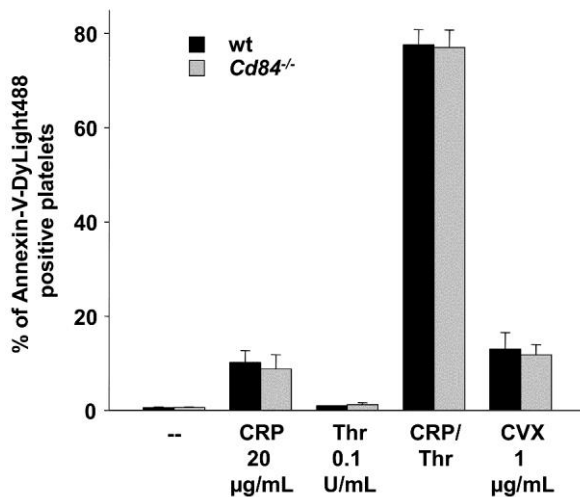


Figure 18. Unaltered procoagulant activity of *Cd84*^{-/-} platelets. Procoagulant activity was determined by Annexin-V-DyLight 488 binding to activated platelets after stimulation with the indicated concentrations of CRP, thrombin (Thr), a combination of CRP (20µg/mL) and thrombin (0.1 U/mL), or CVX. The percentage of Annexin-V-DyLight 488 positive platelets was determined by flow cytometry (n=5 mice per group).

In flowing blood, adhesion of platelets to the exposed subendothelial matrix and subsequent thrombus growth are influenced by shear forces. Under such conditions, lack of receptors that potentially modify platelet aggregate stability could become functionally evident. To test the consequence of CD84 deficiency on aggregate formation under flow, anti-coagulated whole blood was perfused over collagen-coated surfaces in an *ex vivo* flow chamber system, at intermediate (1000 s^{-1}) and high (1700 s^{-1}) shear rates (Figure 19A and B). As in wt controls, platelets from CD84 deficient mice rapidly adhered to collagen and formed three-dimensional thrombi under both intermediate and high shear rates. Evaluation of surface coverage in phase contrast images and relative thrombus volumes, determined by fluorescence intensity measurements, did not reveal statistically significant differences between *Cd84*^{-/-} and wt (Figure 19). These findings indicate that CD84 is not essential for growth and stabilization of platelet rich thrombi under intermediate and high shear *ex vivo*.

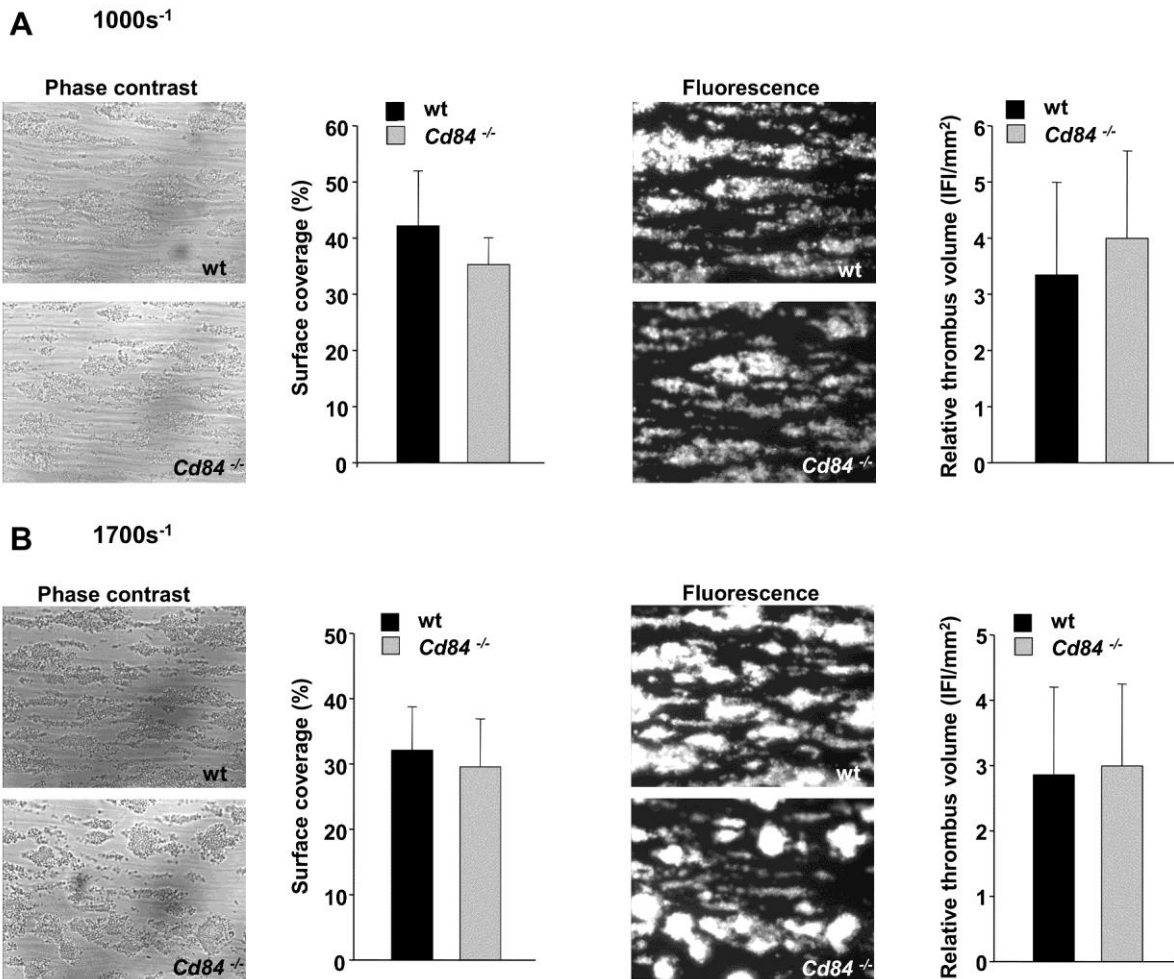


Figure 19. Normal thrombus formation under flow *ex vivo* in *Cd84*^{-/-} blood. Anticoagulated whole blood was perfused over a collagen-coated surface at the indicated shear rates. (A) Representative phase contrast images at the end of the perfusion time of 4 min (1000 s⁻¹) and mean surface coverage ± SD of at least 5 mice are shown (left). Representative fluorescence images obtained by platelet labeling with an anti-GPIX DyLight488 derivative and mean integrated fluorescence intensities (IFI ± SD of at least 5 mice) are shown on the right. (B) Surface coverage and fluorescence intensities for a shear rate of 1700s⁻¹ as described in A.

3.3.5 Thrombus formation *in vivo*

To study thrombus formation *in vivo*, the mice were subjected to two different arterial thrombosis models. These experiments were performed in collaboration with Martina Morowski in our laboratory. Female and male *Cd84*^{-/-} mice were tested separately, to explore whether sex-specific factors may lead to divergent results, as described for SLAM deficient mice by Nanda *et al.*⁵¹ In the first thrombosis model, application of 20% ferric-chloride (FeCl₃) was used to elicit chemical injury in mesenteric arterioles. Thrombus formation was monitored by intravital fluorescence microscopy. The time to beginning of thrombus formation, characterized by adhesion and accumulation of fluorescently labeled platelets, was found to be similar between wt and *Cd84*^{-/-} mice in either sex (Figure 20A, B). The mean

time to complete vessel occlusion was also similar in both groups (males: wt 15.74 ± 3.32 min vs. *Cd84*^{-/-} 15.19 ± 3.69 min; females: wt 17.04 ± 3.15 min vs. *Cd84*^{-/-} 18.47 ± 4.78 min).

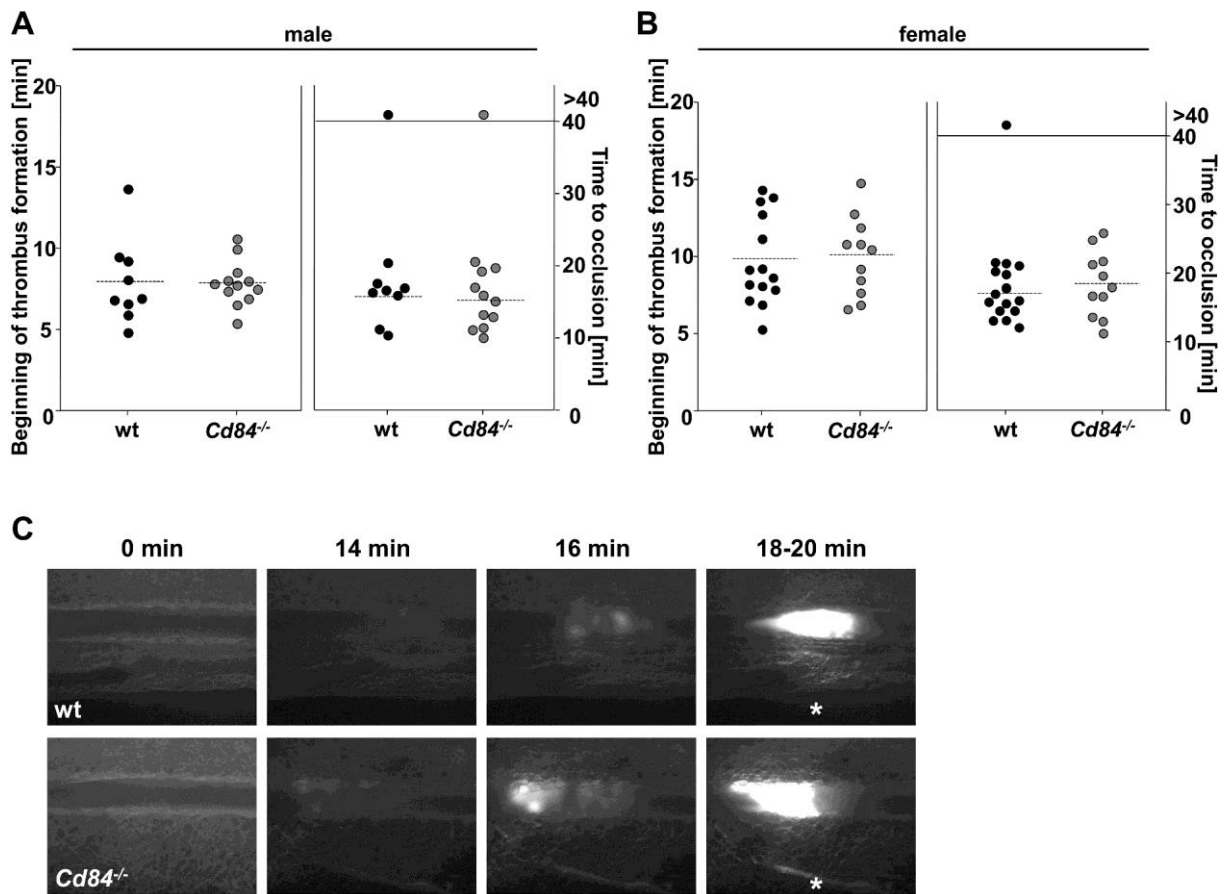


Figure 20. Unaltered arterial thrombus formation in mesenteric arterioles. Mesenteric arterioles were injured by application of FeCl_3 and thrombus formation was monitored by intravital fluorescence microscopy. Time to beginning of thrombus formation (left) and to complete vessel occlusion (right) are shown for male (A) and female (B) mice. Horizontal lines represent mean values. Each symbol represents one arteriole. (C) Representative pictures acquired at the indicated time points. Asterisks indicate complete vessel occlusion.

In a second arterial thrombosis model, mechanical injury was induced in abdominal aortae by firm compression of the vessel. Blood flow was monitored with an ultrasonic flow probe for up to 30 min. In the male animal group, 8 out of 8 wt and 7 out of 8 *Cd84*^{-/-} mice formed irreversible occlusive thrombi within the observation period (mean occlusion time wt: 325 ± 99 vs *Cd84*^{-/-}: 271 ± 72 s; $p=0.25$). In the female animal group, 9 out of 10 wt and 9 out of 10 *Cd84*^{-/-} mice formed irreversible occlusive thrombi (mean occlusion time wt: 392 ± 217 vs *Cd84*^{-/-}: 345 ± 148 s; $p=0.60$; Figure 21).

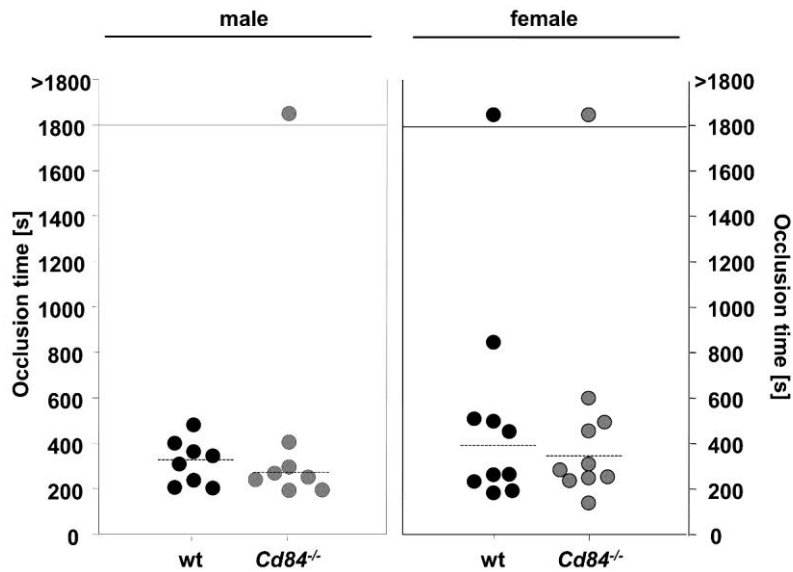


Figure 21. Unaltered occlusion times after mechanical injury of the abdominal aorta. The abdominal aorta was injured by a single firm compression using forceps. Thrombus formation was monitored by blood flow measurements. Occlusion time denotes the time until irreversible occlusion of the vessel. Each symbol represents one individual.

These data, generated in one model of microvascular and one model of macrovascular arterial thrombosis, suggest that absence of CD84 has no major effect on experimentally induced arterial thrombus formation in mice.

3.3.6 Normal hemostasis in *Cd84*^{-/-} mice

Bleeding times were determined by cutting a two millimeter segment from the tail tip and gently absorbing the blood with a filter paper, without making contact with the wound site. Time until arrest of bleeding was not significantly altered in CD84 deficient mice (wt 418 ± 206 s; *Cd84*^{-/-}: 347 ± 201 s; $p=0.29$; Figure 22). When data for female and male mice were analyzed separately, it became evident that females occluded faster than males in general. However there was neither a significant difference between wt and *Cd84*^{-/-} males (wt 532 ± 214 s; *Cd84*^{-/-} 451 ± 173 s; $p=0.39$) nor between wt and *Cd84*^{-/-} females (wt 316 ± 141 s; *Cd84*^{-/-} 254 ± 184 s; $p=0.41$). Another bleeding time model, where the tail tip was immersed in 37°C warm saline did also not reveal alterations in bleeding time (data not shown). These data suggest that CD84 is not an essential player in primary hemostasis in mice.

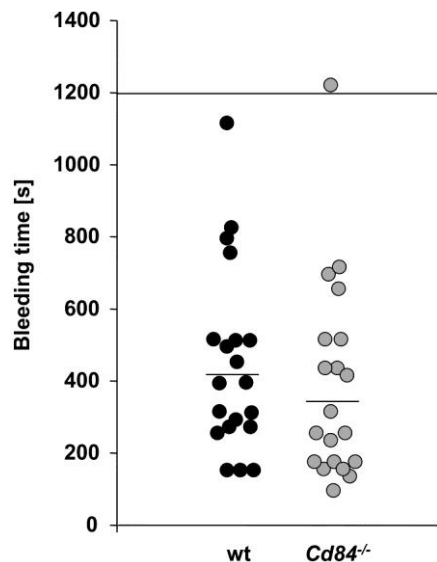


Figure 22. Unaltered tail bleeding times in *Cd84*^{-/-} mice. A 2 mm segment from mouse tail tips was cut with a scalpel and blood was gently absorbed with a filter paper in 20 s intervals. Time until bleeding has ceased is expressed as bleeding time. Each symbol represents one individual (n=20 mice per group).

3.4 Regulation of CD84 receptor levels in platelets

Even though the definite function of CD84 in platelet biology remained elusive, a recent study on human platelets suggested that platelet CD84 may be downregulated in a metalloproteinase-dependent manner,⁹⁶ but the underlying mechanism remained unclear. Therefore, detailed studies on the regulation of CD84 receptor levels were performed in human and mouse platelets in collaboration with Timo Vögtle from our research group, in order to shed light on the mechanism of CD84 receptor regulation.

3.4.1 Ectodomain shedding of CD84 by metalloproteinases in human and murine platelets

Fong *et al.* identified soluble CD84 (sCD84) in the supernatant of activated human platelets in a mass spectrometric approach,⁹⁶ suggesting that the receptor can be downregulated from the platelet surface by proteolytic cleavage. To study this process in more detail, washed human platelets were stimulated with thrombin or the GPVI agonist collagen related peptide (CRP) and surface expression of CD84 was measured by flow cytometry (Figure 23A). Indeed, substantial downregulation of CD84 surface levels in response to CRP and moderate, non-significant, downregulation in response to thrombin were detected and these effects were inhibited in the presence of the broad range metalloproteinase inhibitor GM6001. These data confirmed that CD84 surface expression in human platelets is downregulated in response to agonist stimulation in a metalloproteinase-dependent manner.

Total surface levels of CD84, as measured by flow cytometry, may also be influenced by receptor internalization or exposure of additional CD84 proteins originating from intracellular pools. To circumvent this limitation, an ELISA system was established, using two monoclonal antibodies directed against distinct epitopes on the extracellular domain of the receptor to directly measure soluble human CD84 in the platelet supernatant. As shown in Figure 23B the release of soluble human CD84 from thrombin- and CRP-stimulated human platelets was confirmed by this approach.

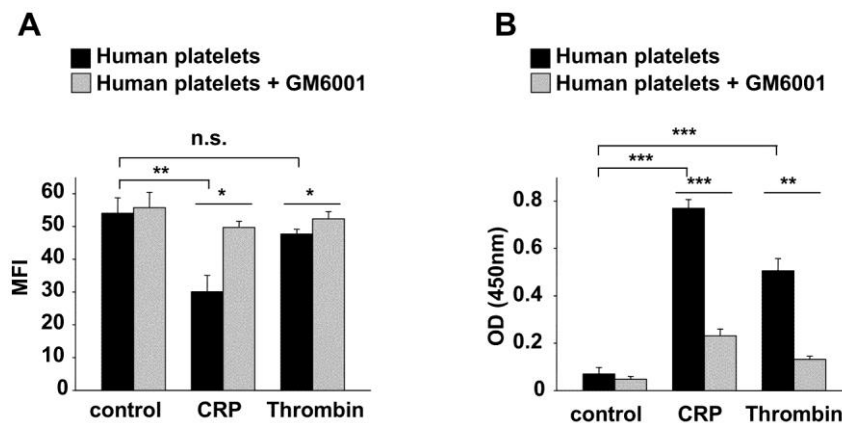


Figure 23. Agonist-induced shedding of CD84 from human platelets is metalloproteinase-dependent. Washed human platelets were incubated with CRP (40 $\mu\text{g}/\text{mL}$) or thrombin (0.5 U/mL) for 1 h at 37°C in the presence or absence of the broad range metalloproteinase inhibitor GM6001 (100 μM). (A) Platelets were stained with FITC-labeled anti-CD84 antibody for 15 min and analyzed directly by flow cytometry. (B) Supernatants were applied on a MAX.3-coated ELISA plate. sCD84 was detected using 2G7-biotin as secondary antibody, followed by HRP-conjugated streptavidin. Results of all experiments are mean \pm SD (n = 3 individuals), * $p < 0.05$, ** $p < 0.01$, *** $p < 0.001$. (Hofmann, Vögtle *et al.*, *JTH* 2012)¹⁶⁴

Next, CD84 regulation was studied in murine platelets. Again, an ELISA system was developed to study CD84 ectodomain shedding. Washed mouse platelets were stimulated with thrombin, CRP, convulxin (CVX) or the CLEC-2 activating snake venom protein rhodocytin (RC), and release of sCD84 was determined with the new ELISA system, designed to detect the cleaved extracellular domain of mouse CD84 (sCD84). High levels of sCD84 were measured in the supernatant of wt platelets in response to stimulation with each of these agonists, compared to the untreated control (Figure 24A). In contrast, virtually no sCD84 was detected when the experiments were performed in the presence of GM6001, strongly suggesting that CD84 cleavage was mediated by metalloproteinases. The ELISA yielded only background signals when the same experiments were performed with platelets from *Cd84*^{-/-} mice, confirming the specificity of the system. When platelet aggregation was blocked by inhibition of integrin $\alpha\text{IIb}\beta 3$ with F(ab)₂ fragments of the JON/A antibody,¹⁶⁶ less sCD84 was detected after CRP and thrombin stimulation. This indicated that cleavage of

CD84 was, at least in part, dependent on platelet aggregation (Figure 24B). Addition of JON/A F(ab)₂ after the agonist incubation period did not reduce the sCD84 signal in ELISA, excluding that the F(ab)₂ interfered with the signal (data not shown).

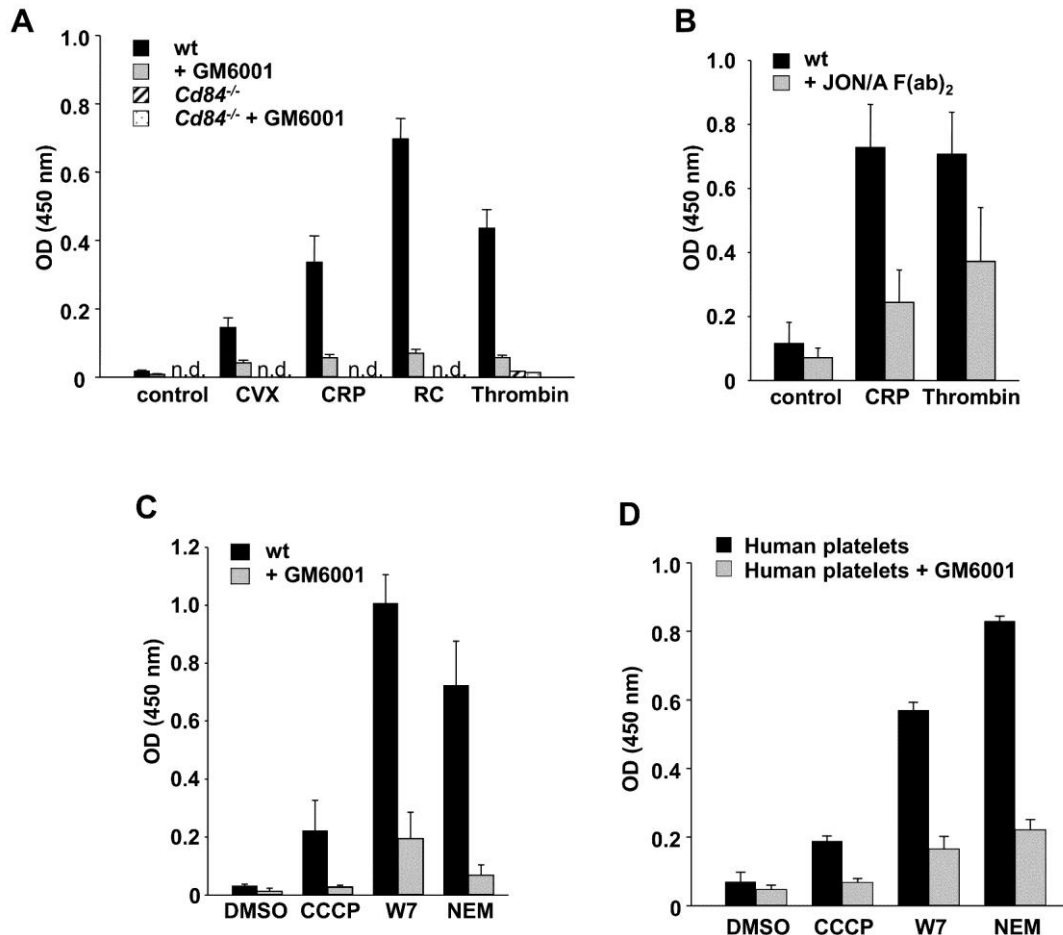


Figure 24. Metalloproteinase-dependent shedding of CD84 from mouse and human platelets. (A) Washed mouse platelets were incubated with the indicated agonists in the presence or absence of GM6001. sCD84 was detected by ELISA as described in materials and methods. n.d. = not detectable (B) Washed mouse platelets were incubated with the indicated agonists in presence or absence of 25 μ g/mL JON/A F(ab)₂ and ELISA was performed. (C) Washed mouse platelets were incubated with CCCP (100 μ M) or W7 (150 μ M) for 1 h at 37°C or NEM (2 mM) for 20 min at 37°C in the presence or absence of GM6001. ELISA was performed. DMSO treatment served as control. Results are mean \pm SD (n = 4 mice per group). (D) Washed human platelets were incubated with CCCP (100 μ M) or W7 (150 μ M) for 1 h at 37°C or NEM (2 mM) for 20 min at 37°C in the presence or absence of GM6001. sCD84 was detected by ELISA as described in material and methods (n=3). (Hofmann, Vögtle *et al.*, *JTH* 2012)¹⁶⁴

To further assess the mechanisms of CD84 ectodomain shedding, washed mouse platelets were treated with different agents that are known to induce shedding of multiple platelet membrane receptors by distinct mechanisms¹² and CD84 cleavage from the platelet surface was measured by sCD84 ELISA. The calmodulin inhibitor W7 induces dissociation of

calmodulin from receptors, thereby facilitating ectodomain shedding, e.g. of GPIb α ^{97,173} and GPV⁹² by ADAM17 and GPVI shedding by ADAM10.^{97,173} N-ethylmaleimide (NEM) is a thiol-modifying reagent which induces shedding by directly activating ADAM10 and ADAM17 independently of platelet activation.¹² Both reagents induced marked ectodomain shedding of CD84 as revealed by detection of high levels of sCD84 in the platelet supernatant compared to untreated control and this effect was virtually abolished in the presence of GM6001 (Figure 24C). Carbonyl cyanide m-chlorophenylhydrazone (CCCP) induces mitochondrial injury by uncoupling oxidative phosphorylation and triggers receptor shedding mainly in an ADAM17 dependent manner.^{88,173} Compared to W7 and NEM, CCCP induced only a mild GM6001-sensitive increase in sCD84 in the platelet supernatant. Similar results were obtained with human platelets (Figure 24D).

3.4.2 Calpain and metalloproteinases cleave CD84

To further analyze the mechanisms underlying CD84 regulation in platelets, CD84 processing in response to shedding inducing agents was assessed by Western blotting using two different antibodies: JER1 (anti-CD84^{N-term}) and the polyclonal antibody M-130, that was raised against the intracellular C-terminal part of CD84 (anti-CD84^{C-term}). The band of the full length CD84 protein appeared between 55 and 72 kDa under non-reducing conditions as previously reported by others.^{51,77} While in unstimulated platelets, M-130 detected only the full length protein, an additional band at a size of approximately 15 kDa appeared in NEM-treated platelets (Figure 25A, lower left). As simultaneously the band intensity of the full length protein decreased, it was hypothesized that this 15 kDa band represents the C-terminal remnant of CD84 that is generated by shedding of the receptor ectodomain. This assumption was confirmed by the finding that GM6001 abrogated the appearance of this additional band in the lysate of NEM treated platelets (Figure 25A, lower left).

Figure 24 shows that W7, and to a lower extent, also CCCP can trigger GM6001-sensitive release of sCD84 into the supernatant. Thus, it was surprising that the C-terminal remnant could not be detected in W7 and CCCP treated platelets although the band of the full length protein was clearly reduced in intensity compared to untreated control, or even absent after W7 treatment (Figure 25, lower left). One possible explanation was that CD84, in addition to ectodomain shedding, may be cleaved in the C-terminal region and that this cleavage interferes with binding of the anti-CD84^{C-term} antibody, M-130. This assumption was also supported by the fact that a shift in the molecular weight of CD84 was detectable with the anti-CD84^{N-term} antibody, JER1, in the lysates of platelets treated with W7 or CCCP. Moreover, this shift, as well as the lack of binding of the anti-CD84^{C-term} antibody was not influenced by GM6001.

One candidate enzyme for mediating this intracellular cleavage was calpain, because shedding by metalloproteinases often occurs concomitantly with activation of calpains¹² and calmodulin-binding proteins are frequently substrates for calpains.¹⁷⁴ This hypothesis was further supported by the analysis of the CD84 C-terminus with an online prediction tool (<http://calpain.org>),¹⁷⁵ which identified a potential cleavage site for calpain in murine CD84, between amino acids 268 and 272 (sequence: V-S-R-N-A), as well as in human CD84.

To test whether calpain indeed mediated the cleavage of the CD84 C-terminus, the calpain-inhibitor calpeptin was used. Strikingly, preincubation of platelets with calpeptin abolished the shift in the molecular weight of CD84 seen in W7 and CCCP treated platelets with the anti-CD84^{N-term} antibody, JER1, (Figure 25A, upper right) and also allowed the detection of the C-terminal remnant with the anti-CD84^{C-term} antibody, M-130 (Figure 25A, lower right). The band intensity for this remnant was strong after W7 and NEM treatment, and weak for CCCP-treated platelets. Importantly, all bands detected by M-130 and JER1 were specific because no signal was obtained when the experiments were performed with *Cd84*^{-/-} platelets (data not shown). These results were in full agreement with the results obtained with the newly established sCD84 ELISA system. When platelets were preincubated with calpeptin and GM6001, both the appearance of the 15 kDa remnant (anti-CD84^{C-term}) as well as the shift in molecular weight and the decrease in band intensity, detected by anti-CD84^{N-term} were abolished, showing additive effects of the two inhibitors (Figure 25A, right). To corroborate the findings using calpeptin and to exclude that its effects on the shift of the CD84 full length band in Western blotting with the anti-CD84^{N-term} antibody were caused by inhibition of other enzymes than calpain¹⁷⁶, two structurally different membrane-permeable calpain inhibitors, MDL28170 and ALLN were used. Calpeptin, MDL28170 and ALLN exerted the same effects on CD84 cleavage (data not shown) confirming the role of calpain in this process. To estimate whether CD84 ectodomain shedding was affected by calpain inhibition, ELISA measurements were performed. Soluble CD84 levels were unaltered in presence of calpeptin (Figure 25B).

These results demonstrated that CD84 is proteolytically regulated by two independent mechanisms: ectodomain shedding by metalloproteinase(s) and intracellular cleavage by calpain. Apparently, metalloproteinase-dependent shedding was functional under calpain-inhibiting conditions and vice versa.

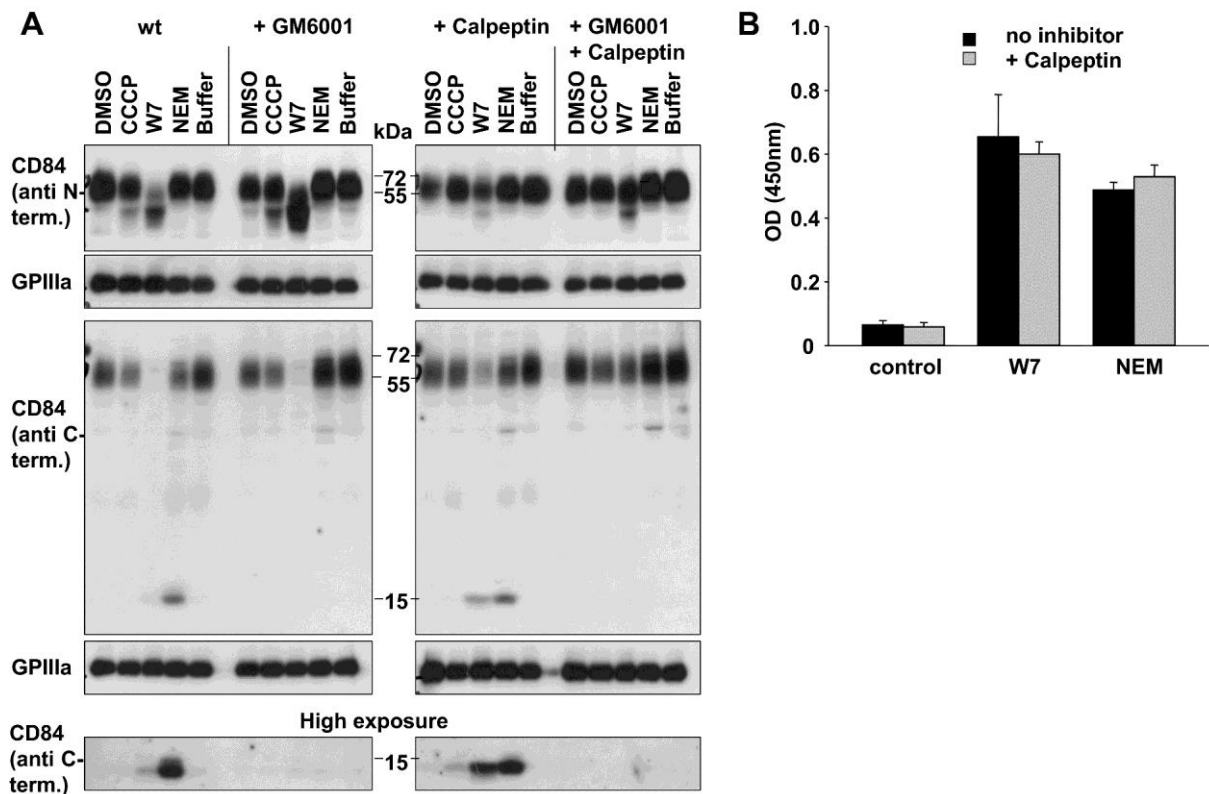


Figure 25. Dual regulation of CD84 by intra- and extracellular cleavage. (A) Washed platelets from wt mice were preincubated in the presence or absence of GM6001 and/or calpeptin. Shedding was induced with CCCP, W7, or NEM. DMSO or buffer served as control. CD84 was detected by Western blotting with anti-CD84 C-term antibody M-130 and anti-CD84 N-term antibody JER-1. GPIIIa was used as a loading control. (B) Washed platelets from wt mice were preincubated in presence or absence of calpeptin. Shedding was induced with W7 or NEM. sCD84 was detected by ELISA. Results are mean \pm SD ($n = 4$ mice per group, representative of 3 individual experiments). (Hofmann, Vögtle *et al.*, *JTH* 2012)¹⁶⁴

3.4.3 ADAM10 is the principal sheddase for CD84 in murine platelets

ADAM10 and ADAM17 are both expressed in platelets¹² and therefore represented potential candidates to mediate CD84 shedding. To test this directly, platelets from *Adam17^{ex/ex}* bone marrow chimeric mice, which exhibit an almost complete loss of ADAM17 protein in hematopoietic cells including platelets,^{106,173} were studied. While shedding of GPIb in response to CCCP, W7 and NEM was abolished in *Adam17^{ex/ex}* platelets (data not shown), levels of released sCD84, as determined by ELISA, were indistinguishable between wt and *Adam17^{ex/ex}* platelets, excluding a major role of ADAM17 in CD84 ectodomain shedding under these experimental conditions (Figure 26A). To investigate the role of ADAM10 in this process, platelets from mice with a megakaryocyte- and platelet-specific deficiency of ADAM10 (*Adam10^{fl/fl}, PF4-Cre* mice, referred to as *Adam10^{-/-}*)¹⁷³ were studied. In sharp contrast to wt and *Adam17^{ex/ex}* platelets stimulated with either agent, sCD84 was virtually undetectable in the supernatant of stimulated *Adam10^{-/-}* platelets (Figure 26B).

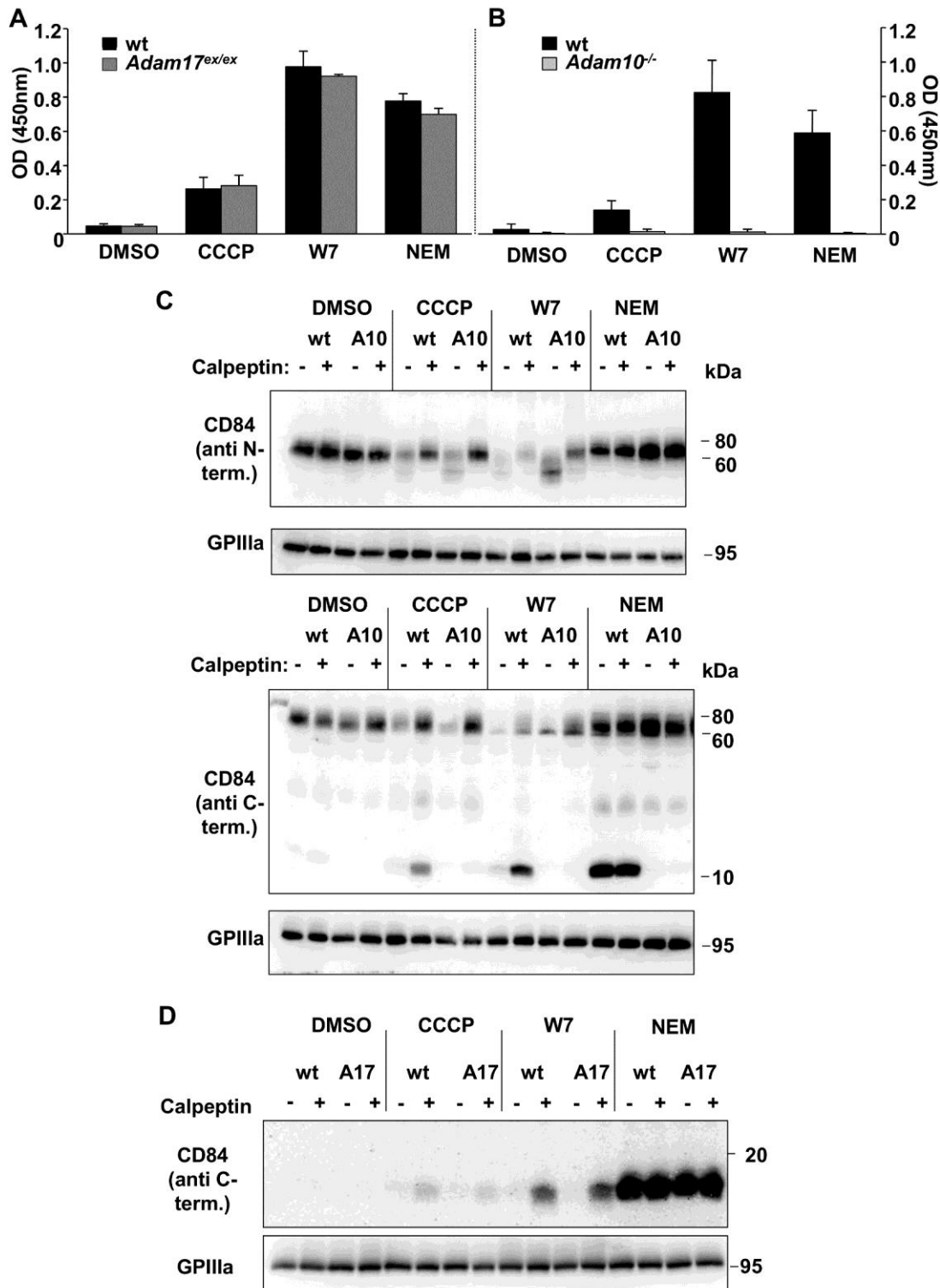


Figure 26. ADAM10 is the principal sheddase for CD84 in murine platelets. Washed platelets from (A) wt and *Adam17^{ex/ex}* BMC mice or (B) wt and *Adam10^{-/-}* mice were treated with CCCP, W7, NEM, or DMSO as a vehicle control. sCD84 in the supernatants was detected by ELISA. Results are mean \pm SD (n=4 mice per group, representative of 2 individual experiments). (C,D) Western Blot detection of CD84 in the lysates of platelets from mice with the indicated genotype (A10: *Adam10^{-/-}*; A17: *Adam17^{ex/ex}*; wt are the respective wt controls). Platelets were incubated with calpeptin or vehicle control and shedding was induced as described above. (2 mice pooled per group, representative of 2-3 individual experiments). (Hofmann, Vögtle *et al.*, *JTH* 2012)¹⁶⁴

These findings were confirmed by Western blot analysis, where no C-terminal remnant was detected in lysates of *Adam10*^{-/-} platelets treated with NEM, W7 and CCCP in presence or absence of calpeptin (Figure 26C). Again, the results from *Adam17*^{ex/ex} platelets did not differ from those obtained with wt platelets (Figure 26D).

Taken together, these data established ADAM10 as the principal sheddase that cleaves CD84 in murine platelets, while ADAM17 is not significantly involved in this process.

3.4.4 ADAM10 and calpain regulate surface expression of CD84 in response to agonist receptor stimulation

To investigate whether ADAM10 is also the principal sheddase for CD84 cleavage in response to agonist receptor stimulation, wt and *Adam10*^{-/-} platelets were activated with CVX, CRP, thrombin or RC. Remarkably, none of these agonists induced significant ectodomain shedding of CD84 in the mutant platelets, in contrast to wt platelets (Figure 27A). To exclude that thrombin directly cleaved CD84 in wt platelets by its protease activity, platelets were also stimulated by PAR-4 activating peptide. This led to generation of soluble CD84 similar to thrombin, confirming that thrombin receptor signaling induced loss of CD84 (Figure 27B). Similar results were obtained with TRAP-6 in human platelets (data not shown). To confirm the results obtained by ELISA, and to get information on shedding kinetics, lysates from wt and *Adam10*^{-/-} platelets that had been stimulated for different times were tested by Western blotting. These experiments were performed in the presence or absence of calpeptin to also detect intracellular cleavage of CD84. Shedding, visualized by detection of the 15 kD remnant with the anti-CD84^{C-term} antibody M-130 occurred within 5 min in response to all agonists and the band intensity increased over time (Figure 27C). RC induced also strong activation of calpain, as indicated by the observation that the remnant was only detectable in the presence of calpeptin as well as by the shortened CD84 protein detected by the anti-CD84^{N-term} antibody JER1 in the absence but not in the presence of calpeptin. In contrast to RC, the other agonists only moderately activated calpain. No C-terminal remnant was detected in lysates of platelets deficient in ADAM10, while calpain activity was unaffected by the absence of the metalloproteinase.

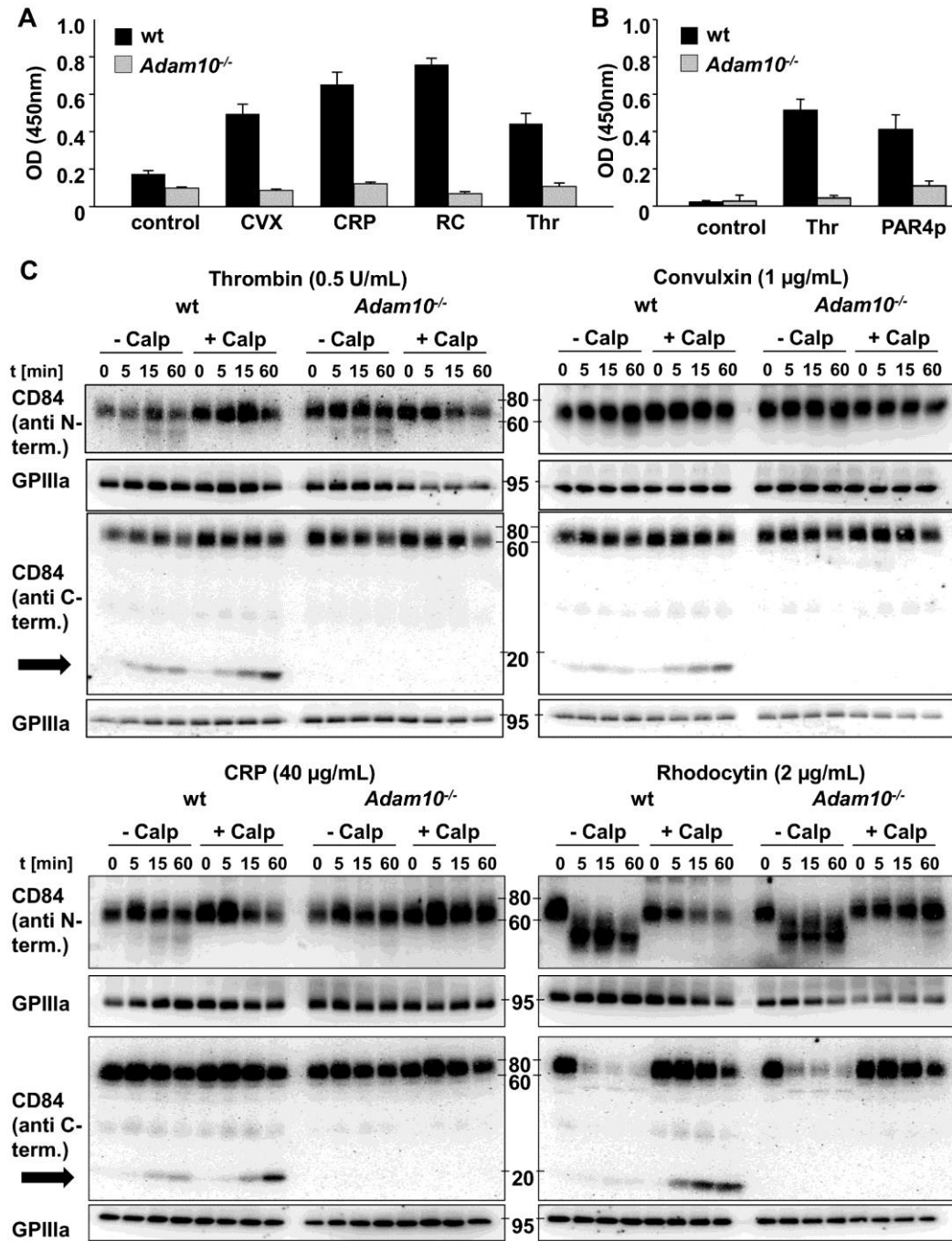


Figure 27. ADAM10 cleaves CD84 in response to platelet receptor stimulation. (A) Washed mouse platelets from wt and *Adam10*^{-/-} mice were incubated with CVX, CRP, rhodocytin or thrombin for 1 h at 37°C. sCD84 was detected by ELISA. Results are mean ± SD (n=4 mice per group, representative of 3 individual experiments). (B) Washed mouse platelets from wt and *Adam10*^{-/-} mice were incubated with thrombin or PAR4 activating peptide (PAR4p, 4mM) for 1 h at 37°C. sCD84 was detected by ELISA. Results are mean ± SD (n=4 mice per group) (C) Washed platelets from wt and *Adam10*^{-/-} mice were preincubated with calpeptin or vehicle control, prior to stimulation for 5 min, 15 min or 1 h with the indicated agonists. Platelet lysates were subjected to Western Blotting. (platelets from 4 mice were pooled per group, representative of 3 individual experiments). (Hofmann, Vögtle *et al.*, *JTH* 2012)¹⁶⁴

3.4.5 High concentrations of sCD84 in plasma of wild-type mice

To test whether CD84 shedding occurs *in vivo*, sCD84 levels were measured in mouse plasma. Indeed, significant levels of sCD84 could be detected in plasma of wt mice, while the ELISA yielded only background signals with plasma from *Cd84*^{-/-} mice (Figure 28A). Remarkably, sCD84 plasma levels in *Adam10*^{-/-} mice were reduced by >50% compared to wt mice, demonstrating that shedding by platelet ADAM10 occurs *in vivo* and accounts for approximately half of the total sCD84 protein found in the plasma of healthy mice. To investigate whether ADAM17 plays a role in CD84 shedding in platelets *in vivo* and thus may be responsible for the sCD84 levels observed in *Adam10*^{-/-} mice, sCD84 levels were measured in the plasma of bone marrow chimeras with platelets double-deficient in ADAM10 and ADAM17 (*Adam10*^{-/-}/*Adam17*^{ex/ex}).¹⁷³ As depicted in Figure 28B, levels of sCD84 were not further reduced in the plasma of double-deficient bone marrow chimeras compared to ADAM10 single-deficient mice, thus excluding a role for ADAM17 in regulating plasma levels of sCD84 *in vivo*. In consistence, plasma levels of wt and *Adam17*^{ex/ex} bone marrow chimeras were indistinguishable (data not shown).

To test whether CD84 shedding occurs during normal blood clotting, non-anticoagulated whole blood was allowed to clot *in vitro* and sCD84 levels were measured in the obtained serum. Indeed, in wt mice levels of sCD84 increased approximately two-fold in serum compared to plasma (Figure 28A). In sharp contrast, sCD84 concentrations in serum of *Adam10*^{-/-} mice did not differ from those found in plasma, demonstrating that ADAM10 is the only proteinase that triggers shedding of CD84 during blood clotting.

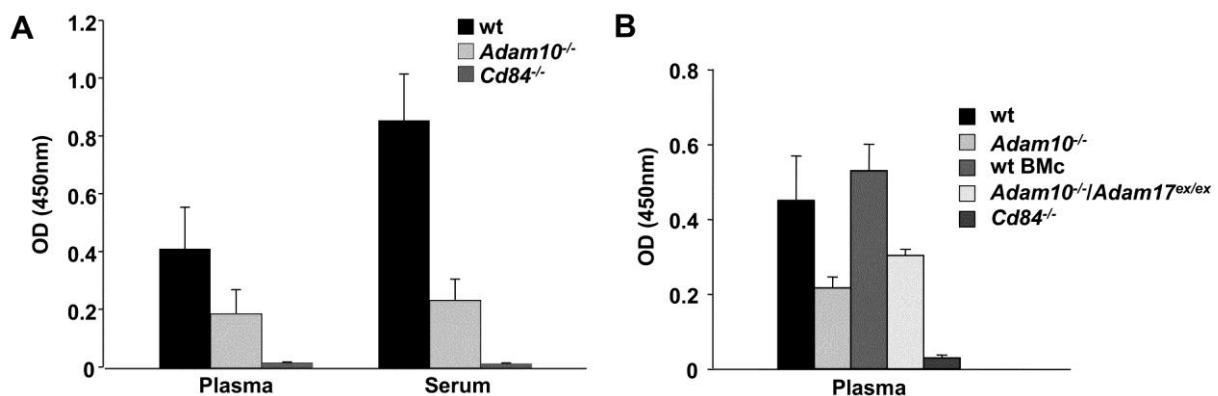


Figure 28. CD84 levels in mouse plasma and serum. (A) sCD84 levels in the plasma and serum of wt, *Adam10*^{-/-} and *Cd84*^{-/-} mice were measured by ELISA. Serum and plasma samples were obtained from the same animals and analyzed within a single experiment. (B) sCD84 levels in the plasma of *Adam10*^{-/-} and *Adam10*^{-/-}/*Adam17*^{ex/ex} mice and their respective controls as determined by ELISA are depicted. Results of all experiments are mean \pm SD (n=4 mice per group representative of 3 individual experiments). (Hofmann, Vögtle *et al.*, *JTH* 2012)¹⁶⁴

3.5 Regulation of GPVI receptor levels in platelets mechanistically differs from CD84 regulation

The collagen receptor GPVI facilitates platelet activation and subsequently firm adhesion upon platelet contact with subendothelial collagen. Metalloproteinases can mediate GPVI downregulation and recent evidence suggested that ADAM10 plays a major role in GPVI cleavage.⁹⁷ *In vivo* downregulation of GPVI receptor levels can be induced experimentally in mice by injection of the monoclonal antibody JAQ1, as reported earlier,⁴¹ making GPVI downregulation a potential approach for antithrombotic therapy. However, the mechanism of GPVI cleavage is not fully understood. In collaboration with Dr. Markus Bender from our research group, genetically modified mice were studied to gain deeper insight into the mechanism of GPVI downregulation *in vitro* and *in vivo*.

3.5.1 GPVI is differentially regulated by ADAM10 and ADAM17 *in vitro*

Downregulation of GPVI can be mediated by internalization as well as proteolytic cleavage.^{41,89} ADAM10 has been proposed to be the metalloproteinase responsible for ectodomain cleavage, based on observations that this enzyme cleaved GPVI-based synthetic peptides.⁹⁷ To test this directly, *Adam10*^{-/-} and wt control platelets were treated with the calmodulin inhibitor W7 and GPVI downregulation was monitored. In wt, this led to almost complete loss of GPVI expression on the platelet surface as shown by flow cytometric analysis (Figure 29A). However, GPVI expression of *Adam10*^{-/-} platelets remained high after W7 treatment, comparable to untreated platelets. As internal control, the expression of GPIb α , which is known to be regulated by ADAM17, was also measured. GPIb α levels were downregulated in controls, as well as in *Adam10*^{-/-} platelets, demonstrating that W7 treatment was effective (data not shown). Consistent with these observations, ELISA measurements demonstrated absence of soluble GPVI (sGPVI) in supernatants of *Adam10*^{-/-} platelets treated with W7, whereas strong signals were detectable with wt platelets (Figure 29B). Additionally, Western blot analysis confirmed loss of intact GPVI in wt platelets after W7-treatment, but not in *Adam10*^{-/-} platelets (Figure 29C). These findings provided direct evidence that ADAM10 is responsible for GPVI shedding after calmodulin inhibition, and support earlier findings by Gardiner *et al.*⁹⁷ Unexpectedly, however, different results were obtained when receptor shedding was induced by the mitochondrial damage-inducing reagent CCCP.⁸⁸ This treatment resulted in comparable downregulation of GPVI in wt and in *Adam10*^{-/-} platelets (Figure 29A). ELISA measurements confirmed cleavage of GPVI from the platelet surface by detection of sGPVI in the supernatant of wt and *Adam10*^{-/-} platelets

(Figure 29B), and Western blots revealed almost complete absence of intact GPVI (Figure 29C).

These data show that ADAM10 cleaves GPVI after W7-treatment, but probably another proteinase triggers GPVI downregulation in response to mitochondrial damage induced by CCCP. Because ADAM17 is a well-described sheddase of platelet receptors GPIb α ⁸⁸ and GPV,⁹² platelets from *Adam17^{ex/ex}* bone marrow chimeric mice, which exhibit an almost complete loss of ADAM17 protein in hematopoietic cells,^{106,173} were studied with regard to GPVI shedding. Compared to wt controls, downregulation of GPVI from the platelet surface was nearly unaltered for *Adam17^{ex/ex}* platelets in response to W7 treatment, but almost completely abrogated in response to CCCP (Figure 29D). ELISA measurements supported these findings, with low amounts of sGPVI in supernatants of *Adam17^{ex/ex}* platelets and high amounts for wt controls (Figure 29E), whereas intact GPVI was still found in lysates from *Adam17^{ex/ex}* platelets in Western blots (Figure 29F). Together, these data revealed that GPVI is differentially regulated by ADAM10 or ADAM17 *in vitro*, depending on the stimulus.

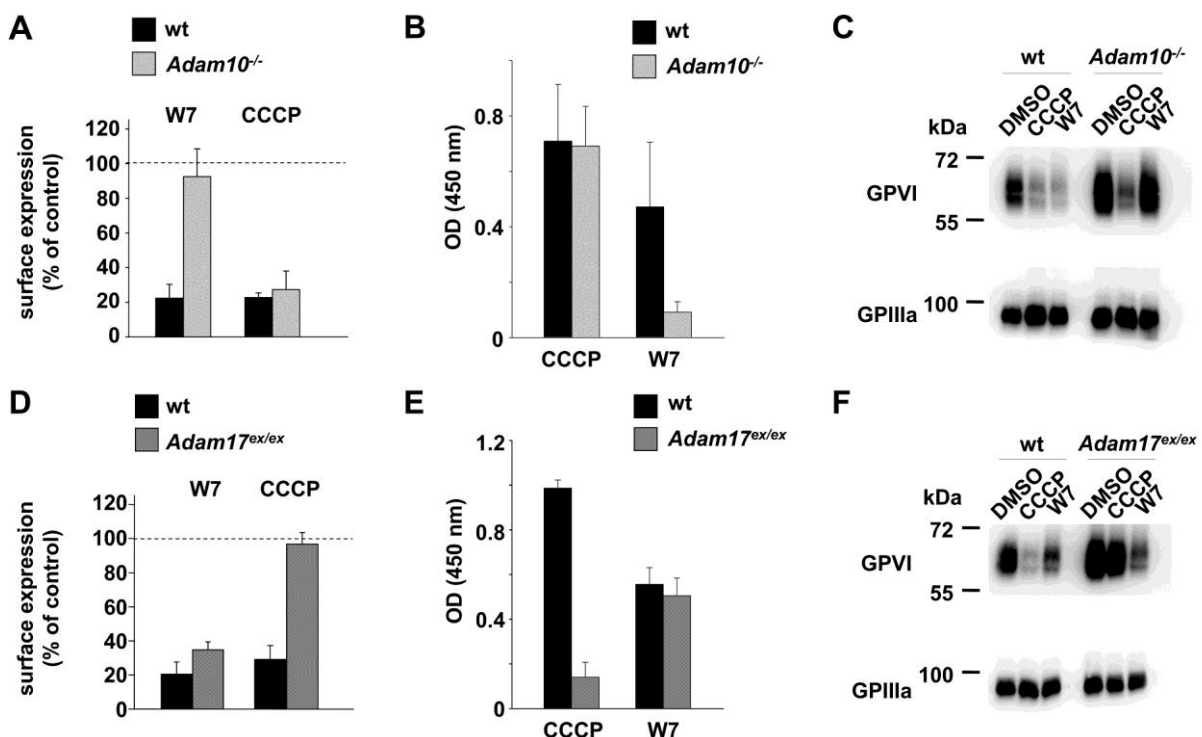


Figure 29. Abrogated GPVI shedding in *Adam10^{-/-}* platelets after W7 treatment and in *Adam17^{ex/ex}* platelets after CCCP treatment. (A, D) Washed platelets were treated with W7 or CCCP for 1 h at 37°C, stained with FITC-labeled anti-GPVI antibody and analyzed by flow cytometry. (B, E) Washed platelets were incubated with biotinylated JAQ1 and then treated with CCCP or W7 for 1 h at 37°C. Supernatants were applied on a JAQ3-coated ELISA plate and GPVI-JAQ1-biotin complexes were detected with HRP-conjugated streptavidin. (C, F) Western blot detection of intact GPVI (JAQ1-HRP) in CCCP, W7, or vehicle treated platelets. GPIIIa served as loading control. Results are mean \pm SD (n = 4 mice per group, representative of 3 experiments). (Bender, Hofmann *et al.*, *Blood* 2010)¹⁷³

3.5.2 GPVI shedding *in vivo* is unaltered in *Adam10*^{-/-} and *Adam17*^{ex/ex} mice

Mice were injected with biotinylated JAQ1⁴¹ to test the roles of ADAM10 and ADAM17 in antibody-induced GPVI shedding *in vivo* and the associated transient thrombocytopenia. JAQ1 injection led to a comparable transient thrombocytopenia in wt, *Adam10*^{-/-}, and *Adam17*^{ex/ex} mice (Figure 30A) with a maximal drop of platelet counts after 30 min (down to ~20% of vehicle treated mice) and the platelet count returned to normal levels at later time points. GPVI downregulation from the platelet surface occurred in all mice (Figure 30B). It is likely that ectodomain shedding was responsible for this downregulation, as comparably high levels of sGPVI were detected in plasma of wt and mutant mice by ELISA measurements 30 min and 3 h after JAQ1 injection (Figure 30C). These data demonstrated that JAQ1-induced GPVI shedding *in vivo* and the associated transient thrombocytopenia is unaltered in the absence of ADAM10 or ADAM17 suggesting that neither ADAM10 nor ADAM17 is the GPVI cleaving sheddase *in vivo*.

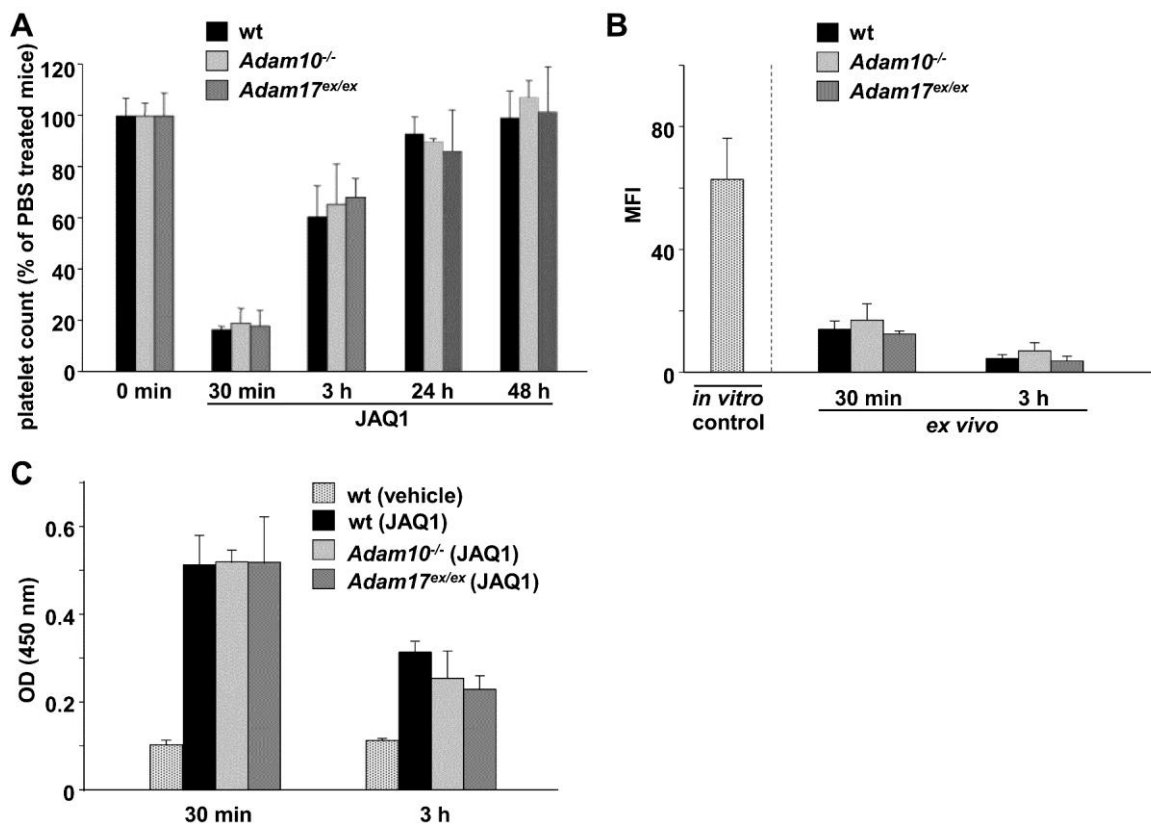


Figure 30. GPVI is cleaved in *Adam10*^{-/-} and *Adam17*^{ex/ex} mice *in vivo*. Wt and mutant mice were injected i.v. with 100 µg of biotinylated anti-GPVI (JAQ1) antibody. (A) Flow cytometric analysis of platelet count and (B) GPVI surface expression (indirectly with streptavidin-FITC) was performed. As positive control in (B), wt platelets from untreated mice were incubated with 10 µg/mL biotinylated-JAQ1 *in vitro* and stained with streptavidin-FITC. (C) Mice were injected with 100 µg biotinylated-JAQ1 and plasma was collected at the indicated time points. Levels of GPVI-JAQ1-biotin complexes in plasma were determined by ELISA. Results of all experiments are mean ± SD (n = 4 mice per group, representative for 3 individual experiments). (Bender, Hofmann *et al.*, *Blood* 2010)¹⁷³.

3.5.3 Abrogated GPVI shedding in *Adam10^{-/-}/Adam17^{ex/ex}* double-mutant platelets *in vitro*

Platelets from *Adam10^{-/-}/Adam17^{ex/ex}* bone marrow chimeric mice were treated with W7 or CCCP to study the effect of ADAM10/ADAM17 double-deficiency. In contrast to wt platelets, double-deficient platelets were not able to downregulate GPVI from their surface (Figure 31A). This was expected based on the results obtained with the single mutant mice (Figure 29). Accordingly, no cleaved GPVI was detectable by ELISA in supernatants of W7- or CCCP-treated double-mutant platelets (Figure 31B) and levels of intact GPVI were unaltered in platelet lysates (Figure 31C).

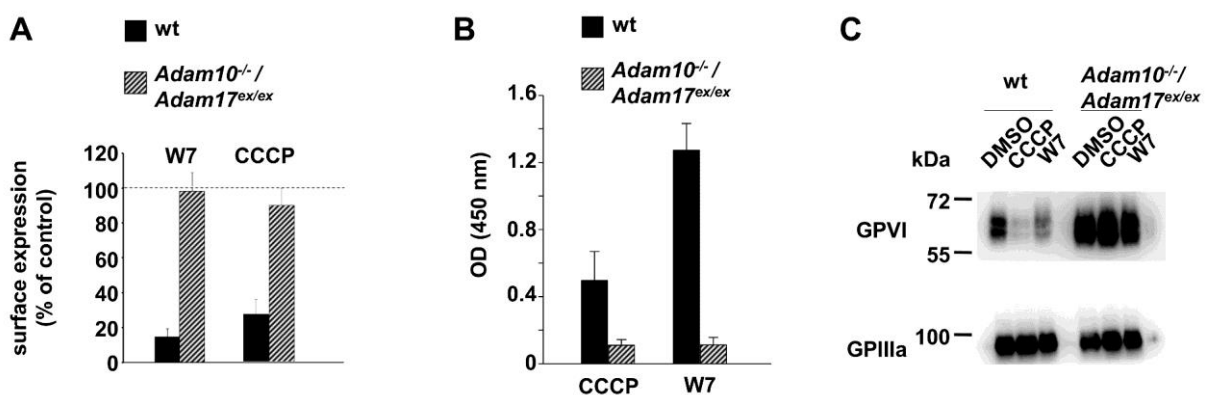


Figure 31. GPVI shedding is abolished in *Adam10^{-/-}/Adam17^{ex/ex}* platelets *in vitro*. (A) Washed platelets were treated with W7 (150 μ M) or CCCP (100 μ M) for 1 h at 37°C, stained with FITC-labeled anti-GPVI antibody and analyzed by flow cytometry. (B) Washed platelets were incubated with biotinylated JAQ1 and then treated with CCCP (100 μ M) or W7 (150 μ M) for 1 h at 37°C. Supernatants were applied on a JAQ3-coated ELISA plate and incubated with HRP-conjugated streptavidin. (C) Western blot detection of intact GPVI (JAQ1-HRP) in CCCP (100 μ M), W7 (150 μ M) or vehicle treated platelets. GPIIIa served as loading control. Results of experiments (A, B) are mean \pm SD ($n = 4$ mice per group, representative for 3 individual experiments). (Bender, Hofmann *et al.*, *Blood* 2010)¹⁷³.

3.5.4 Unaltered JAQ1-induced GPVI shedding in *Adam10^{-/-}/Adam17^{ex/ex}* mice

Adam10^{-/-}/Adam17^{ex/ex} BMc mice were injected with biotinylated JAQ1 in order to test the effect of the metalloproteinase double-deficiency on antibody-induced GPVI ectodomain shedding and the associated thrombocytopenia *in vivo*. Platelet counts, GPVI surface expression and soluble GPVI levels in plasma were determined. The transient thrombocytopenia induced by JAQ1 injection was comparable in wt and double-mutant mice (Figure 32A). Surprisingly, GPVI was downregulated from the surface of *Adam10^{-/-}/Adam17^{ex/ex}* platelets with the same kinetics and to the same extent as in wt (Figure 32B). Further, similar levels of soluble GPVI were detected in plasma of both groups of mice (Figure 32C).

Hence, antibody-induced ectodomain shedding of GPVI *in vivo* occurs independently of the two major ADAM sheddases which are responsible for shedding of the receptor *in vitro*. These experimental data suggested the existence of a third metalloproteinase, which is able to shed GPVI from the platelet surface *in vivo*.

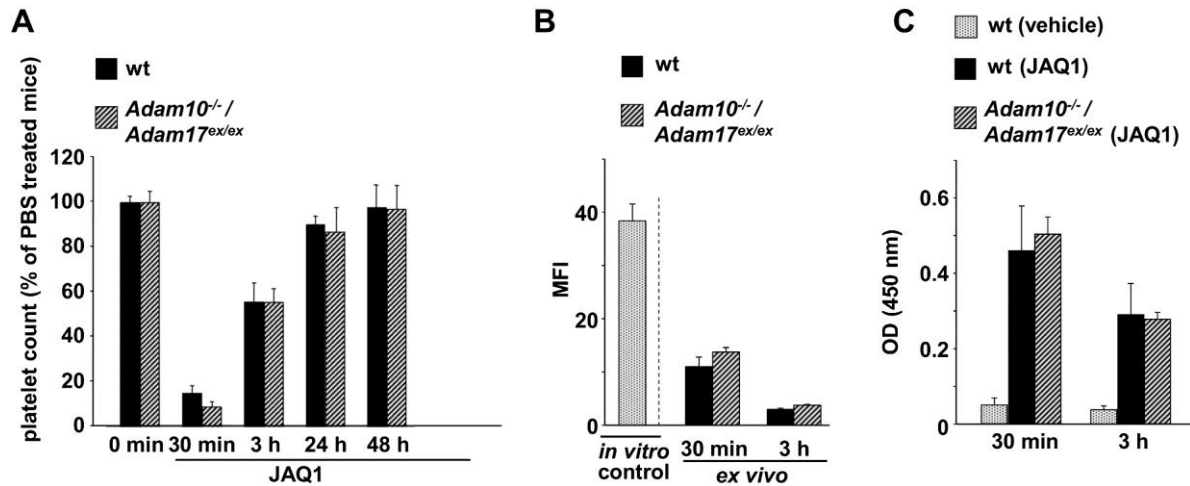


Figure 32. JAQ1-induced GPVI shedding occurs in *Adam10*^{-/-}/*Adam17*^{ex/ex} double-mutant mice. Wt and *Adam10*^{-/-}/*Adam17*^{ex/ex} BMC mice were injected i.v. with 100 μ g biotinylated JAQ1. Flow cytometric analysis of platelet count (A) and GPVI expression (B) (indirectly: streptavidin-FITC) was performed. As positive control in (B), wt platelets from untreated mice were incubated with 10 μ g/mL biotinylated JAQ1 and stained with streptavidin-FITC. (C) Plasma was collected at the indicated time points from mice after injection of 100 μ g biotinylated-JAQ1. GPVI levels were determined by ELISA. Results of all experiments are mean \pm SD ($n = 4$ mice per group, representative for 3 individual experiments). (Bender, Hofmann *et al.*, *Blood* 2010)¹⁷³

3.5.5 Differential effects of JER1 antibody administration compared to JAQ1 *in vivo*

Inducible GPVI downregulation and the associated thrombocytopenia by *in vivo* administration of JAQ1 antibody in mice is an established process, as mentioned in the previous paragraphs. To study whether CD84 downregulation in platelets can be induced experimentally by *in vivo* administration of an anti-CD84 antibody, JER1 was injected intravenously into wt mice. Four mice per group received either 20 μ g/mL JER1 or PBS. After injection, platelet counts were monitored daily. Mice injected with JER1 became thrombocytopenic, with a platelet count of approximately 50% of initial value after 24 h, whereas platelet counts in controls remained unaltered. This thrombocytopenia was transient, since platelet counts returned to normal values after 5 days (Figure 33A). Injection of 100 μ g JER1 induced a more pronounced and longer lasting thrombocytopenia (~40% of initial value), with platelet counts turning back to normal values at day 7 (data not shown). To study whether CD84 becomes downregulated from the platelet surface after JER1 injection,

platelets were stained with JER1-FITC or anti rat-IgG-FITC at different time points. JER1-FITC did not bind to platelets isolated after 1 h or 24 h but binding capacity increased over time before it reached its maximal value after 5 days (Figure 33B). Platelets from JER1-injected mice stained with anti rat-IgG-FITC (washed blood) displayed MFIs which almost reached values of *in vitro* stained positive controls, after 1 h or 24 h. MFIs decreased over the following days until they reached background signals (Figure 33C). These data demonstrated that CD84 is neither cleaved, nor internalized after JER1 injection, but remains occupied by the injected antibody. In conclusion, JER1 injection induces transient thrombocytopenia upon *in vivo* administration, but does not trigger CD84 downregulation.

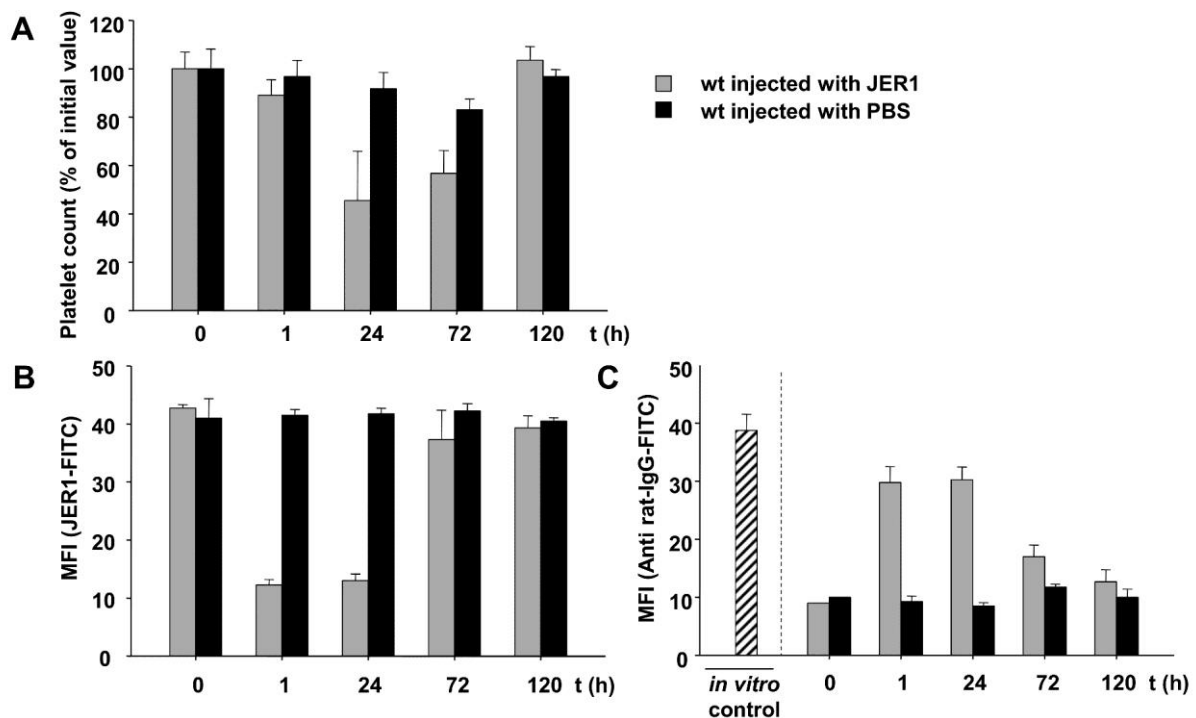


Figure 33. CD84 is not cleaved upon injection of JER1 *in vivo*. Mice were injected with 20 μ g unlabeled anti-CD84 antibody (JER1) and platelet count was determined at different time points by flow cytometry (A). (B) Platelets were stained with JER1 FITC. (C) Platelets were stained with anti rat-IgG-FITC to detect JER1-occupied platelets. Untreated platelets preincubated with 10 μ g/mL JER1 served as *in vitro* controls. (n=4 mice per group).

In summary, different mechanisms are operative in CD84 and GPVI ectodomain shedding in mouse platelets. While GPVI is differentially regulated by ADAM10 and ADAM17, CD84 is exclusively regulated by ADAM10. In addition, intracellular cleavage of CD84 is mediated by calpain. GPVI can be depleted by JAQ1 antibody administration *in vivo*, a process that probably involves ectodomain shedding, however the responsible metalloproteinase(s) remain to be identified. In contrast, *in vivo* cleavage of CD84 cannot be induced by injection of the monoclonal antibody JER1.

3.6 CD84 deficient mice are protected from ischemic stroke

Stroke is the second leading cause of death and disability worldwide¹²³ and is mostly caused by focal cerebral ischemia subsequent to arterial occlusion.¹²⁵ Ischemic stroke can be described as a complex thrombo-inflammatory disease,^{129,177} with platelets and immune cells essentially contributing to the severity of stroke outcome in experimental mouse models.^{45,139} However, the signaling and adhesion events involved in microvascular thrombus formation and immune cell activation in the ischemic brain are still not fully understood. Since CD84 exhibits a broad expression in platelets and immune cells (see 3.2.2), we wanted to study whether CD84 deficiency would influence ischemic stroke outcome in mice. Thus, mice were challenged in the tMCAO (transient middle cerebral artery occlusion) model,¹³¹ an experimental model for ischemic stroke. Stroke experiments were conducted by Dr. Peter Kraft in the research group of Prof. Dr. Guido Stoll at the Neurology Department of the University of Würzburg. To induce transient cerebral ischemia, a thread was advanced through the carotid artery into the middle cerebral artery. This leads to a local reduction of cerebral blood flow by approximately 95%.⁴⁵ After one h the filament was removed to allow reperfusion for 24 h. Then brains were harvested, sectioned and 2,3,5-triphenyltetrazolium chloride (TTC) staining was performed to analyze infarct sizes. In CD84 deficient mice, infarct volumes were significantly reduced (wt: $94.44 \pm 20.98 \text{ mm}^3$; *Cd84*^{-/-}: $65.53 \pm 24.73 \text{ mm}^3$; $p=0.01$; Figure 34A). This reduction in ischemic lesions also resulted in significantly less neurological deficits compared to wt mice, as determined by the Bederson score¹⁶⁹ assessing global neurological function (wt median 3.0 vs *Cd84*^{-/-} median 2.0; $p=0.02$; Figure 34B) and the grip test¹⁷⁰ which indicates motor function and coordination of the mice (wt median 3.0 vs *Cd84*^{-/-} median 4.0; $p=0.019$; Figure 34B).

The platelet adhesion receptors GPIb and GPVI have been shown to essentially contribute to infarct growth, because their inhibition confers protection in the tMCAO model.⁴⁵ For CD84 deficient mice, the results are more difficult to interpret, as it is unclear whether lack of CD84 in platelets or other cell types exerts protective effects. Smaller infarct sizes in *Cd84*^{-/-} mice could be due to reduced immune cell adhesion to the endothelium or reduced infiltration into the brain parenchyma following ischemia. However, no significant differences in number of neutrophils or CD11b⁺ leukocytes were found in brain sections of wt and *Cd84*^{-/-} mice (data not shown). Reduced infarct sizes in CD84 deficient mice could also be explained by reduction of necrotic or apoptotic brain cells. Inflammatory cytokines like TNF- α and IFN- γ might lead to apoptosis in cells of the ischemic brain.¹⁷⁸ Therefore, RT-PCR studies were performed to determine the expression of inflammatory cytokines in brains from wt and *Cd84*^{-/-} mice 24 h after tMCAO. Strikingly, in brain cortices of *Cd84*^{-/-} mice, expression of

TNF- α as well as IFN- γ was significantly reduced as compared to wt controls (Figure 34C,D). In basal ganglia, levels of these cytokines also showed a tendency towards reduction.

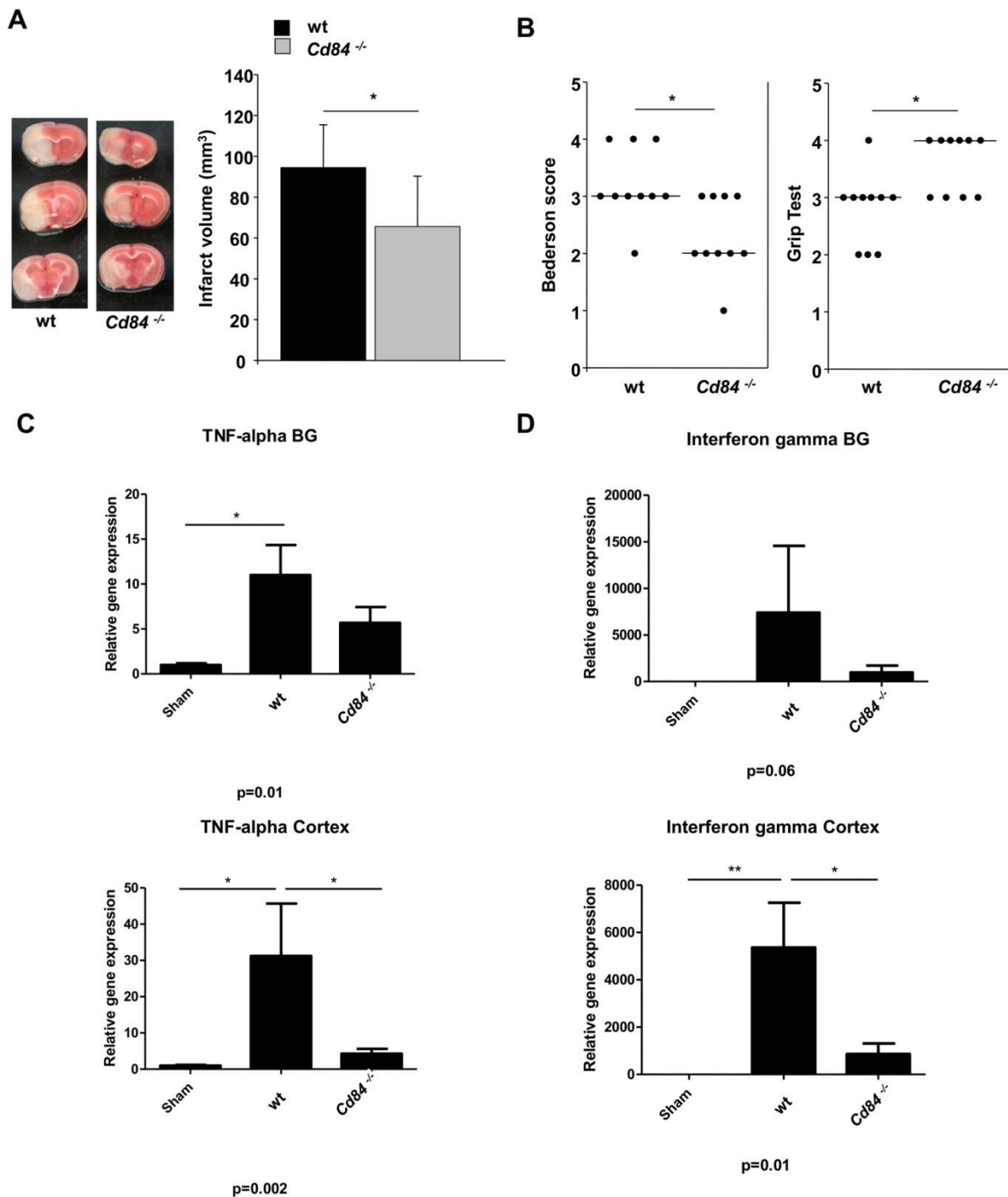


Figure 34. CD84 deficient mice are protected from ischemic stroke. tMCAO was performed and neurological defects were investigated. (A) Representative images of three corresponding TTC-stained coronal brain sections from wt and *Cd84*^{-/-} mice 24 h after tMCAO (left). Brain infarct volumes in wt and *Cd84*^{-/-} mice (n=10) presented as mean \pm SD (right). Infarct areas are stained white and non-infarcted tissue in red. (B) Bederson score and grip test, determined 24 h after tMCAO of wt and *Cd84*^{-/-} mice; horizontal bar indicates the median. (C) RNA was isolated from basal ganglia (BG) or cortices 24h after tMCAO and relative gene expression of TNF- α as well as IFN- γ were determined by RT-PCR. Figure C was kindly provided by Dr. P. Kraft; *p<0.05; **p<0.01.

Inflammatory cytokines can be produced by various immune cells, but especially T cells have become the focus of attention in stroke studies, because recent findings demonstrated their detrimental contributions to infarct development.^{138,139} To study whether CD84 in T cells has a role in experimental stroke, wt or *Cd84*^{-/-} CD4⁺ T cells were transferred into *Rag1*^{-/-} mice,¹⁷⁹ which lack T and B lymphocytes. Remarkably, 24 h after tMCAO, *Rag1*^{-/-} mice reconstituted with *Cd84*^{-/-} T cells displayed significantly lower infarct volumes than *Rag1*^{-/-} mice reconstituted with wt T cells (*Cd84*^{-/-} CD4⁺→*Rag1*^{-/-}: 62.96 ± 49.76 mm³; wt CD4⁺→*Rag1*^{-/-}: 122.93 ± 13.03 mm³; p=0.009; Figure 35A).

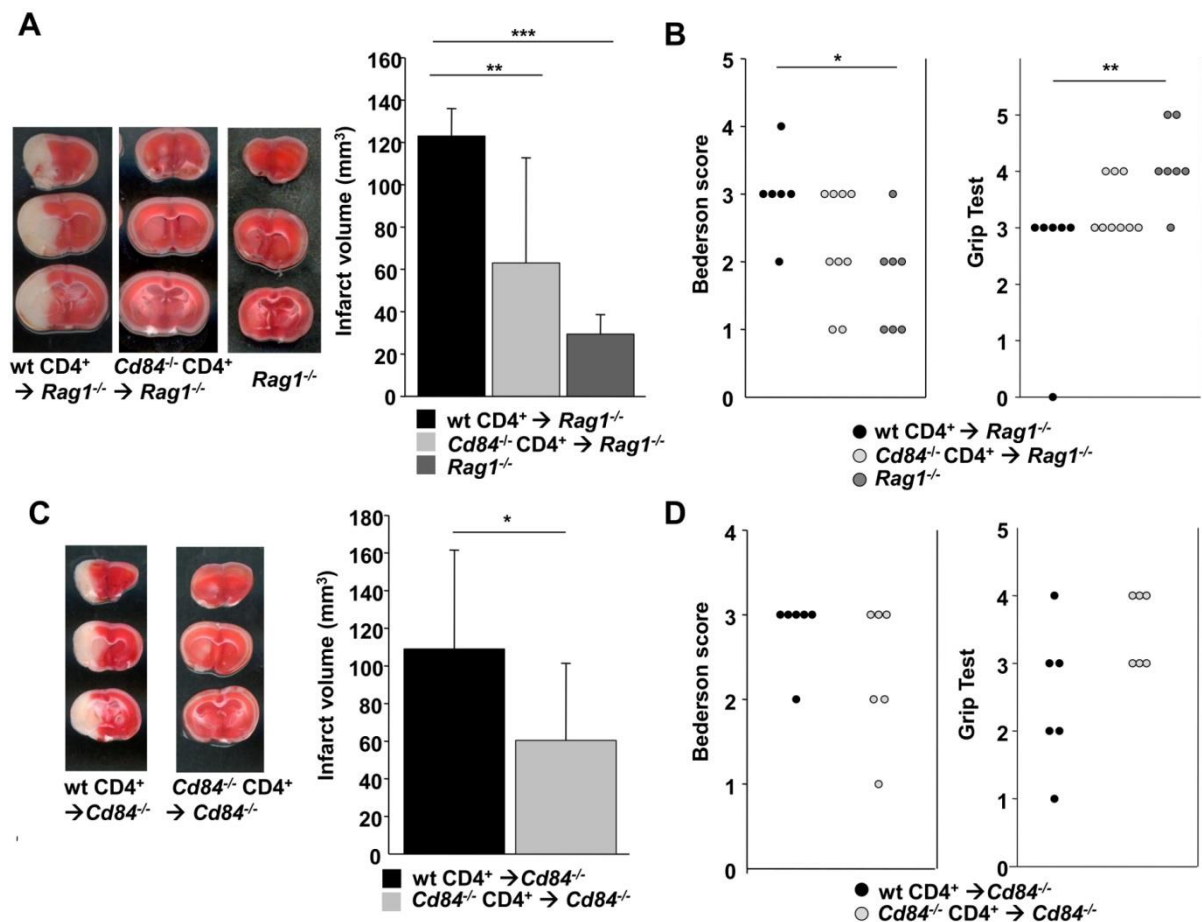


Figure 35. CD84 on T cells determines ischemic stroke outcome. (A-B) *Rag1*^{-/-} mice were reconstituted with wt or *Cd84*^{-/-} CD4⁺ T cells. Untreated *Rag1*^{-/-} mice served as control. The tMCAO model was performed and neurological defects were investigated. (A) Representative images of three corresponding coronal brain sections from the indicated groups of mice stained with TTC 24 h after tMCAO (left). Brain infarct volumes from the indicated groups of mice (n=10) presented as mean ± SD (right). (B) Bederson score and grip test, determined 24h after tMCAO. (C-D) Wt or *Cd84*^{-/-} T cells were transferred into *Cd84*^{-/-} mice and tMCAO was performed. (C) Representative images of three corresponding coronal brain sections from the indicated groups of mice stained with TTC 24 h after tMCAO (left). Brain infarct volumes from the indicated groups of mice (n=8) presented as mean ± SD (right). (D) Bederson score and grip test was determined 24h after tMCAO. *p<0.05; **p<0.01, ***p<0.001.

Noteworthy, 4 out of 10 *Rag1*^{-/-} mice reconstituted with wt T cells, but only one mouse reconstituted with *Cd84*^{-/-} T cells died within 24 h after tMCAO, an observation also pointing towards ameliorated stroke outcome when CD84 is absent in T cells. The reduction in ischemic lesions also led to a tendency towards reduced neurological deficits and better motor function in *Rag1*^{-/-} mice reconstituted with *Cd84*^{-/-} T cells, compared to those reconstituted with wt T cells (Figure 35B). The findings from the T cell transfer experiment into *Rag1*^{-/-} mice strongly suggested that CD84 in T cells significantly influenced ischemic stroke outcome. It was not clear whether CD84 in other cell types, e.g. in platelets, was required as (homophilic) ligand for CD84 in wt T cells in this setting. Thus, CD84 deficient mice were transplanted with wt or *Cd84*^{-/-} CD4⁺ T cells. In this experimental setup, the transplanted wt T cells are the only cell type expressing CD84, since the recipient mice are lacking CD84 in all their cells. Transfer of *Cd84*^{-/-} T cells into *Cd84*^{-/-} mice served as control. Surprisingly, transfer of wt T cells restored susceptibility to ischemic stroke in *Cd84*^{-/-} mice, whereas controls (*Cd84*^{-/-} mice + *Cd84*^{-/-} T cells) displayed smaller infarct volumes. ($109.00 \pm 52.56 \text{ mm}^3$ vs. $60.43 \pm 41.03 \text{ mm}^3$; $p=0.04$; Figure 35C). The increased ischemic lesions after wt T cell transfer also led to a tendency towards higher neurological deficits and reduced motor function than in *Cd84*^{-/-} mice + *Cd84*^{-/-} T cells (Figure 35D).

In summary, CD84 deficient mice were protected from ischemic stroke and reduced inflammatory cytokine expression might be mechanistically linked to the observed protection. T cell transfer experiments have demonstrated that presence of CD84 in T cells contributes to detrimental outcome of ischemic stroke. As presence of CD84 in T cells alone was sufficient to induce large infarcts, the question remains which ligand CD84 binds to in this setting, because homophilic binding to CD84 in other cell types can be excluded.

3.7 Generation of Orai2 deficient mice

Recent studies from our research group established STIM1 and Orai1 as crucial Ca²⁺ sensor and store operated Ca²⁺ (SOC) channel subunit in platelets,^{22,23} respectively. However, low expression of Orai2 has also been detected in platelets.²³ Another study from our laboratory demonstrated that the Ca²⁺ sensor STIM2 is the major STIM isoform in brain, which mediates Ca²⁺ influx in neurons in response to ischemia, but the corresponding SOC channel remained unknown.¹⁵³ To explore the relevance of Orai2 for platelet function, as well as in experimental brain ischemia, Orai2 mice deficient were generated and analyzed in this thesis.

3.7.1 Cloning of a targeting vector for disrupting the *Orai2* gene

According to bioinformatics analysis, the murine *Orai2* gene contains 3 exons, two of which are translated into a 250 aa protein (<http://www.ensembl.org>; transcript ID ENSMUST00000041048). The start codon (ATG) lies within exon 2, which codes only for the N-terminal part of *Orai2* and a part of the first transmembrane domain. Exon 3 contains the majority of the coding sequence for *Orai2* (Figure 36A). Together with Dr. Attila Braun a targeting strategy was developed, which aimed at the disruption of exon 3 of the *Orai2* gene, by replacement with a neomycin resistance cassette. According to this strategy, no functional *Orai2* mRNA can be produced in the mutant animals.

Briefly, physical mapping of the *Orai2* gene was performed to find restriction enzyme sites flanking exon 3. *EcoRV* endonuclease restriction sites were chosen, in order to distinguish between the wt and targeted allele in Southern blot, because the newly introduced gene targeting sequence introduces an additional *EcoRV* restriction site (Figure 37A). To generate the targeting construct, a modified pBluescriptKS vector was used, which contains a Neo resistance cassette under the PGK promoter, flanked by loxP sites and two multiple cloning sites for insertion of the homologous arms. 5' and 3' arms were generated and inserted into this targeting vector (Figure 36B). These arms (flanking regions) contain 4.5 and 4.9 kb long homologous sequences identical to the corresponding upstream and downstream sequences of the protein coding region of *Orai2* exon 3. To amplify the homologous arms by long range PCR from 129/Sv ES cell DNA, primers containing additional restriction enzyme sites for insertion into the vector backbone were designed. *NotI* site-containing primers were chosen for amplification of the 5' arm, and *SalI*- and *XhoI*-containing primers for the 3' arm. After purification, the homologous arms were subcloned into the TOPO XL vectors. Competent cells were transformed and DNA test digestions using several restriction endonucleases were performed. Bacteria exhibiting DNA with the correct restriction patterns were chosen. The purified DNA was sent for sequencing (MWG Eurofins, Ebersberg). All sequencing results were aligned with the mouse genome using UCSC Blat search (<http://genome.ucsc.edu/>) to check for correctness. Next, the 5' arm and the Neo vector were ligated, and competent cells were transformed. Clones with correct insert orientation of the 5' were also checked by sequencing. Finally, the 3' flanking was inserted into the vector already containing the 5' flanking, which was linearized before using the *XhoI* endonuclease. According to this method, the correct orientation of the insert was easily detected in test digestions, because a *SalI/XhoI* site at the 5' end of the 3' arm was eliminated after correct ligation. Test digestions of the final vector showed the correct restriction pattern (Figure 36C).

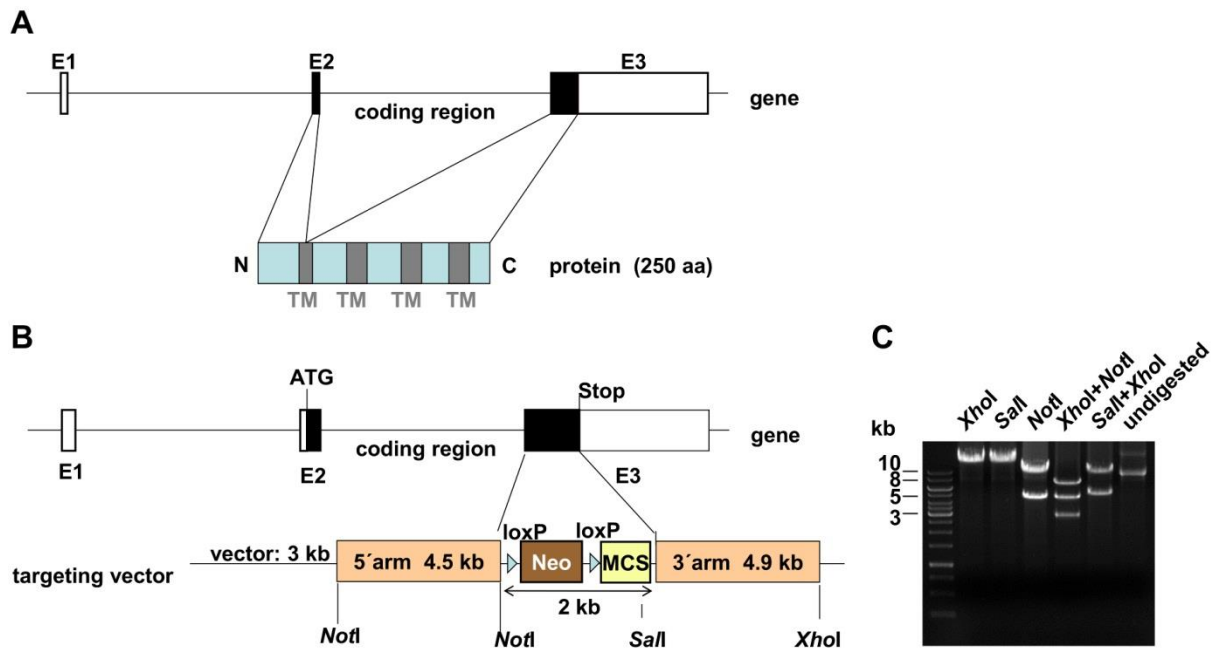


Figure 36. Targeting strategy and test digestion of the final vector. (A) The mouse *Orai2* gene contains 3 exons. Only exon 2 and a part of exon 3 are translated into a 250 aa protein containing 4 transmembrane (TM) domains. (B) The scheme depicts the strategy for the generation of an *Orai2* ko allele. A neomycin resistance cassette (Neo+MCS) replaces the protein coding part of exon 3. The majority of the protein coding region of *Orai2* is deleted by this strategy. (C) Test digestions of the targeting vector showed the expected restriction fragment lengths.

3.7.2 Electroporation of *Orai2* targeting vector and analysis of recombinant clones

The final targeting vector was linearized with *XhoI* and electroporated into 129/Sv ES cells.¹⁶⁰ After electroporation, 448 stem cell clones, which had survived the Geneticin selection process, were picked. DNA samples of all ES cell clones were digested with *EcoRV* and screened for homologous recombination in Southern blot (see Figure 37A for Southern blot strategy). According to the strategy, the radioactively labeled external probe binds to a DNA sequence downstream of exon 3, located downstream of the 3' arm (flanking). Homologous recombination will introduce a new *EcoRV* site into the targeted allele, allowing for detection of a 7.8 kb ko allele, whereas the wt allele will appear as a 11.7 kb fragment. Southern blot screening of all 448 ES cell clones that had survived Geneticin selection, revealed three homologous-recombinant stem cell clones. These clones (*Orai2*^{+/−}) showed the wt band at 11.7 kb and the knockout band at the expected size of 7.8 kb (Figure 37B).

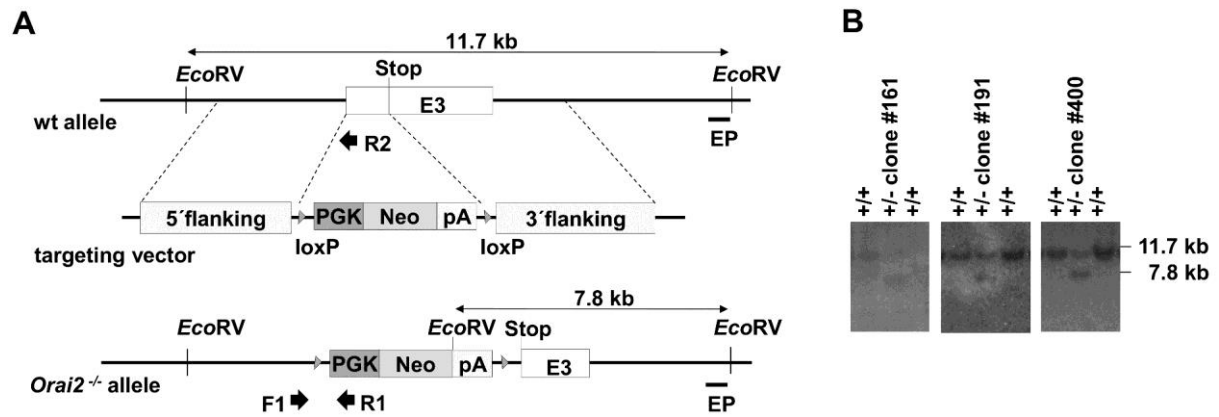


Figure 37. Detection of homologous-recombinant ES cell clones by Southern blot. (A) The scheme illustrates the detection of wt and *Orai2* knockout (targeted) alleles. The external probe (EP) recognizes a sequence downstream of 3' flanking. The wt band between the two *EcoRV* restriction sites is approx. 11.7 kb. The Neo resistance cassette contains an additional *EcoRV* site. The mutant band is approx. 7.8 kb. (B) Southern blot pictures showing 3 different homologous-recombinant stem cells clones (+/-).

3.7.3 Breeding of homozygous *Orai2*^{-/-} mice

The three homologous-recombinant clones were recultured and retested by Southern blot analysis. ES cells were then injected into C57Bl/6J blastocysts in collaboration with Dr. Michael Bösl (Max Planck Institute of Neurobiology, Martinsried), to generate chimeric mice. Only one (#400) of three ES cell clones gave rise to chimeric mice (Table 5).

chimeric mice	derived from ES cell clone #	chimerism (%)	germline transmission
male	400	60	Yes
male	400	60	No
male	400	50	No
female	400	80	No
female	400	50	No

Table 5. Chimeric mice obtained after blastocyst injection of *Orai2*^{+/-} ES cells. Germline transmission was obtained in one mouse, as indicated.

The chimerism of mice obtained after blastocyst injection was estimated according to their coat color. Since the injected stem cells were from a 129/Sv ES cell line¹⁶⁰ and the blastocyst was from C57BL/6J mice, a high percentage of brown coat color indicates high chimerism, and thus a high chance of germline transmission. Chimeric male mice were crossed with female C57BL/6J and chimeric females were crossed with male C57BL/6J mice. Germline transmission occurred only in one chimeric male, i.e. offspring with brown coat color was

obtained. Subsequently, *Orai2*^{+/-} mice were intercrossed to finally obtain *Orai2*^{-/-} mice. Mouse genotypes were determined by Southern blot (Figure 38A) and by PCR (Figure 38B). Loss of *Orai2* gene expression was detected on mRNA level by semiquantitative RT-PCR. Primers were designed, which cannot anneal to cDNA when exon 3 is deleted. Therefore, no band will be obtained in homozygous *Orai2*^{-/-} mice. In wt mice, high *Orai2* mRNA expression was detected in brain tissue and spleen, weak expression was found in heart, and only a faint band occurred in platelets. None of these RNA samples of *Orai2*^{-/-} mice contained *Orai2* mRNA (Figure 38C). This demonstrates that the targeting strategy was successful.

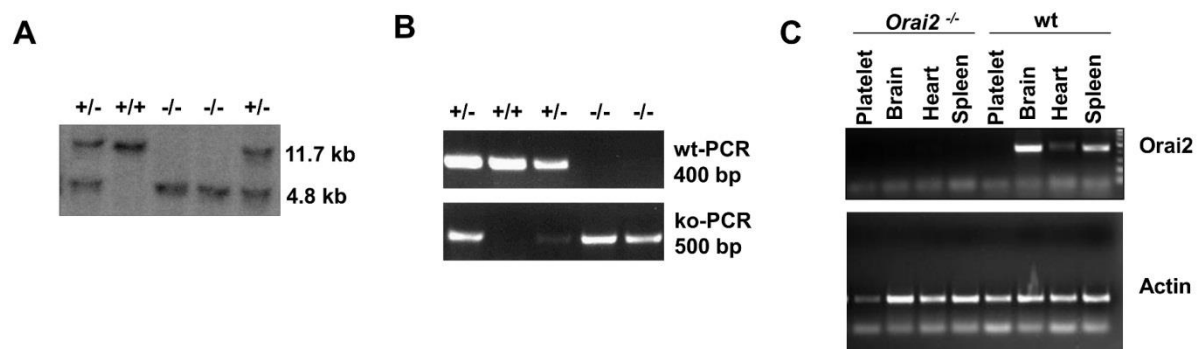


Figure 38. Successful generation of homozygous *Orai2* ko mice. (A) Southern blot and (B) PCR strategy to detect wt (+/+), heterozygous (+/-) and ko (-/-) mice. (C) RT-PCR detecting absence of *Orai2* in platelets, brain, heart, and spleen of *Orai2*^{-/-} mice. In wt, expression of *Orai2* was detected in brain>spleen>heart>platelets. Actin served as loading control.

3.8 Analysis of *Orai2* deficient mice

3.8.1 *Orai2* deficient mice are born in Mendelian ratio and develop normally

Among offspring from heterozygous matings, *Orai2*^{-/-} (ko) and *Orai2*^{+/+} (wt) mice were born approximately in Mendelian ratio (Table 6). Therefore it was concluded that loss of *Orai2* does not severely impair embryonic development.

Genotype <i>Orai2</i>	number of mice	percentage	expected percentage
+/+	43	27%	25%
+/-	81	51%	50%
-/-	34	22%	25%
total	158	100%	100%

Table 6. *Orai2*^{-/-} mice were born in Mendelian ratio after intercrossing of heterozygous animals

In contrast to *Stim2*^{-/-} mice, which die spontaneously starting at the age of 10 weeks,¹⁵³ in *Orai2*^{-/-} mice spontaneous death was not observed. *Orai2*^{-/-} mice developed normally, did not show any signs of illness and were indistinguishable from wt mice. Intercrossing of *Orai2*^{-/-} mice yielded approximately same litter sizes as intercrossing of wt mice. Litters from ko mouse intercrossing also developed normally, indicating that ko females had no deficit in feeding their offspring. An analysis of basal hematologic parameters (Table 7) did not reveal significant differences between wt and *Orai2*^{-/-} mice.

Genotype <i>Orai2</i>	WBC	RBC	HGB	HCT
+/+	7.45± 3.46	9.09± 0.96	14.45±1.66	46.33±4.77
-/-	5.15± 2.20	8.32±1.21	13.62±2.20	44.42±6.82
p	n.s.	n.s.	n.s.	n.s.

Table 7. Normal hematologic parameters in *Orai2*^{-/-} mice. White blood cell count (WBC; $\times 10^3/\mu\text{L}$), erythrocytes (RBC; $\times 10^6/\mu\text{L}$), hemoglobin (HGB; g/dl) and hematocrit (HCT; %) as determined by a hematologic analyzer (Sysmex) were unaltered in *Orai2* deficient mice. n=10. n.s.: not significant.

3.8.2 Normal platelet function and hemostasis in *Orai2* deficient mice

Orai1 has been shown to be the major SOC channel subunit in platelets and to be critically involved in pathological thrombus formation.²³ Interestingly, weak *Orai2* expression was detected in platelets²³. *Orai2*^{-/-} mice were analyzed to study whether lack of *Orai2* has an impact on platelet activation *in vitro* or (pathological) thrombus formation *in vivo*.

Platelet count (wt: $898 \pm 159 \times 10^3$ plt/ μL ; *Orai2*^{-/-}: $915 \pm 199 \times 10^3$ plt/ μL ; $p \geq 0.05$) and platelet size (FSC wt: 286.6 ± 20.6 ; FSC *Orai2*^{-/-}: 298.8 ± 20.7 ; $p \geq 0.05$) in *Orai2*^{-/-} mice were unaltered as compared to wt control mice (Figure 39A, B). The expression of prominent platelet receptors was measured by flow cytometry and also found to be comparable to control mice (Figure 39C).

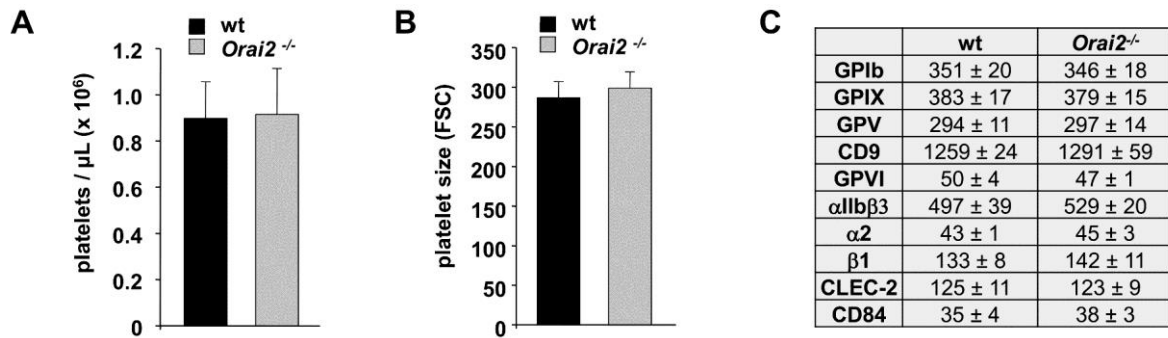


Figure 39. Normal platelet count, size, and glycoprotein expression in *Orai2*^{-/-} platelets. (A) platelet counts (platelets $\times 10^6/\mu\text{L}$) and (B) platelet size (expressed as forward scatter) were determined either by a hematologic analyzer (Sysmex) or flow cytometry. Values are mean \pm SD, $n \geq 8$ per group. (C) Expression levels of prominent platelet surface receptors were measured by flow cytometry and expressed as mean fluorescence intensity \pm SD, $n=5$ per group.

To study whether lack of *Orai2* leads to altered platelet activation *in vitro*, platelets were stimulated with various agonists, and activated platelet integrin $\alpha\text{IIb}\beta\text{3}$, as well as degranulation-dependent P-selectin exposure were measured by flow cytometry. *Orai2* deficient platelets showed normal activation in response to thrombin, ADP/U46619, CRP, convulxin and rhodocytin. Therefore, *Orai2* is dispensable for platelet integrin activation and degranulation in response to G-protein coupled or ITAM coupled receptor stimulation (Figure 40).

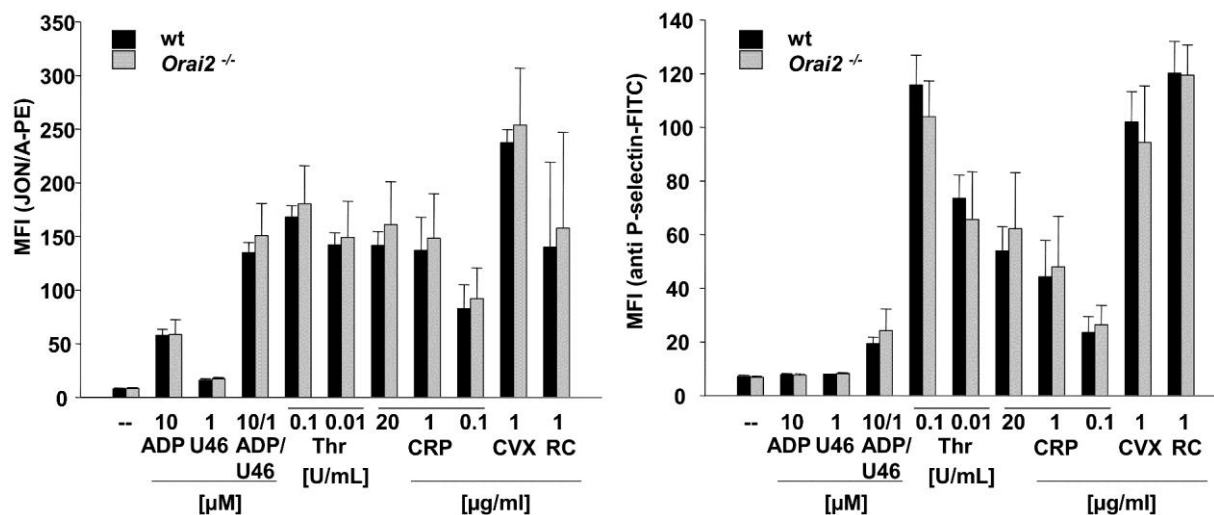


Figure 40. Flow cytometric analysis of $\alpha\text{IIb}\beta\text{3}$ integrin activation (binding of JON/A-PE, left) and degranulation-dependent P-selectin exposure (right) in response to the indicated agonists. Values are mean fluorescence intensity (MFI) \pm SD; 5 mice per group. U46=U46619, Thr=thrombin, CVX=convulxin, RC=rhodocytin.

Next, potential effects of *Orai2* deficiency on thrombosis were studied *in vivo*. Arterial thrombosis was analyzed in collaboration with Martina Morowski in our laboratory. To elicit chemical injury, 20% ferric-chloride (FeCl_3) was applied to mesenteric arterioles and thrombus formation was monitored by intravital fluorescence microscopy. The time to beginning of thrombus formation, characterized by adhesion and accumulation of fluorescently labeled platelets, was found to be similar between wt and *Orai2*^{-/-} mice (Figure 41A). The mean time to complete vessel occlusion was not significantly different between the two groups (wt 15.6 ± 2.8 min vs. *Orai2*^{-/-} 19.3 ± 4.2 min; $p > 0.05$).

Bleeding times were determined by cutting a two millimeter segment from the tail tip and gently absorbing the blood with a filter paper, without making contact with the wound site. Time until arrest of bleeding was not significantly altered in *Orai2* deficient mice (wt 618.6 ± 221.4 s; *Orai2*^{-/-} 566.7 ± 296.2 s; $p > 0.05$; Figure 41B). These data suggest that *Orai2* is neither essential for (pathological) arterial thrombus formation, nor for primary hemostasis.

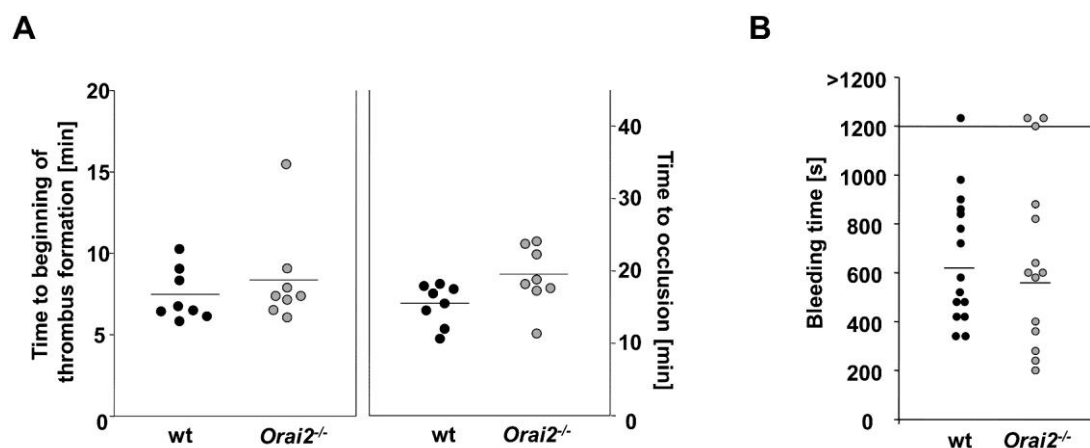


Figure 41. Unaltered arterial thrombus formation in mesenteric arterioles and normal hemostasis in *Orai2*^{-/-} mice. (A) Mesenteric arterioles were injured by application of FeCl_3 and thrombus formation was monitored by intravital fluorescence microscopy. Time to beginning of thrombus formation (left) and to complete vessel occlusion (right) are shown. Horizontal lines represent mean values. Each symbol represents one arteriole. $p > 0.05$. (B) A 2 mm segment from mouse tail tips was cut with a sharp scalpel and blood was gently absorbed with a filter paper in 20 s intervals. Time until bleeding has ceased is expressed as bleeding time [s]. Each symbol represents one individual. $p > 0.05$.

In conclusion, *Orai2* is dispensable for platelet activation *in vitro* and thrombus formation *in vivo*. In accordance with previously published data,²³ *Orai1* is the most critical *Orai* isoform in platelets.

3.8.3 *Orai2* deficient mice are protected from ischemic stroke and show reduced SOCE in neurons

High expression of *Orai2* has been shown in brain.¹⁵⁶ Recently, Berna-Erro *et al.* demonstrated that the Ca^{2+} sensor STIM2 is the major STIM isoform in the brain and lack of STIM2 led to protection from ischemic stroke in mice that were challenged in the tMCAO model.¹⁵³ Therefore we hypothesized that *Orai2* and STIM2 could be mechanistically linked to facilitate SOCE in neurons. *Orai2* deficient mice were therefore studied in the tMCAO model. Stroke experiments were performed by Dr. Peter Kraft in the research group of Prof. Guido Stoll at the Department of Neurology at the University of Würzburg.

Orai2^{-/-} mice were protected from ischemic stroke, as infarct volumes were significantly reduced (wt: $104.58 \pm 27.96 \text{ mm}^3$; *Orai2*^{-/-}: $57.0 \pm 32.68 \text{ mm}^3$; $p=0.007$; Figure 42A). This reduction in ischemic lesions also resulted in significantly reduced neurological deficits compared to wt, as determined by the Bederson score¹⁶⁹ assessing global neurological function (wt median 3.0 vs *Orai2*^{-/-} median 2.0; $p=0.04$; Figure 42B) and the grip test¹⁷⁰ which indicates motor function and coordination of the mice (wt median 3.0 vs *Orai2*^{-/-} median 4.0; $p=0.021$; Figure 42B).

Since *Orai2* is also expressed in immune cells,^{158,180} it was unclear whether the observed protection of *Orai2*^{-/-} mice in the tMCAO model was immune cell- or rather neuron-intrinsic. To address this, wt and *Orai2*^{-/-} mice were lethally irradiated and afterwards bone marrow cells from donor mice were injected intravenously into the irradiated mice, in order to generate bone marrow chimeras (BMc). *Orai2*^{-/-} mice were injected with wt BM, wt mice were injected with *Orai2*^{-/-} BM, and as control group, wt mice were injected with wt BM. After 8 weeks, these mice were subjected to tMCAO.

Orai2^{-/-} mice transplanted with wt BM developed significantly smaller infarct sizes than wt mice with *Orai2*^{-/-} BM cells, which displayed normal infarct sizes as compared to the wt control group with wt BM (*Orai2*^{-/-} + wt BM: $47.40 \pm 25.83 \text{ mm}^3$; wt + *Orai2*^{-/-} BM: $109.31 \pm 35.02 \text{ mm}^3$, $p=0.004$; wt + wt BM: $95.30 \pm 41.83 \text{ mm}^3$; $p=0.016$; p-values as compared to *Orai2*^{-/-} + wt BM, Figure 42C). The reduction in ischemic lesions in *Orai2*^{-/-} + wt BM mice also resulted in significantly less neurological deficits compared to the two control groups, determined as Bederson score and grip test. Details on statistical evaluation are summarized in Figure 42D.

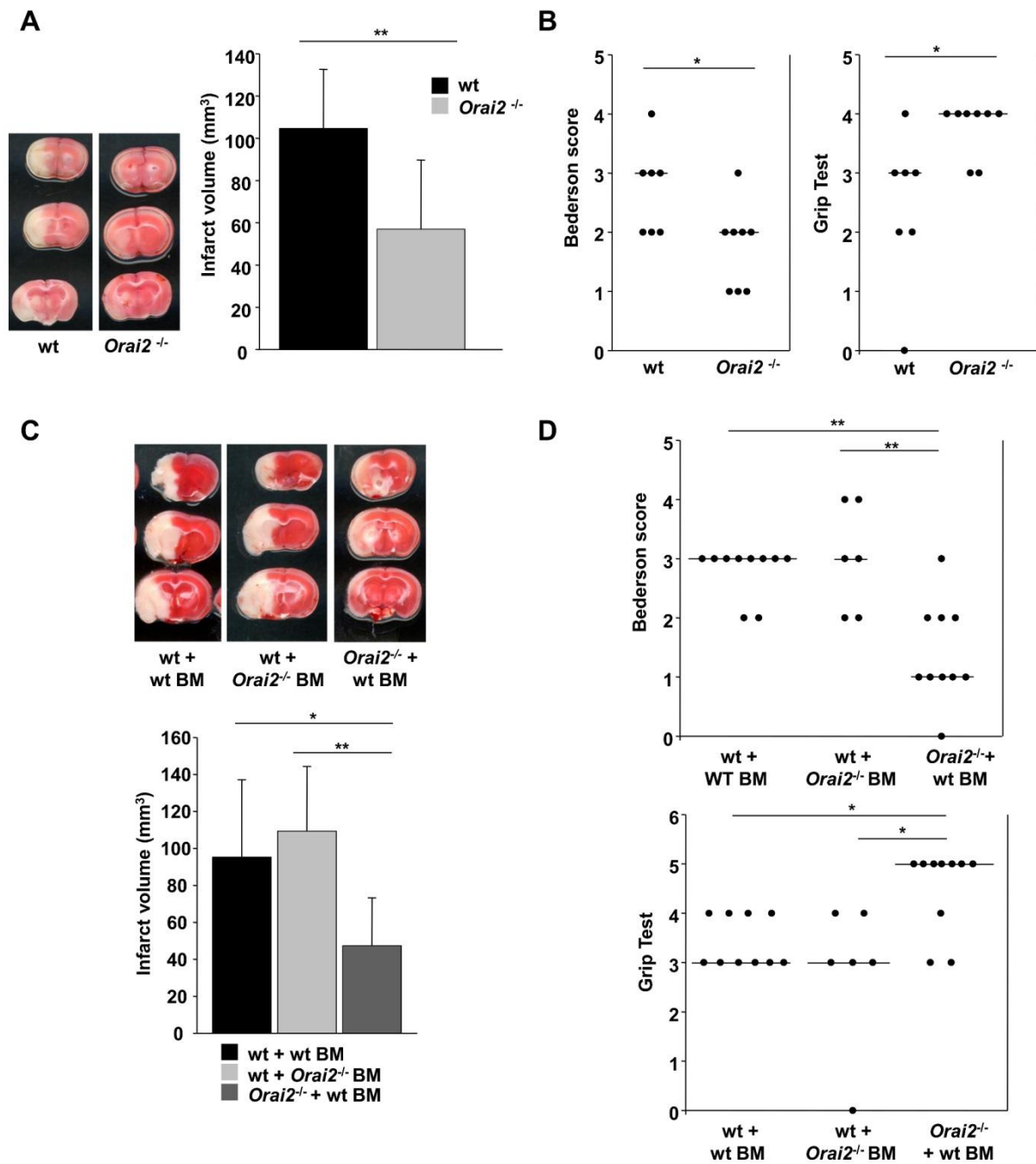


Figure 42. *Orai2* deficient mice are protected from neuronal damage after cerebral ischemia. The tMCAO model was performed and neurological defects were investigated. (A) Representative images of three corresponding coronal brain sections from wt and *Orai2*^{-/-} mice stained with TTC 24 h after tMCAO (left). Brain infarct volumes in wt and *Orai2*^{-/-} mice (n=8) presented as mean ± SD (right). Infarct areas are stained white and non-infarcted tissue in red. (B) Bederson score and grip test, as assessed 24 h after tMCAO for wt and *Orai2*^{-/-} mice. (C) Representative images of three corresponding TTC stained coronal brain sections from BMC mice of the indicated genotype transplanted with BM from the indicated donor mice, 24 h after tMCAO. Brain infarct volumes of the indicated BMC mice (n=8 to 10 mice per group) are presented as mean ± SD. One-way ANOVA, Bonferroni post hoc test for comparison between groups. (D) Bederson score and grip test, as assessed 24 h after tMCAO in the indicated BMC mice. Kruskal-Wallis, Dunns multiple comparison post hoc test for comparison between groups. Horizontal bars indicate the median. *p<0.05; **p<0.01.

The stroke experiments using BMC mice clearly demonstrated that protection was not blood cell intrinsic, because wt mice transplanted with *Orai2*^{-/-} BM cells were not protected. Further, *Orai2*^{-/-} mice that received wt BM cells were significantly protected. Loss of Orai2 in several non-hematopoietic cells, e.g. endothelial cells, could mediate this protection. In light of similar observations made in *Stim2*^{-/-} BMC mice,¹⁵³ it appeared more likely that Orai2 plays a critical role in neurons. To study this in more detail, Ca²⁺ measurements were performed in cortical neurons isolated from *Orai2*^{-/-} mice and controls, in collaboration with Dr. Robert Kraft, University of Leipzig. Remarkably, Ca²⁺ influx was significantly impaired in Orai2 deficient cortical neurons. Further, store depletion with the sarcoendoplasmic reticulum Ca²⁺ adenosine-5'-triphosphatase (SERCA) pump inhibitor cyclopiazonic acid (CPA) in the absence of extracellular Ca²⁺ suggested that *Orai2*^{-/-} neurons had reduced store content of Ca²⁺ (Figure 43A). To study the role of Orai2-mediated SOCE under ischemic conditions, Ca²⁺ imaging experiments on neuronal cultures under conditions of oxygen-glucose deprivation (OGD) were performed. OGD led to a robust increase in intracellular Ca²⁺ levels ([Ca²⁺]_i) in the wt neurons, but significantly smaller increase in [Ca²⁺]_i after 90 min of OGD in *Orai2*^{-/-} neurons (Figure 43B).

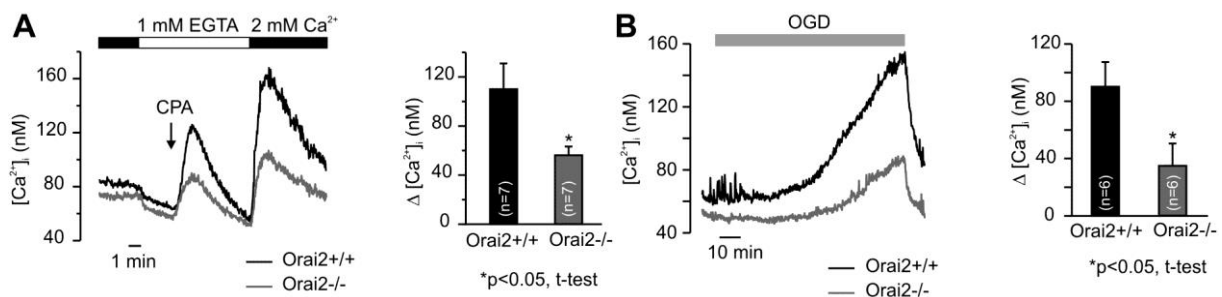


Figure 43. Reduced calcium influx in cortical neurons. (A) Neuronal cultures were loaded with fura-2 and averaged [Ca²⁺]_i responses in *Orai2*^{-/-} neurons were compared to those in cells from wt (*Orai2*^{+/+}) littermates. Cells were treated with CPA (20 μM) followed by replacement of 1 mM EGTA with 2 mM Ca²⁺. Increases in [Ca²⁺]_i (Δ[Ca²⁺]_i) were calculated by subtracting basal [Ca²⁺]_i from peak [Ca²⁺]_i prior to and after re-addition of extracellular Ca²⁺, respectively. (B) Neurons were exposed to oxygen-glucose deprivation (OGD) conditions (a glucose-free bath solution continuously bubbled with N₂) and changes in [Ca²⁺]_i were determined from [Ca²⁺]_i measured 0 min and 90 min after start of OGD, respectively. Figure was kindly provided by Dr. Robert Kraft, Leipzig. *p<0.05.

These data argue for a critical role of Orai2 as SOC channel component in neurons, because mice deficient in Orai2 were significantly protected from ischemia-induced neuronal damage, and Ca²⁺ influx was impaired in isolated neurons. Neurological studies are currently ongoing in collaboration with the above mentioned research groups and will provide new insights into this novel, previously unidentified role of Orai2.

4 Discussion

Arterial thrombosis and the resulting ischemic cardio- and cerebrovascular events are major causes of death and disability worldwide.¹²³ However, the use of established antithrombotic drugs has always been associated with elevated bleeding risk.¹²⁴ Therefore, the development of new therapeutic options is highly desirable. Advances in understanding of platelet receptor signaling and regulation may lead to discovery of novel targets for antithrombotic drug development. In recent years, genetic methods that enable targeted manipulations of the mouse genome have opened new ways to study protein function and to unravel signaling pathways in platelets both *in vitro* and *in vivo*.¹⁸¹ It is important to point out that some differences in expression or function of platelet proteins exist between humans and mice. Nevertheless the knowledge obtained from the mouse system may serve as a basis for the development of new antithrombotic therapies for humans.

In this thesis, function and regulation of the SLAM family member CD84 were studied. Since CD84 was known to be expressed in platelets and immune cells, studying this receptor appeared not only interesting in the context of its function in thrombus formation, but also in its role in the development of ischemic stroke. In this pathophysiological disease state, earlier studies using the tMCAO model in mice have revealed pivotal roles of platelets and immune cells for infarct progression.^{125,139} In the work presented here, CD84 deficient mice were generated and analyzed. The novel data revealed that, surprisingly, CD84 does not play a critical role in thrombosis and hemostasis but is of pathophysiological relevance in ischemic stroke. Additionally, novel regulatory mechanisms involving extra- and intracellular cleavage were shown to facilitate downregulation of CD84 from platelets in response to platelet activation. The presence of cleaved CD84 in murine plasma indicated an *in vivo* relevance of the newly discovered CD84 regulation in platelets.

The platelet collagen receptor GPVI has been proposed as a promising antithrombotic target, since “immunodepletion” of the receptor by administration of the monoclonal anti-GPVI antibody JAQ1 leads to protection from arterial thrombosis in mice without severe side effects.⁴¹ Earlier studies demonstrated that depletion of GPVI is mediated by internalization as well as metalloproteinase-dependent ectodomain shedding,⁴⁸ but the identity of the metalloproteinase(s) remained elusive. Results from the current study showed that GPVI shedding is differentially regulated by two metalloproteinases *in vitro*. Shedding of GPVI still occurred *in vivo* upon injection of the monoclonal anti-GPVI antibody JAQ1 in mice that carried a double-deficiency of these two metalloproteinases in their platelets, suggesting the involvement of a third, unidentified (metallo-)proteinase in this process.

Store-operated calcium entry is established as the most ubiquitous way of regulated Ca^{2+} entry in mammalian cells. Previous studies established STIM1 as an essential Ca^{2+} sensor and Orai1 as the major store SOC channel in platelets.^{22,23} The Ca^{2+} sensor STIM2 is the main STIM isoform in brain, but the corresponding SOC channel was unknown.¹⁵³ In the last part of this thesis, Orai2 deficient mice were generated and analyzed. The novel data demonstrated that Orai2 is dispensable in platelets, but revealed for the first time a role of Orai2 for SOCE in neurons. Further data indicated that Orai2 may represent a future target for stroke therapy.

4.1 Analysis of CD84 deficient mice

In the present study, CD84 deficient mice were generated by targeting of the *Cd84* gene in a 129/Sv ES cell line. Loss of the CD84 protein was confirmed by Western blot (Figure 10) and flow cytometry (Figure 11). CD84 deficient mice were born in Mendelian ratio, were fertile, and did not display any obvious abnormalities. Basal hematologic parameters were unaltered compared to wt controls, and cell fractions in thymus, lymph nodes and spleen were also unaltered (Figure 12, Figure 13). This is in line with another recent study by Cannons *et al.* reporting on the generation of CD84 deficient mice, where a different ES cell line (C57BL/6) was used for ko mouse generation.⁸⁴ These mice also did not display abnormalities in development or cellularity of lymphoid organs.

4.1.1 CD84 is dispensable for platelet function in thrombosis and hemostasis

CD84 expression in platelets has been reported in earlier studies,^{51,77} but its role in platelet activation and thrombus formation has been elusive. Nanda *et al.* detected tyrosine phosphorylation of CD84 in response to platelet aggregation.⁵¹ One of the two phosphorylated cytoplasmic tyrosines was found in an ITSM motif, a putative recognition motif for the adaptor proteins SAP and EAT-2. These adaptor molecules were both detected in mouse platelets by Western blot. When aggregation was blocked using an $\alpha\text{IIb}\beta\text{3}$ inhibitor, no tyrosine phosphorylation of CD84 was detected. Consequently, CD84 was proposed as aggregation-induced signaling receptor that synergizes with integrins to mediate platelet thrombosis. In the same study, Nanda *et al.* detected tyrosine phosphorylation of CD150 (SLAM) in response to platelet aggregation. As for CD84, this CD150 phosphorylation was prevented in presence of an integrin blocker. In addition, the authors reported that CD150 deficient female mice displayed a delay in thrombus formation in a FeCl_3 -induced thrombosis model in mesenteric arteries. Tail bleeding times were normal, but CD150 deficient platelets displayed weaker aggregation in response to collagen and a thrombin receptor activating peptide. Nanda *et al.* then proposed CD84 and CD150 as novel receptors in their new

concept of the “platelet synapse”. This is initiated by platelet-platelet proximity, mediated by $\alpha\text{IIb}\beta\text{3}$ -induced aggregation, in analogy with the lymphocyte synapse induced during immune responses.²⁶ Importantly, CD84 has recently been demonstrated to be crucial for sustained B cell: T cell interaction, which is also primarily integrin dependent.⁸⁴ Taken together, CD84 and CD150 were proposed to stabilize thrombi in response to platelet aggregation.⁵¹ SLAM family members were also suggested to represent novel targets for antithrombotic drug discovery.²⁶ However, Nanda *et al.* only reported on the phenotype of mice deficient in CD150 in their study, and mice deficient in CD84 were not available at that time.⁵¹

The current thesis provides the first analysis of CD84 deficient platelets. Except a slightly elevated platelet size, *Cd84*^{-/-} platelets did not display any abnormalities. Platelet production, as well as activation parameters in response to various agonists were unaltered (Figure 15). CD84 was proposed as an aggregation-induced co-receptor which may stabilize thrombi,²⁶ but aggregation of washed *Cd84*^{-/-} platelets *in vitro* did not reveal any defect (Figure 16), indicating that CD84 has no major role in platelet aggregation *in vitro*. This was different from CD150 deficient platelets, which displayed defective aggregation in response to collagen or TRAP in the study by Nanda *et al.*⁵¹ Spreading of platelets on ECM proteins requires integrin outside-in signaling.¹⁷¹ This was obviously not affected in *Cd84*^{-/-} platelets, because they were able to fully spread. Thrombus formation at different shear rates under flow *ex vivo* (Figure 19) indicated that lack of CD84 does not affect platelet aggregate stability, even under conditions of high shear. This was also observed for thrombus formation *in vivo*, where *Cd84*^{-/-} mice formed stable occlusive thrombi (Figure 21 and Figure 20). This differs in part from the observations that were made by Nanda *et al.* in CD150 deficient mice. Female *Cd150*^{-/-} mice displayed a defect in stable aggregate formation *in vivo* and this sex-specific defect was attributed to differences in the vasculature between male and female mice.⁵¹ Unaltered tail bleeding times (Figure 22) indicated that CD84 is not essentially involved in primary hemostasis.

In conclusion, CD84 is of minor relevance for thrombus formation, at least under the conditions studied here. It is conceivable that there is a potential redundancy between the SLAM family members CD84 and CD150. Lack of CD84 may be fully compensated by CD150. In light of the study by Nanda *et al.*,⁵¹ who found weaker aggregation of CD150 deficient platelets, CD150 might be more important for thrombus formation than CD84. Potential cooperation of SLAM family members has also been shown for stabilization of T cell:B cell contacts, where both CD84 and Ly108 participate,⁸⁴ however both appeared to participate equally in this setting. The generation of CD84/CD150 double-deficient mice to study the effect of lack of both of these SLAM family members in platelets, however, is hardly feasible. As depicted in Figure 3, CD84 and CD150 are localized in a syntenic genomic

region closely together on the same chromosome. Obtaining double-deficient mice by intercrossing of CD84 deficient and CD150 deficient mice would require a very unlikely chromosomal crossing over. On the other hand, it is also conceivable that CD84 acts as a negative regulator of thrombus formation. In mast cells, homophilic interaction of CD84 has been shown to negatively regulate Fc ϵ RI signaling.¹⁸² Later, this inhibitory mechanism was found to be independent of SAP and EAT-2, but dependent on the inhibitory kinase Fes.⁸⁶ Whether there is a SAP and EAT-2 independent role of CD84 in platelets has not been addressed. It cannot be completely ruled out that CD84 negatively influences thrombus stability, because the effect of CD84 deficiency might be rather weak and hardly detectable. One example of an inhibitory receptor that signals through an ITIM is PECAM-1, but deficiency of this receptor was found to have only minimal effects on platelet activity.¹⁸³ Potentially also a compensation by other inhibitory signaling receptors may occur in CD84 deficient mice.

In summary, the data from this thesis indicate that CD84 in platelets is dispensable for thrombosis and hemostasis. CD84 in platelets may serve other, yet unidentified functions. Given the fact that CD84 is broadly expressed in immune cells and platelets, it is tempting to speculate that interaction of platelets with immune cells via CD84 plays a role at sites of inflammation. There are several prominent examples of platelet receptors that have been described to mediate interaction with leukocytes, thereby assisting and modulating inflammation.¹⁸⁴ The interaction of platelet P-selectin with PSGL-1 (P-selectin glycoprotein ligand-1), contributes to recruitment of neutrophils and other immune cells to inflamed tissue.¹⁸⁵ Platelet CD40L can bind to CD40, which is expressed on B cells, monocytes, macrophages and dendritic cells. This interaction induces inflammatory and immune responses.¹⁸⁶ The platelet receptor GPIIb α can bind to a variety of ligands, including Mac-1 (CD11b/CD18) in leukocytes. This interaction may lead to recruitment of leukocytes to thrombotic sites.¹⁸⁷ The complex process of atherosclerotic lesion formation involves lymphocyte infiltration and several lines of evidence suggest that platelet adhesion to the arterial wall initiates this process.¹⁸⁸ Recent experimental data showed that multiple platelet adhesion molecules contribute to lymphocyte adhesion under arterial flow conditions.¹⁸⁹ It remains to be addressed, whether CD84 on platelets is among the molecules that contribute to recruitment of immune cells to sites of inflammation or vascular injury, but in light of its broad expression on immune cells, this appears to be possible.

4.1.2 Loss of CD84 provides protection from ischemic stroke

Stroke is a major cause of death and disability worldwide.¹²³ Arterial occlusion resulting in focal cerebral ischemia accounts for approximately 80% of strokes.¹²⁵ Since platelets as well as immune cells represent critical cell types that influence stroke outcome in experimental mouse models,^{45,139} ischemic stroke has recently been proposed to be a complex thrombo-inflammatory disease.^{129,177} The signaling and adhesion events that are involved in microvascular thrombus formation and immune cell activation in the ischemic brain are still incompletely understood. CD84 is broadly expressed in platelets and immune cells, but the role of the receptor in the development of ischemic stroke has been unclear.

Remarkably, deficiency of CD84 in mice led to significant protection from infarct progression in the tMCAO model (Figure 34A and B). Earlier studies revealed the involvement of platelet adhesion receptors GPIb and GPVI in the development of ischemic lesions. Inhibition of these receptors by *in vivo* administration of Fab fragments or antibodies, respectively, led to protection in the tMCAO model.⁴⁵ The interpretation of the novel tMCAO data on CD84 deficient mice was more complex, as it was unclear whether deficiency of CD84 in platelets or other cell types led to the protective effect. The smaller infarct sizes in *Cd84*^{-/-} mice could be caused by impaired immune cell adhesion to the endothelium or reduced infiltration into brain parenchyma following ischemia. Notably, no significant differences in number of neutrophils or CD11b⁺ leukocytes were found in brain sections of wt and *Cd84*^{-/-} mice (Dr. Peter Kraft, data not shown). Smaller infarct sizes in *Cd84*^{-/-} mice can also be due to reduction of necrotic or apoptotic brain cells. Inflammatory cytokines, such as TNF- α and IFN- γ can lead to apoptosis in cells of the ischemic brain.¹⁷⁸ Importantly, significantly reduced expression of these inflammatory cytokines was revealed in cortices of *Cd84*^{-/-} mice 24 h after tMCAO, compared to controls (Figure 34C). Less TNF- α and IFN- γ gamma production in absence of CD84 is in agreement with findings by several authors. Cannons *et al.*⁸⁴ detected reduced IFN- γ gamma production in stimulated *Cd84*^{-/-} T cells. Another study demonstrated reduced TNF- α production after LPS stimulation when CD84 was knocked down in bone marrow derived macrophages.⁸³ Accordingly, Martin *et al.* found that CD84 ligation enhances IFN- γ secretion in lymphocytes.⁸¹ In the setting of ischemic stroke, reduced levels of proinflammatory cytokines may lead to reduced tissue necrosis,¹³⁸ reduced apoptosis, but also less activated cerebrovascular endothelium.¹⁷⁸ The beneficial effects of weaker endothelial activation may also include less platelet adhesion. IFN- γ has been described as a mediator of inflammatory and thrombogenic responses in the postischemic brain microvasculature.¹³⁸ TNF- α can be produced by mast cells and macrophages, but also by T cells¹³⁷ and there is increasing evidence in the literature that T cells exert detrimental effects in ischemic stroke.^{139,178} In the acute phase of ischemic stroke, unprimed T cells

contribute to damage in an antigen-independent manner.¹³⁷ Adoptive transfer experiments of wt or *Cd84*^{-/-} CD4⁺ T cells into *Rag1*^{-/-} mice revealed that CD84 in T cells significantly influenced ischemic stroke outcome. Since it has remained unclear whether CD84 in other cell types, e.g. in platelets, was required as ligand for CD84 in wt T cells, adoptive transfer experiments with *Cd84*^{-/-} mice as recipients were performed. Unexpectedly, wt T cells restored susceptibility to ischemic stroke after tMCAO in *Cd84*^{-/-} mice, whereas *Cd84*^{-/-} T cells induced smaller infarcts (Figure 35).

Taken together, a T cell intrinsic phenotype was revealed in CD84 deficient mice in ischemic stroke. However, adoptive transfer experiments suggested that homophilic interaction of CD84 on platelets and T cells appeared not to be functionally relevant in the setting of ischemic stroke. CD84 in T cells might bind to another, yet unidentified ligand on platelets, and this interaction is disrupted by T cell-specific CD84 deficiency. As another explanation, an unknown ligand of CD84 might be present on endothelial cells. Absence of CD84 in T cells may lead to abolished interaction with this postulated ligand, and therefore T cells may be less stimulated and less cytokines might be produced. This is, however, highly speculative and must be proved experimentally by cytokine measurements in mice with transferred T cells. In light of recently published findings that also regulatory T cells (Tregs) are detrimental in experimental ischemic stroke,¹⁴⁰ it will be interesting to study whether CD84 is relevant in Tregs. Lymphocytes adhere to platelets but also to endothelial cells during the reperfusion phase after tMCAO. These interactions can lead to obstruction of blood flow in cerebral microvessels. The recent study on the role of regulatory T cells in ischemic stroke demonstrated that blockade of LFA-1 interaction with ICAM-1 on the endothelium leads to less adhesion of Tregs under ischemic conditions, reduced intravascular thrombosis and improved tissue reperfusion.¹⁴⁰ Whether CD84 is involved in such processes remains to be determined and the question remains, whether T cell CD84, which has been described to undergo homophilic interaction, can bind to other unknown ligands present in platelets or endothelial cells.

It is tempting to speculate that pharmacological blockade of CD84 may become a future option for treatment of ischemic stroke. At least loss of CD84 on T cells was found to provide protection from ischemic stroke in the tMCAO model. It is unclear whether CD84 binds to an unknown ligand on the endothelium or on platelets, but blockade of this postulated interaction might be protective. Blockade of the platelet receptor GPIb by injection of mice with p0p/B Fab fragments led to 60% reduction of infarct size in the tMCAO model,⁴⁵ and this effect was preserved even when GPIb α blockade was induced 1 h after tMCAO. GPIb has several binding partners besides vWF (Mac-1, Factor XII, P-selectin)¹⁸⁷ and the relevance of different binding partners in ischemic stroke is not fully understood yet. Mice deficient in

Mac-1 were also less susceptible to cerebral ischemia/reperfusion injury.¹⁹⁰ Therefore, it was speculated that the interaction of platelet GPIb with Mac-1 might recruit leukocytes to sites of thrombosis after cerebral ischemia.¹²⁵

Even though the molecular interactions of CD84 in ischemic stroke are not fully understood, therapeutic blockade of CD84 might provide protection from ischemic stroke, comparable to the observed protection in CD84 deficient mice. Therefore, CD84 rather seems to be a target for stroke therapy than a target for antithrombotic therapy, which was originally proposed by Nanda *et al.*²⁶ Given that the CD84 deficient mice generated in this thesis did not display obvious abnormalities, short term pharmacological blockade of CD84 might be feasible for stroke therapy. The findings from Cannons *et al.*, who also reported that their CD84 deficient mice were healthy and only displayed a specific defect in long term immunity,⁸⁴ support the notion that short term CD84 blockade may be applicable without inducing perturbing effects on immunity. Even though data gained in the mouse stroke model cannot be directly transferred to the human situation, these findings may serve as a basis for the development of novel stroke therapeutics.

4.2 Regulation of CD84 in platelets by ADAM10 and calpain

A recent study on human platelets provided first evidence that platelet CD84, among several other platelet receptors, is regulated in a metalloproteinase-dependent manner.⁹⁶ However, the mechanism of CD84 receptor regulation remained unknown. Here, studies on human and mouse platelets were performed to elucidate the mechanism of CD84 receptor regulation. The experimental data revealed that CD84 is regulated by two distinct proteolytic mechanisms in platelets: metalloproteinase-dependent ectodomain shedding and calpain-mediated cleavage of the intracellular C-terminal domain. ADAM10 was established as the principal sheddase to mediate CD84 cleavage under all tested conditions, whereas ADAM17 did not play a significant role in this process (Figure 26). This was surprising, since other studies have shown that prominent platelet receptors are either cleaved only by ADAM17 (GPIb α , semaphorin 4D)^{88,93} or by ADAM10 and ADAM17, depending on the shedding-inducing stimulus (GPV, GPVI).^{97,173} Importantly, ADAM10 also appeared to be the only protease to mediate CD84 ectodomain shedding in clotting blood suggesting that even under conditions of maximal agonist receptor stimulation no other proteinase can cleave the receptor, at least in mouse platelets. In contrast, Fong *et al.* observed a significant reduction of CD84 shedding in human platelets in the presence of a putatively selective ADAM17 inhibitor, but it was not analyzed in detail whether ADAM10 activity was also affected by this

inhibitor.⁹⁶ Additional studies are necessary to elucidate whether there are minor differences in the substrate selectivity of ADAM family sheddases between mouse and human platelets.

Furthermore, consistently low amounts of sCD84 were detected in the supernatant of unstimulated wt, but not *Adam10*^{-/-} or GM6001-treated platelets. Together with the elevated sCD84 plasma levels of wt compared to *Adam10*^{-/-} mice, this strongly suggests that CD84 is continuously shed from the platelet surface by ADAM10, similar to the described constitutive shedding of GPIb α by ADAM17.⁸⁸ Residual sCD84 levels in plasma of *Adam10*^{-/-} mice might be due to shedding from other cell types or trans-shedding of platelet CD84 by non-platelet ADAM10. The high basal sCD84 levels in plasma of wt mice indicated that its use as a marker of thrombotic/inflammatory activity might be limited. Additional sCD84, which might be locally generated upon platelet activation *in vivo*, e.g. during thrombotic events, might not lead to a significant elevation in the systemic plasma concentration above the basal level. Measurements of sCD84 in murine plasma after local thrombotic events, e.g. after injury of the abdominal aorta, did not reveal elevated levels as compared to sham-treated mice (data not shown). The use of sCD84 as a biomarker in ischemic stroke is still questionable. In plasma samples of healthy human volunteers, no significant levels of CD84 in plasma could be detected. It is important to mention that factors in human plasma might mask sCD84, at least in the ELISA system used here, since supernatant of NEM-stimulated platelets yielded lower ODs when diluted in plasma, compared to buffer (data not shown). One receptor which may serve as diagnostic biomarker in the future is GPVI, because it is cleaved from human platelets after its stimulation.⁹⁰ Elevated levels of sGPVI were detected in patients with ischemic stroke¹⁹¹ and another study revealed elevated levels of sGPVI in response to pathologic shear.¹⁹² It will be interesting to study whether sCD84 is elevated in patients with thrombotic events, but this requires the establishment of a new sensitive ELISA system for human sCD84.

As mentioned above, high basal levels of sCD84 were detected in plasma of wt mice. Glycocalicin, the shed extracellular fragment of GPIb α , is another platelet receptor fragment that has likewise been detected in considerable amounts in plasma of normal healthy mice¹⁹³ and is also not a sensitive marker of platelet activity. In addition, it cannot be excluded that sCD84 in plasma is just derived from aging platelets, with CD84 being cleaved from the platelet surface, before old platelets are cleared from the blood stream. However, this is just speculative and further experiments on CD84 levels during platelet aging are required to answer this question. Earlier studies from our laboratory demonstrated that GPIb α levels decrease during platelet aging *in vitro* and proposed GPIb α surface levels as a marker for quality of human platelet concentrates for transfusion.¹⁹⁴ Similarly, CD84 surface expression

on human platelet concentrates might represent a potential quality marker for transfusion, but this remains to be addressed in future studies.

Treatment of platelets with the calmodulin inhibitor W7 induced strong shedding and calpain-dependent degradation of the C-terminal part of CD84, indicating that CD84 is a calmodulin-binding protein. The platelet receptors GPVI,⁹⁸ GPIIb β and GPV¹⁹⁵ bind calmodulin by their positively charged, membrane-proximal sequences within their cytoplasmic domains. By analyzing sequence data of the murine as well as the human CD84 C-terminus, positively charged, membrane-proximal sequences were also found, further supporting the hypothesis that CD84 is a calmodulin-binding protein. Calpain-mediated cleavage of the C-terminus may attenuate or completely terminate signaling. Calpain-mediated intracellular receptor downregulation in platelets has been described for PECAM-1,¹¹² Fc γ RIIa¹¹¹ and the β 3 integrin subunit.¹¹⁰ This study clearly shows a dual regulation of CD84 by ADAM10 and calpain and both processes can occur independently of each other (Figure 25). Calpain was able to cleave both the full length protein, as well as the C-terminal remnant that is generated by ADAM10 activity. Although it is recognized that stimuli inducing extracellular shedding also have the potential to activate intracellular calpain cleavage^{12,196} this is the first study showing that a single platelet receptor is simultaneously targeted by calpain and a metalloproteinase in response to a single stimulus (W7 or RC). It has been shown in cell culture experiments, e.g. for IL6R,¹⁹⁷ that γ -secretase-mediated cleavage of the C-terminal protein remnant can occur subsequent to ADAM-mediated ectodomain shedding, leading to degradation of the remnant. The data in the current thesis indicate, however, that this mechanism does not play a role for the degradation of the C-terminal remnant of platelet CD84, since calpeptin, an inhibitor of calpain, was sufficient to inhibit the degradation.

Platelet receptor shedding has been proposed as a mechanism to regulate principal platelet functions, e.g. by modulation of adhesive properties or modification of receptor signaling, thereby regulating thrombus growth and stability.¹⁹⁶ Ectodomain cleavage could limit the response to agonists, and concomitantly release soluble receptor fragments into the plasma, which may have a role as regulators of distinct biological functions.¹² Shedding of CD84 could be of specific relevance in this context, because of its broad expression on platelets and immune cells and its ability to undergo homophilic interaction.⁵⁶ As recently shown, CD84 stabilizes B cell:T cell interaction.⁸⁴ Therefore, it is tempting to speculate that sCD84 of platelet origin might have the potential to modulate immune cell interactions, but this needs further investigation.

Several functional roles are conceivable for extracellular CD84 cleavage. First, ectodomain shedding may downregulate platelet reactivity by lowering surface density of receptors, thus

attenuating signaling and decreasing platelet-matrix contacts.¹² For CD84 this may be true, as it might be a receptor that contributes to thrombus stability, acting in concert with other stabilizing receptors. However, loss of CD84 may not become evident in thrombosis and hemostasis models, since loss of this receptor might be compensated by other receptors. The data from the first part of this thesis support this notion. On the other hand, soluble receptor fragments generated by shedding may have stimulatory or antagonistic functions. An antagonistic role of receptor ectodomains was shown for Sema4D, because the soluble bioactive fragment impaired monocyte migration.⁹³ Similarly, soluble JAM-A exhibited antagonistic effects, by blocking migration of endothelial cells and reducing transendothelial migration of neutrophils.⁹⁴ Stimulatory effects of soluble receptor fragments have been described, e.g. for Sema4D, which can evoke angiogenic responses of endothelial cells.⁹³ Whether soluble CD84 acts in a stimulatory or antagonizing manner on other cell types remains to be determined. Shedding of platelet receptors may also downregulate the inflammatory potential of platelets, as proposed for P-Selectin.⁸⁷ Similarly, ectodomain shedding of CD84 in platelets may also play a role in resolution of inflammation. It could be that homophilic interaction of CD84 on platelets and leukocytes promotes initial phases of platelet-immune cell interaction. Shedding of CD84 on platelets might subsequently dampen these processes, providing a layer of regulation that prevents overshooting immune reactions. Since CD84 is expressed in neutrophils,⁷⁸ shedding of platelet CD84 may dampen platelet-neutrophil interaction, a process wherein platelets have been described as amplifiers of acute inflammation.¹⁸⁵

In summary, the surface expression of the SLAM family receptor CD84 is tightly regulated by two proteolytic mechanisms involving ADAM10 and calpain and ectodomain shedding of CD84 constitutively occurs *in vivo* through ADAM10. Several functional roles of CD84 shedding are conceivable. It appears possible that the receptor is of functional importance in platelet-immune cell rather than in platelet-platelet interactions. Shedding of CD84 on platelets might therefore represent a novel mechanism to regulate such interactions. Future studies on platelet-immune cell interaction in *Cd84*^{-/-} mice will be required to better understand the role of this receptor in thrombotic, inflammatory, and/or immunologic processes.

4.3 Regulation of GPVI by ADAM10 and ADAM17

Metalloproteinase-dependent shedding has been established as a mechanism to regulate surface expression of the central platelet-activating collagen receptor GPVI. Based on recent experimental evidence, ADAM10 was proposed as the GPVI-cleaving enzyme.⁹⁷ Downregulation of GPVI occurs in mice after injection of the monoclonal antibody JAQ1,⁴¹

and antibody-induced loss of GPVI has also been reported in human patients with autoantibodies.^{46,47} Importantly, in JAQ1-treated mice, as well as in patients with autoantibodies against GPVI, only a mild bleeding disorder was observed. Further, JAQ1-treated mice were protected from intravascular thrombosis,⁴¹ making GPVI downregulation a potential antithrombotic approach. Alternatively, selective activation of platelet metalloproteinases might result in reduction of GPVI levels and lead to protection from undesired platelet activation. So far, it was unclear whether only one or several platelet metalloproteinases mediate GPVI ectodomain cleavage.

To explore GPVI shedding in platelets, different metalloproteinase deficient mice were used. The novel findings indicated complex regulation of GPVI involving differentially activated metalloproteinases, which may represent novel molecular targets for therapy in patients with increased risk of thrombosis. In response to W7 treatment of platelets *in vitro*, GPVI was found to be cleaved by ADAM10, confirming previous data on GPVI-based peptides by Gardiner *et al.*⁹⁷ In addition, ADAM17-dependent shedding occurred after treatment with CCCP (Figure 29), providing the first evidence that GPVI can be differentially regulated by two different metalloproteinases. In contrast, CD84 ectodomain shedding was exclusively mediated by ADAM10 (Figure 26) and in addition, calpain-mediated intracellular cleavage of CD84 was revealed. However, it is unlikely that GPVI is also regulated by calpain, since in contrast to CD84, Western blots using an antibody against the N-terminus of GPVI (JAQ1) did not reveal a shift in the molecular weight of GPVI in response to different stimuli (e.g. Figure 29C). Studies on platelets that lack both ADAM10 and ADAM17 revealed that these two metalloproteinases are the only enzymes that mediate GPVI ectodomain shedding *in vitro* (Figure 31). Unexpectedly, however, *in vivo* administration of JAQ1 induced GPVI downregulation from the surface of *Adam10*^{-/-}/*Adam17*^{ex/ex} platelets which was comparable to the downregulation of GPVI in wt controls. Similar levels of soluble GPVI were detected in plasma of both groups of mice (Figure 32). In conclusion, antibody-induced ectodomain shedding of GPVI *in vivo* requires other or additional mechanisms, compared to GPVI shedding *in vitro*.

ADAM10 and/or ADAM17 present in other cell types might cleave GPVI from the platelet surface (trans-shedding). This possibility cannot be excluded since mice with a platelet-specific ADAM10 deficiency and lack of functional ADAM17 only in the hematopoietic system were used. However, given the high numbers of platelets in the blood stream of mice ($\sim 10^6$ / μL) and the rapid time course and high efficiency of antibody-induced GPVI shedding *in vivo*, this can be considered rather unlikely. As an alternative explanation, another unidentified metalloproteinase in platelets may cleave GPVI *in vivo* and this process requires further signals which are not present in isolated platelets *in vitro*. This notion is supported by the

observation that the kinetics and the extent of JAQ1-induced GPVI shedding in the double-mutant mice were comparable to the wt control, indicating that neither ADAM10 nor ADAM17 play a major role in this process. ADAM9 in platelets is a candidate enzyme which might be able to shed GPVI, since it is a catalytically active metalloproteinase which is expressed in various tissues and highly conserved between species.¹⁹⁸ However, platelets also express many other proteases, including matrix metalloproteinases, which could potentially mediate GPVI cleavage. Notably, JAQ1-induced GPVI downregulation in murine platelets occurs efficiently *in vivo*,⁴¹ but not *in vitro*. Comparable observations have been reported for human platelets in a NOD/SCID mouse model.¹⁹⁹ These observations indicate that the antibody-induced activation of the GPVI sheddase(s) requires a costimulus that is present *in vivo* but not *in vitro*. On the other hand, studies from our research group previously showed that the GPVI signaling pathway via LAT and PLC γ 2 is required for JAQ1-induced GPVI shedding *in vivo* and this is associated with a transient thrombocytopenia.⁴⁸ It is still unclear whether the activation of metalloproteinases is mechanistically linked to the thrombocytopenia but the data shown here clearly exclude a role of ADAM10 or ADAM17 in this process.

Taken together, our data demonstrated that GPVI can be differentially regulated *in vitro* by ADAM10 and ADAM17 depending on the shedding-inducing stimulus. Additionally, indirect evidence for the existence of a third GPVI cleaving enzyme in platelets that has the capacity to efficiently mediate antibody-induced “therapeutic” GPVI downregulation *in vivo* has been provided. These data may provide a basis for development of anti-GPVI agents, which may be used for treatment of thrombotic and inflammatory diseases.²⁰⁰

Notably, differential effects of antibodies against CD84 or GPVI were observed upon *in vivo* administration, demonstrating that not all platelet receptors are amenable to antibody-induced downregulation. While JAQ1 injection induced rapid downregulation of GPVI from the platelet surface, injection of JER1 antibody did not lead to downregulation of CD84. Instead, the receptor was occupied by the antibody for several days, as detected by anti rat-IgG-FITC *ex vivo*. On the other hand, considerable amounts of sCD84 were detected in plasma of untreated wt mice, but sCD84 levels were lower in mice with a platelet specific ADAM10 deficiency. Thus, constitutive shedding of CD84 by ADAM10 *in vivo* was proposed. These findings underscore that for each regulated platelet receptor, several factors synergize that determine their usefulness as antithrombotic or anti-inflammatory target, like metalloproteinase selectivity, constitutive shedding, and amenability to selective depletion by specific antibodies.

4.4 Orai2 deficiency protects from ischemia-induced neuronal damage

SOCE is established as the most ubiquitous way of regulated Ca^{2+} entry in mammalian cells and is not only important for replenishment of ER Ca^{2+} stores, but also controls diverse processes like lymphocyte activation and cell proliferation.¹⁴³ With the identification of STIM1 as the principal ER Ca^{2+} sensor^{144,145} and Orai1^{146,147} as critical SOC channel pore subunit in several independent studies in 2005 and 2006, great progress in understanding the molecular mechanisms of SOCE has been made. STIM2 is another Ca^{2+} sensor residing in the ER. It was shown to activate SOCE upon smaller decreases of ER Ca^{2+} levels and to regulate basal cytosolic and ER Ca^{2+} levels in eukaryotic cells.¹⁵² In contrast, the function of Orai2 is not well explored, with only a few data on immune cell expression being available. While Orai1 was described as essential SOC channel component in human T cells,¹⁴⁶ studies by Vig *et al.*¹⁵⁷ indicated that rather Orai2 and Orai3 might be essential in mouse thymocytes. In contrast, Gwack *et al.*¹⁸⁰ revealed an essential role for Orai1 in mouse T cell SOCE. However, in the same study, Orai2 was supposed to be able to compensate to a certain degree for the loss of Orai1, since SOCE was not completely abolished in Orai1 deficient T cells. In a recent study, Orai2 was shown to interact selectively with STIM2 upon store depletion in mouse dendritic cells,¹⁵⁸ indicating a cell type specific use of Orai molecules. However, studies published so far have used either transfection methods in cultured cells or semiquantitative methods to investigate channel properties or expression levels of Orai2 in cells and on tissue level. No *in vivo* studies have been available so far.

This thesis provides the first description of Orai2 deficient mice. *Orai2*^{-/-} mice were born in a Mendelian ratio, developed normally, and were healthy and fertile. Deficiency of Orai2 was proved on mRNA level (Figure 38), since antibodies available were unsuitable for Western blot (not shown). In contrast to STIM2 deficiency, where mice had a reduced life expectancy, due to unknown reasons and female mice displayed lactation problems,²⁰¹ Orai2 deficient mice did not display any of these abnormalities. Further, in *Stim2*^{-/-} mice a pronounced cognitive defect became apparent.¹⁵³ Whether subtle differences in cognitive abilities exist between wt and *Orai2*^{-/-} mice, needs to be tested in behavioral studies. Tests like the Morris Water Maze Task,²⁰² a standard test for hippocampus-dependent spatial memory, will be performed in the future.

Orai1 is essential for SOCE in platelets,²³ but residual Ca^{2+} influx was detected in Orai1 deficient platelets, suggesting Orai2 to be a candidate that facilitates this residual Ca^{2+} influx. Orai2 has been shown to be expressed at low levels in platelets from mice and humans, however the studies performed in this thesis indicated that Orai2 does not to play an essential role in platelets. Platelets from Orai2 deficient mice were normal in number and size and had normal expression of prominent platelet glycoproteins (Figure 39). *In vitro*,

Orai2^{-/-} platelets displayed normal activation and degranulation induced by different G-protein coupled and (hem)ITAM receptor coupled agonists (Figure 40). This is in sharp contrast to *Orai1*^{-/-} platelets, which displayed defective activation and degranulation in response to ITAM coupled receptor stimulation.²³ Further, *Orai2* deficient mice displayed unaltered arterial thrombus formation and hemostasis was also not impaired (Figure 41). Thus the relevance of SOCE through *Orai2* in platelets is negligible, and/or the observed residual Ca²⁺ influx in *Orai1* deficient platelets²³ may be due to non-SOCE, which for example can be triggered by TRPC6 channel activation by DAG.²⁰³ In conclusion, *Orai2* is not required for platelet activation *in vitro* and thrombus formation *in vivo*. This supports previous studies,²³ which concluded that *Orai1* is the most relevant *Orai* isoform in platelets.

However, *Orai2* deficient mice were protected from ischemic stroke, since infarct volumes were significantly smaller and overall neurological functions were significantly better as compared to wt controls (Figure 42A,B). The mechanisms that contribute to neuronal damage in response to ischemic stroke are complex and only partly understood. Ca²⁺ overload is a common mechanism contributing to neurodegeneration in ischemia. Mechanisms that lead to Ca²⁺ overload include excessive release of the neurotransmitter glutamate, referred to as glutamate excitotoxicity.¹²⁷ Glutamate is the major excitatory neurotransmitter in the mammalian central nervous system. Following glutamate release, postsynaptic responses occur through both metabotropic and ionotropic receptors, like the N-methyl-D-aspartate (NMDA) receptor and some 2-amino-3-(3-hydroxy-5-methylisoxazol-4-yl) proprionate receptors (AMPA). Metabotropic receptors mediate their actions through GTP-binding-protein-dependent mechanisms that cause mobilization of Ca²⁺ from internal stores.²⁰⁴ Ca²⁺ release from the ER can occur in neurons via IP₃ receptors, which are ubiquitously expressed, and via ryanodine receptors (RyR), which are found in neurons and muscle cells.²⁰⁵ So far, most knowledge about SOCE has been gained from non-excitabile cells. SOCE, frequently referred to as CCE (capacitive calcium entry) also plays an important physiological role in many, but not all excitable cells where it is important for the generation of cytoplasmic Ca²⁺ signals with cell-specific functions.²⁰⁶ A recent study from our laboratory provided first compelling evidence that SOCE in neurons significantly contributes to neuronal cell death under ischemic conditions, as *STIM2* deficient mice were shown to be protected from ischemic stroke and isolated neurons displayed reduced Ca²⁺ influx and elevated survival upon conditions of oxygen-glucose deprivation, as compared to wt.¹⁵³ In light of the findings of the current thesis and the previously published data on *STIM2*, it appears likely that *STIM2* and *Orai2* form the Ca²⁺ sensor-SOC channel unit in neurons. This idea is supported by early studies from Parvez *et al.*, already providing evidence that the Ca²⁺ sensor *STIM2* can also couple to *Orai2* and *Orai3*.²⁰⁷ The protection of *Orai2*^{-/-} mice from

ischemic stroke in the tMCAO model (Figure 42A,B) strongly suggested that SOCE is significantly involved in pathological Ca^{2+} accumulation in ischemic neurons. In accordance, Ca^{2+} measurements performed in collaboration with Dr. Robert Kraft (University of Leipzig) clearly demonstrated that *Orai2* significantly contributes to SOCE in neurons. In addition, *Orai2* deficient neurons displayed significantly less Ca^{2+} influx in response to oxygen-glucose deprivation (Figure 43). Interestingly, store depletion with the SERCA pump inhibitor CPA in cortical neurons in the absence of extracellular Ca^{2+} suggested that *Orai2*^{-/-} neurons had reduced Ca^{2+} store content. This implies the question whether *Orai2* also facilitates the Ca^{2+} store filling or whether it is involved in controlling the filling state.

Experiments with bone marrow chimeric (BMc) mice were performed to study whether the protection of *Orai2*^{-/-} mice from ischemic stroke was attributed (in part) to *Orai2* deficiency in blood cells. *Orai2* expression has been described in immune cells, e.g. T and B cells¹⁸⁰ and during the last years especially T cells were described to play a detrimental role in ischemic stroke progression.^{139,178} The stroke experiments using BMc mice clearly demonstrated that protection was not blood cell intrinsic (Figure 42C,D). Also alterations in brain vasculature which may affect brain sensitivity to ischemia can be excluded since experiments using ink perfusion did not reveal significant differences in the Circle of Willis and major brain arteries (Dr. Peter Kraft, University of Würzburg, personal communication). These findings, together with Ca^{2+} measurements on isolated neurons (Figure 43) strongly suggest that protection from ischemic stroke in *Orai2*^{-/-} mice is primarily or even exclusively neuron-intrinsic.

Therapeutic blockade of *Orai2* in acute cerebral ischemia might be safer than interference with STIM2, because *Stim2*^{-/-} mice exhibited severe abnormalities, like reduced life expectancy,¹⁵³ and lactation problems in females whereas *Orai2*^{-/-} mice did not show these abnormalities. Further, *Orai2* is expressed in the plasma membrane and thus may be more easily accessible to pharmacological inhibition than STIM2 to prevent or treat ischemic stroke. The healthier status of *Orai2*^{-/-} mice in comparison to *Stim2*^{-/-} mice under normal conditions implies that other *Orai* isoforms, e.g. *Orai3*, might contribute to physiological SOCE in neurons. First evidence has been provided that STIM2 also couples to *Orai2* and *Orai3*.²⁰⁷ Also formation of *Orai* heteromultimers was proposed to facilitate SOC channel formation.¹⁵⁴ Therefore, *Orai2* may be a SOC channel component in neurons that is essential for excessive Ca^{2+} influx in ischemia, but its lack may be compensated for by other SOC channels under healthy conditions. Nevertheless, deficiency of *Orai2* was neuroprotective in mice under ischemic conditions and therefore administration of *Orai2* blockers may provide a future medication to treat patients suffering from acute ischemic stroke. To inhibit excessive Ca^{2+} accumulation in the ischemic territory, blockade of *Orai2* might be more suitable than glutamate receptor antagonists, which due to massive psychotic side effects and a short

therapeutic time window have not proven clinically useful.²⁰⁸ It is tempting to speculate that short term inhibition of Ca^{2+} accumulation in ischemic neurons via blockade of Orai2 in combination with established platelet inhibitors might provide effective therapeutic means to restrict neuronal damage in stroke patients. It is obvious that comprehensive further studies will be required to address the feasibility of this concept.

4.5 Concluding remarks and future plans

In the work presented here, CD84 deficient mice were generated and characterized. Further, new insights into the regulation of the glycoproteins CD84 and GPVI in platelets were provided. In addition, insights into the biological role of Orai2 were obtained by generation and initial analysis of Orai2 deficient mice.

Studies on CD84 deficient mice revealed that, in contrast to what was expected before, CD84 does not play a critical role in thrombus formation. However, the novel findings demonstrated tight regulation of CD84 in platelets by ADAM10 and calpain and pointed towards a role of platelet CD84 in biological processes other than thrombus formation. CD84 might be involved in platelet-immune cell interaction in inflammatory processes and it is tempting to speculate that shedding of CD84 on platelets may regulate such processes. Future studies will be performed to gain deeper insights into platelet-immune cell interaction.

In contrast to CD84, which was found to be shed exclusively by ADAM10, GPVI was shown to be differentially regulated by both ADAM10 and ADAM17 *in vitro*. Unexpectedly, shedding of GPVI in ADAM10/ADAM17 deficient mice still occurred *in vivo* upon injection of the monoclonal anti GPVI antibody JAQ1. It remains to be addressed in the future, which additional mechanisms drive extracellular cleavage of GPVI *in vivo*.

Ischemic cardio- and cerebrovascular diseases are leading causes of death and disability worldwide.¹²³ Clinical use of antithrombotic drugs has always been inevitably connected with increased bleeding risk. That is why alternative therapeutic options are strongly required. A series of complex processes involving diverse cell types act in concert to promote infarct development in ischemic stroke. CD84 deficiency was found to provide protection from ischemic stroke and this was further attributed to CD84 deficiency in T cells. Additional studies are required to unravel the molecular mechanism how CD84 on T cells contributes to neuronal damage. In addition, this thesis demonstrates for the first time that Orai2 is an essential player in SOCE in neurons and proposes the concept that Orai2 may represent a promising target for pharmacological intervention in the pathophysiological context of ischemic stroke. To further delineate how Orai2 and SOCE influence neuronal processes, behavioral studies and neuronal cell culture studies will be performed together with

collaboration partners in the field of neurology. Taken together, CD84 and Orai2 may represent novel pharmacological targets for future treatment of ischemic stroke.

5 References

1. Chang Y, Bluteau D, Debili N, Vainchenker W. From hematopoietic stem cells to platelets. *J Thromb Haemost.* 2007;5 Suppl 1:318-327.
2. Italiano JE, Jr., Patel-Hett S, Hartwig JH. Mechanics of proplatelet elaboration. *J Thromb Haemost.* 2007;5 Suppl 1:18-23.
3. Junt T, Schulze H, Chen Z, Massberg S, Goerge T, Krueger A, Wagner DD, et al. Dynamic visualization of thrombopoiesis within bone marrow. *Science.* 2007;317(5845):1767-1770.
4. Tsakiris DA, Scudder L, Hodivala-Dilke K, Hynes RO, Collier BS. Hemostasis in the mouse (*Mus musculus*): a review. *Thromb Haemost.* 1999;81(2):177-188.
5. Ault KA, Knowles C. In vivo biotinylation demonstrates that reticulated platelets are the youngest platelets in circulation. *Exp Hematol.* 1995;23(9):996-1001.
6. Davi G, Patrono C. Platelet activation and atherothrombosis. *N Engl J Med.* 2007;357(24):2482-2494.
7. White JG, Clawson CC. The surface-connected canalicular system of blood platelets-a fenestrated membrane system. *Am J Pathol.* 1980;101(2):353-364.
8. Rendu F, Brohard-Bohn B. The platelet release reaction: granules' constituents, secretion and functions. *Platelets.* 2001;12(5):261-273.
9. Nieswandt B, Pleines I, Bender M. Platelet adhesion and activation mechanisms in arterial thrombosis and ischaemic stroke. *J Thromb Haemost.* 2011;9 Suppl 1:92-104.
10. Varga-Szabo D, Pleines I, Nieswandt B. Cell adhesion mechanisms in platelets. *Arterioscler Thromb Vasc Biol.* 2008;28(3):403-412.
11. Wong C, Liu Y, Yip J, Chand R, Wee JL, Oates L, Nieswandt B, et al. CEACAM1 negatively regulates platelet-collagen interactions and thrombus growth in vitro and in vivo. *Blood.* 2009;113(8):1818-1828.
12. Andrews RK, Karunakaran D, Gardiner EE, Berndt MC. Platelet receptor proteolysis: a mechanism for downregulating platelet reactivity. *Arterioscler Thromb Vasc Biol.* 2007;27(7):1511-1520.
13. Savage B, Almus-Jacobs F, Ruggeri ZM. Specific synergy of multiple substrate-receptor interactions in platelet thrombus formation under flow. *Cell.* 1998;94(5):657-666.
14. Ruggeri ZM. Von Willebrand factor, platelets and endothelial cell interactions. *J Thromb Haemost.* 2003;1(7):1335-1342.
15. Nieswandt B, Watson SP. Platelet-collagen interaction: is GPVI the central receptor? *Blood.* 2003;102(2):449-461.
16. Offermanns S. Activation of platelet function through G protein-coupled receptors. *Circ Res.* 2006;99(12):1293-1304.
17. Nieswandt B, Aktas B, Moers A, Sachs UJ. Platelets in atherothrombosis: lessons from mouse models. *J Thromb Haemost.* 2005;3(8):1725-1736.

18. Ruggeri ZM, Orje JN, Habermann R, Federici AB, Reininger AJ. Activation-independent platelet adhesion and aggregation under elevated shear stress. *Blood*. 2006;108(6):1903-1910.
19. Maxwell MJ, Westein E, Nesbitt WS, Giuliano S, Dopheide SM, Jackson SP. Identification of a 2-stage platelet aggregation process mediating shear-dependent thrombus formation. *Blood*. 2007;109(2):566-576.
20. Varga-Szabo D, Braun A, Nieswandt B. Calcium signaling in platelets. *J Thromb Haemost*. 2009;7(7):1057-1066.
21. Hagedorn I, Vogtle T, Nieswandt B. Arterial thrombus formation. Novel mechanisms and targets. *Hamostaseologie*. 2010;30(3):127-135.
22. Varga-Szabo D, Braun A, Kleinschnitz C, Bender M, Pleines I, Pham M, Renne T, Stoll G, Nieswandt B. The calcium sensor STIM1 is an essential mediator of arterial thrombosis and ischemic brain infarction. *The Journal of experimental medicine*. 2008;205(7):1583-1591.
23. Braun A, Varga-Szabo D, Kleinschnitz C, Pleines I, Bender M, Austinat M, Bosl M, Stoll G, Nieswandt B. Orai1 (CRACM1) is the platelet SOC channel and essential for pathological thrombus formation. *Blood*. 2009;113(9):2056-2063.
24. Shattil SJ, Kashiwagi H, Pampori N. Integrin signaling: the platelet paradigm. *Blood*. 1998;91(8):2645-2657.
25. Prevost N, Woulfe D, Tognolini M, Brass LF. Contact-dependent signaling during the late events of platelet activation. *J Thromb Haemost*. 2003;1(7):1613-1627.
26. Nanda N, Phillips DR. Novel targets for antithrombotic drug discovery. *Blood Cells Mol Dis*. 2006;36(2):228-231.
27. Andre P, Prasad KS, Denis CV, He M, Papalia JM, Hynes RO, Phillips DR, Wagner DD. CD40L stabilizes arterial thrombi by a beta3 integrin--dependent mechanism. *Nat Med*. 2002;8(3):247-252.
28. Angelillo-Scherrer A, Burnier L, Flores N, Savi P, DeMol M, Schaeffer P, Herbert JM, et al. Role of Gas6 receptors in platelet signaling during thrombus stabilization and implications for antithrombotic therapy. *J Clin Invest*. 2005;115(2):237-246.
29. Prevost N, Woulfe DS, Jiang H, Stalker TJ, Marchese P, Ruggeri ZM, Brass LF. Eph kinases and ephrins support thrombus growth and stability by regulating integrin outside-in signaling in platelets. *Proc Natl Acad Sci U S A*. 2005;102(28):9820-9825.
30. Brass LF, Zhu L, Stalker TJ. Minding the gaps to promote thrombus growth and stability. *J Clin Invest*. 2005;115(12):3385-3392.
31. Clemetson JM, Polgar J, Magnenat E, Wells TN, Clemetson KJ. The platelet collagen receptor glycoprotein VI is a member of the immunoglobulin superfamily closely related to FcalphaR and the natural killer receptors. *J Biol Chem*. 1999;274(41):29019-29024.
32. Jandrot-Perrus M, Busfield S, Lagrue AH, Xiong X, Debili N, Chickering T, Le Couedic JP, et al. Cloning, characterization, and functional studies of human and mouse glycoprotein VI: a platelet-specific collagen receptor from the immunoglobulin superfamily. *Blood*. 2000;96(5):1798-1807.
33. Watson SP, Auger JM, McCarty OJ, Pearce AC. GPVI and integrin alphaIIb beta3 signaling in platelets. *J Thromb Haemost*. 2005;3(8):1752-1762.
34. Nieswandt B, Bergmeier W, Schulte V, Rackebrandt K, Gessner JE, Zirngibl H. Expression and function of the mouse collagen receptor glycoprotein VI is strictly

- dependent on its association with the FcRgamma chain. *J Biol Chem.* 2000;275(31):23998-24002.
35. Berlanga O, Tulasne D, Bori T, Snell DC, Miura Y, Jung S, Moroi M, Frampton J, Watson SP. The Fc receptor gamma-chain is necessary and sufficient to initiate signalling through glycoprotein VI in transfected cells by the snake C-type lectin, convulxin. *Eur J Biochem.* 2002;269(12):2951-2960.
36. Jung SM, Tsuji K, Moroi M. Glycoprotein (GP) VI dimer as a major collagen-binding site of native platelets: direct evidence obtained with dimeric GPVI-specific Fabs. *J Thromb Haemost.* 2009;7(8):1347-1355.
37. Loyau S, Dumont B, Ollivier V, Boulaftali Y, Feldman L, Ajzenberg N, Jandrot-Perrus M. Platelet glycoprotein VI dimerization, an active process inducing receptor competence, is an indicator of platelet reactivity. *Arterioscler Thromb Vasc Biol.* 2012;32(3):778-785.
38. Polgar J, Clemetson JM, Kehrel BE, Wiedemann M, Magnenat EM, Wells TN, Clemetson KJ. Platelet activation and signal transduction by convulxin, a C-type lectin from *Crotalus durissus terrificus* (tropical rattlesnake) venom via the p62/GPVI collagen receptor. *J Biol Chem.* 1997;272(21):13576-13583.
39. Poole A, Gibbins JM, Turner M, van Vugt MJ, van de Winkel JG, Saito T, Tybulewicz VL, Watson SP. The Fc receptor gamma-chain and the tyrosine kinase Syk are essential for activation of mouse platelets by collagen. *EMBO J.* 1997;16(9):2333-2341.
40. Dutting S, Bender M, Nieswandt B. Platelet GPVI: a target for antithrombotic therapy?! *Trends Pharmacol Sci.* 2012;33(11):583-590.
41. Nieswandt B, Schulte V, Bergmeier W, Mokhtari-Nejad R, Rackebrandt K, Cazenave JP, Ohlmann P, Gachet C, Zirngibl H. Long-term antithrombotic protection by in vivo depletion of platelet glycoprotein VI in mice. *The Journal of experimental medicine.* 2001;193(4):459-469.
42. Schulte V, Rabie T, Prostedna M, Aktas B, Gruner S, Nieswandt B. Targeting of the collagen-binding site on glycoprotein VI is not essential for in vivo depletion of the receptor. *Blood.* 2003;101(10):3948-3952.
43. Gruner S, Prostedna M, Koch M, Miura Y, Schulte V, Jung SM, Moroi M, Nieswandt B. Relative antithrombotic effect of soluble GPVI dimer compared with anti-GPVI antibodies in mice. *Blood.* 2005;105(4):1492-1499.
44. Massberg S, Gawaz M, Gruner S, Schulte V, Konrad I, Zohlhofer D, Heinzmann U, Nieswandt B. A crucial role of glycoprotein VI for platelet recruitment to the injured arterial wall in vivo. *The Journal of experimental medicine.* 2003;197(1):41-49.
45. Kleinschnitz C, Pozgajova M, Pham M, Bendszus M, Nieswandt B, Stoll G. Targeting platelets in acute experimental stroke: impact of glycoprotein Ib, VI, and IIb/IIIa blockade on infarct size, functional outcome, and intracranial bleeding. *Circulation.* 2007;115(17):2323-2330.
46. Moroi M, Jung SM, Okuma M, Shinmyozu K. A patient with platelets deficient in glycoprotein VI that lack both collagen-induced aggregation and adhesion. *J Clin Invest.* 1989;84(5):1440-1445.
47. Boylan B, Chen H, Rathore V, Paddock C, Salacz M, Friedman KD, Curtis BR, et al. Anti-GPVI-associated ITP: an acquired platelet disorder caused by autoantibody-mediated clearance of the GPVI/FcRgamma-chain complex from the human platelet surface. *Blood.* 2004;104(5):1350-1355.

48. Rabie T, Varga-Szabo D, Bender M, Pozgaj R, Lanza F, Saito T, Watson SP, Nieswandt B. Diverging signaling events control the pathway of GPVI down-regulation in vivo. *Blood*. 2007;110(2):529-535.
49. Cannons JL, Tangye SG, Schwartzberg PL. SLAM family receptors and SAP adaptors in immunity. *Annu Rev Immunol*. 2011;29:665-705.
50. Ma CS, Nichols KE, Tangye SG. Regulation of cellular and humoral immune responses by the SLAM and SAP families of molecules. *Annu Rev Immunol*. 2007;25:337-379.
51. Nanda N, Andre P, Bao M, Clauser K, Deguzman F, Howie D, Conley PB, Terhorst C, Phillips DR. Platelet aggregation induces platelet aggregate stability via SLAM family receptor signaling. *Blood*. 2005;106(9):3028-3034.
52. Calpe S, Wang N, Romero X, Berger SB, Lanyi A, Engel P, Terhorst C. The SLAM and SAP gene families control innate and adaptive immune responses. *Adv Immunol*. 2008;97:177-250.
53. Fraser CC, Howie D, Morra M, Qiu Y, Murphy C, Shen Q, Gutierrez-Ramos JC, et al. Identification and characterization of SF2000 and SF2001, two new members of the immune receptor SLAM/CD2 family. *Immunogenetics*. 2002;53(10-11):843-850.
54. Engel P, Eck MJ, Terhorst C. The SAP and SLAM families in immune responses and X-linked lymphoproliferative disease. *Nat Rev Immunol*. 2003;3(10):813-821.
55. Veillette A, Dong Z, Latour S. Consequence of the SLAM-SAP signaling pathway in innate-like and conventional lymphocytes. *Immunity*. 2007;27(5):698-710.
56. Yan Q, Malashkevich VN, Fedorov A, Fedorov E, Cao E, Lary JW, Cole JL, Nathanson SG, Almo SC. Structure of CD84 provides insight into SLAM family function. *Proc Natl Acad Sci U S A*. 2007;104(25):10583-10588.
57. Veillette A. Immune regulation by SLAM family receptors and SAP-related adaptors. *Nat Rev Immunol*. 2006;6(1):56-66.
58. Ostrakhovitch EA, Li SS. The role of SLAM family receptors in immune cell signaling. *Biochem Cell Biol*. 2006;84(6):832-843.
59. Clements JL, Boerth NJ, Lee JR, Koretzky GA. Integration of T cell receptor-dependent signaling pathways by adapter proteins. *Annu Rev Immunol*. 1999;17:89-108.
60. Li C, Iosef C, Jia CY, Han VK, Li SS. Dual functional roles for the X-linked lymphoproliferative syndrome gene product SAP/SH2D1A in signaling through the signaling lymphocyte activation molecule (SLAM) family of immune receptors. *J Biol Chem*. 2003;278(6):3852-3859.
61. Mikhalap SV, Shlapatska LM, Berdova AG, Law CL, Clark EA, Sidorenko SP. CDw150 associates with src-homology 2-containing inositol phosphatase and modulates CD95-mediated apoptosis. *J Immunol*. 1999;162(10):5719-5727.
62. Latour S, Gish G, Helgason CD, Humphries RK, Pawson T, Veillette A. Regulation of SLAM-mediated signal transduction by SAP, the X-linked lymphoproliferative gene product. *Nat Immunol*. 2001;2(8):681-690.
63. Sayos J, Martin M, Chen A, Simarro M, Howie D, Morra M, Engel P, Terhorst C. Cell surface receptors Ly-9 and CD84 recruit the X-linked lymphoproliferative disease gene product SAP. *Blood*. 2001;97(12):3867-3874.
64. Nichols KE, Ma CS, Cannons JL, Schwartzberg PL, Tangye SG. Molecular and cellular pathogenesis of X-linked lymphoproliferative disease. *Immunol Rev*. 2005;203:180-199.

65. Roncagalli R, Taylor JE, Zhang S, Shi X, Chen R, Cruz-Munoz ME, Yin L, Latour S, Veillette A. Negative regulation of natural killer cell function by EAT-2, a SAP-related adaptor. *Nat Immunol.* 2005;6(10):1002-1010.
66. Simarro M, Lanyi A, Howie D, Poy F, Bruggeman J, Choi M, Sumegi J, Eck MJ, Terhorst C. SAP increases FynT kinase activity and is required for phosphorylation of SLAM and Ly9. *Int Immunol.* 2004;16(5):727-736.
67. Romero X, Benitez D, March S, Vilella R, Miralpeix M, Engel P. Differential expression of SAP and EAT-2-binding leukocyte cell-surface molecules CD84, CD150 (SLAM), CD229 (Ly9) and CD244 (2B4). *Tissue Antigens.* 2004;64(2):132-144.
68. Bottino C, Falco M, Parolini S, Marcenaro E, Augugliaro R, Sivori S, Landi E, et al. NTB-A [correction of GNTB-A], a novel SH2D1A-associated surface molecule contributing to the inability of natural killer cells to kill Epstein-Barr virus-infected B cells in X-linked lymphoproliferative disease. *The Journal of experimental medicine.* 2001;194(3):235-246.
69. Yilmaz OH, Kiel MJ, Morrison SJ. SLAM family markers are conserved among hematopoietic stem cells from old and reconstituted mice and markedly increase their purity. *Blood.* 2006;107(3):924-930.
70. Sintes J, Romero X, Marin P, Terhorst C, Engel P. Differential expression of CD150 (SLAM) family receptors by human hematopoietic stem and progenitor cells. *Exp Hematol.* 2008;36(9):1199-1204.
71. Bhat R, Eissmann P, Endt J, Hoffmann S, Watzl C. Fine-tuning of immune responses by SLAM-related receptors. *J Leukoc Biol.* 2006;79(3):417-424.
72. Coffey AJ, Brooksbank RA, Brandau O, Oohashi T, Howell GR, Bye JM, Cahn AP, et al. Host response to EBV infection in X-linked lymphoproliferative disease results from mutations in an SH2-domain encoding gene. *Nat Genet.* 1998;20(2):129-135.
73. Al-Alem U, Li C, Forey N, Relouzat F, Fondaneche MC, Tavtigian SV, Wang ZQ, Latour S, Yin L. Impaired Ig class switch in mice deficient for the X-linked lymphoproliferative disease gene Sap. *Blood.* 2005;106(6):2069-2075.
74. Kumar KR, Li L, Yan M, Bhaskarabhatla M, Mobley AB, Nguyen C, Mooney JM, et al. Regulation of B cell tolerance by the lupus susceptibility gene Ly108. *Science.* 2006;312(5780):1665-1669.
75. de la Fuente MA, Pizcueta P, Nadal M, Bosch J, Engel P. CD84 leukocyte antigen is a new member of the Ig superfamily. *Blood.* 1997;90(6):2398-2405.
76. Palou E, Piroto F, Sole J, Freed JH, Peral B, Vilardell C, Vilella R, Vives J, Gaya A. Genomic characterization of CD84 reveals the existence of five isoforms differing in their cytoplasmic domains. *Tissue Antigens.* 2000;55(2):118-127.
77. Krause SW, Rehli M, Heinz S, Ebner R, Andreesen R. Characterization of MAX.3 antigen, a glycoprotein expressed on mature macrophages, dendritic cells and blood platelets: identity with CD84. *Biochem J.* 2000;346 Pt 3:729-736.
78. Zaiss M, Hirtreiter C, Rehli M, Rehm A, Kunz-Schughart LA, Andreesen R, Hennemann B. CD84 expression on human hematopoietic progenitor cells. *Exp Hematol.* 2003;31(9):798-805.
79. Tangye SG, van de Weerd BC, Avery DT, Hodgkin PD. CD84 is up-regulated on a major population of human memory B cells and recruits the SH2 domain containing proteins SAP and EAT-2. *Eur J Immunol.* 2002;32(6):1640-1649.

80. Tangye SG, Nichols KE, Hare NJ, van de Weerd BC. Functional requirements for interactions between CD84 and Src homology 2 domain-containing proteins and their contribution to human T cell activation. *J Immunol.* 2003;171(5):2485-2495.
81. Martin M, Romero X, de la Fuente MA, Tovar V, Zapater N, Esplugues E, Pizcueta P, Bosch J, Engel P. CD84 functions as a homophilic adhesion molecule and enhances IFN-gamma secretion: adhesion is mediated by Ig-like domain 1. *J Immunol.* 2001;167(7):3668-3676.
82. Howie D, Okamoto S, Rietdijk S, Clarke K, Wang N, Gullo C, Bruggeman JP, et al. The role of SAP in murine CD150 (SLAM)-mediated T-cell proliferation and interferon gamma production. *Blood.* 2002;100(8):2899-2907.
83. Sintes J, Romero X, de Salort J, Terhorst C, Engel P. Mouse CD84 is a pan-leukocyte cell-surface molecule that modulates LPS-induced cytokine secretion by macrophages. *J Leukoc Biol.* 2010;88(4):687-697.
84. Cannons JL, Qi H, Lu KT, Dutta M, Gomez-Rodriguez J, Cheng J, Wakeland EK, Germain RN, Schwartzberg PL. Optimal germinal center responses require a multistage T cell:B cell adhesion process involving integrins, SLAM-associated protein, and CD84. *Immunity.* 2010;32(2):253-265.
85. Morra M, Lu J, Poy F, Martin M, Sayos J, Calpe S, Gullo C, et al. Structural basis for the interaction of the free SH2 domain EAT-2 with SLAM receptors in hematopoietic cells. *EMBO J.* 2001;20(21):5840-5852.
86. Alvarez-Errico D, Oliver-Vila I, Ainsua-Enrich E, Gilfillan AM, Picado C, Sayos J, Martin M. CD84 negatively regulates IgE high-affinity receptor signaling in human mast cells. *J Immunol.* 2011;187(11):5577-5586.
87. Dole VS, Bergmeier W, Patten IS, Hirahashi J, Mayadas TN, Wagner DD. PSGL-1 regulates platelet P-selectin-mediated endothelial activation and shedding of P-selectin from activated platelets. *Thromb Haemost.* 2007;98(4):806-812.
88. Bergmeier W, Piffath CL, Cheng G, Dole VS, Zhang Y, von Andrian UH, Wagner DD. Tumor necrosis factor-alpha-converting enzyme (ADAM17) mediates GPIIb/IIIa shedding from platelets in vitro and in vivo. *Circ Res.* 2004;95(7):677-683.
89. Bergmeier W, Rabie T, Strehl A, Piffath CL, Prostredna M, Wagner DD, Nieswandt B. GPVI down-regulation in murine platelets through metalloproteinase-dependent shedding. *Thromb Haemost.* 2004;91(5):951-958.
90. Gardiner EE, Arthur JF, Kahn ML, Berndt MC, Andrews RK. Regulation of platelet membrane levels of glycoprotein VI by a platelet-derived metalloproteinase. *Blood.* 2004;104(12):3611-3617.
91. Aktas B, Pozgajova M, Bergmeier W, Sunnarborg S, Offermanns S, Lee D, Wagner DD, Nieswandt B. Aspirin induces platelet receptor shedding via ADAM17 (TACE). *J Biol Chem.* 2005;280(48):39716-39722.
92. Rabie T, Strehl A, Ludwig A, Nieswandt B. Evidence for a role of ADAM17 (TACE) in the regulation of platelet glycoprotein V. *J Biol Chem.* 2005;280(15):14462-14468.
93. Zhu L, Bergmeier W, Wu J, Jiang H, Stalker TJ, Cieslak M, Fan R, et al. Regulated surface expression and shedding support a dual role for semaphorin 4D in platelet responses to vascular injury. *Proc Natl Acad Sci U S A.* 2007;104(5):1621-1626.
94. Koenen RR, Pruessmeyer J, Soehnlein O, Fraemohs L, Zernecke A, Schwarz N, Reiss K, et al. Regulated release and functional modulation of junctional adhesion molecule A by disintegrin metalloproteinases. *Blood.* 2009;113(19):4799-4809.

95. Furman MI, Krueger LA, Linden MD, Barnard MR, Frelinger AL, 3rd, Michelson AD. Release of soluble CD40L from platelets is regulated by glycoprotein IIb/IIIa and actin polymerization. *J Am Coll Cardiol.* 2004;43(12):2319-2325.
96. Fong KP, Barry C, Tran AN, Traxler EA, Wannemacher KM, Tang HY, Speicher KD, et al. Deciphering the human platelet sheddome. *Blood.* 2011;117(1):e15-26.
97. Gardiner EE, Karunakaran D, Shen Y, Arthur JF, Andrews RK, Berndt MC. Controlled shedding of platelet glycoprotein (GP)VI and GPIb-IX-V by ADAM family metalloproteinases. *J Thromb Haemost.* 2007;5(7):1530-1537.
98. Andrews RK, Suzuki-Inoue K, Shen Y, Tulasne D, Watson SP, Berndt MC. Interaction of calmodulin with the cytoplasmic domain of platelet glycoprotein VI. *Blood.* 2002;99(11):4219-4221.
99. Seals DF, Courtneidge SA. The ADAMs family of metalloproteases: multidomain proteins with multiple functions. *Genes & development.* 2003;17(1):7-30.
100. Blobel CP. ADAMs: key components in EGFR signalling and development. *Nat Rev Mol Cell Biol.* 2005;6(1):32-43.
101. Leonard JD, Lin F, Milla ME. Chaperone-like properties of the prodomain of TNFalpha-converting enzyme (TACE) and the functional role of its cysteine switch. *Biochem J.* 2005;387(Pt 3):797-805.
102. Huovila AP, Turner AJ, Pelto-Huikko M, Karkkainen I, Ortiz RM. Shedding light on ADAM metalloproteinases. *Trends Biochem Sci.* 2005;30(7):413-422.
103. Mohammed FF, Smookler DS, Taylor SE, Fingleton B, Kassiri Z, Sanchez OH, English JL, et al. Abnormal TNF activity in Timp3^{-/-} mice leads to chronic hepatic inflammation and failure of liver regeneration. *Nat Genet.* 2004;36(9):969-977.
104. Hartmann D, de Strooper B, Serneels L, Craessaerts K, Herreman A, Annaert W, Umans L, et al. The disintegrin/metalloprotease ADAM 10 is essential for Notch signalling but not for alpha-secretase activity in fibroblasts. *Hum Mol Genet.* 2002;11(21):2615-2624.
105. Horiuchi K, Kimura T, Miyamoto T, Takaishi H, Okada Y, Toyama Y, Blobel CP. Cutting edge: TNF-alpha-converting enzyme (TACE/ADAM17) inactivation in mouse myeloid cells prevents lethality from endotoxin shock. *J Immunol.* 2007;179(5):2686-2689.
106. Chalaris A, Adam N, Sina C, Rosenstiel P, Lehmann-Koch J, Schirmacher P, Hartmann D, et al. Critical role of the disintegrin metalloprotease ADAM17 for intestinal inflammation and regeneration in mice. *The Journal of experimental medicine.* 2010;207(8):1617-1624.
107. Gardiner EE, Al-Tamimi M, Andrews RK, Berndt MC. Platelet receptor shedding. *Methods Mol Biol.* 2012;788:321-339.
108. Flevaris P, Stojanovic A, Gong H, Chishti A, Welch E, Du X. A molecular switch that controls cell spreading and retraction. *The Journal of cell biology.* 2007;179(3):553-565.
109. Goll DE, Thompson VF, Li H, Wei W, Cong J. The calpain system. *Physiological reviews.* 2003;83(3):731-801.
110. Du X, Saido TC, Tsubuki S, Indig FE, Williams MJ, Ginsberg MH. Calpain cleavage of the cytoplasmic domain of the integrin beta 3 subunit. *J Biol Chem.* 1995;270(44):26146-26151.

111. Gardiner EE, Karunakaran D, Arthur JF, Mu FT, Powell MS, Baker RI, Hogarth PM, et al. Dual ITAM-mediated proteolytic pathways for irreversible inactivation of platelet receptors: de-ITAM-izing FcγRIIIa. *Blood*. 2008;111(1):165-174.
112. Naganuma Y, Satoh K, Yi Q, Asazuma N, Yatomi Y, Ozaki Y. Cleavage of platelet endothelial cell adhesion molecule-1 (PECAM-1) in platelets exposed to high shear stress. *J Thromb Haemost*. 2004;2(11):1998-2008.
113. Azam M, Andrabi SS, Sahr KE, Kamath L, Kuliopulos A, Chishti AH. Disruption of the mouse mu-calpain gene reveals an essential role in platelet function. *Molecular and cellular biology*. 2001;21(6):2213-2220.
114. Kuchay SM, Kim N, Grunz EA, Fay WP, Chishti AH. Double knockouts reveal that protein tyrosine phosphatase 1B is a physiological target of calpain-1 in platelets. *Molecular and cellular biology*. 2007;27(17):6038-6052.
115. Kuchay SM, Wieschhaus AJ, Marinkovic M, Herman IM, Chishti AH. Targeted gene inactivation reveals a functional role of calpain-1 in platelet spreading. *J Thromb Haemost*. 2012;10(6):1120-1132.
116. Roger VL, Go AS, Lloyd-Jones DM, Adams RJ, Berry JD, Brown TM, Carnethon MR, et al. Heart disease and stroke statistics--2011 update: a report from the American Heart Association. *Circulation*. 2011;123(4):e18-e209.
117. von Bruhl ML, Stark K, Steinhart A, Chandraratne S, Konrad I, Lorenz M, Khandoga A, et al. Monocytes, neutrophils, and platelets cooperate to initiate and propagate venous thrombosis in mice in vivo. *The Journal of experimental medicine*. 2012;209(4):819-835.
118. Bauersachs R, Berkowitz SD, Brenner B, Buller HR, Decousus H, Gallus AS, Lensing AW, et al. Oral rivaroxaban for symptomatic venous thromboembolism. *N Engl J Med*. 2010;363(26):2499-2510.
119. Ruggeri ZM. Platelets in atherothrombosis. *Nat Med*. 2002;8(11):1227-1234.
120. Jackson SP. Arterial thrombosis--insidious, unpredictable and deadly. *Nat Med*. 2011;17(11):1423-1436.
121. Falk E. Plaque rupture with severe pre-existing stenosis precipitating coronary thrombosis. Characteristics of coronary atherosclerotic plaques underlying fatal occlusive thrombi. *Br Heart J*. 1983;50(2):127-134.
122. WHO. The Global Burden of Disease: 2004 Update. Geneva: World Health Organization; 2008. 978-9241563710.
123. Lopez AD, Mathers CD, Ezzati M, Jamison DT, Murray CJ. Global and regional burden of disease and risk factors, 2001: systematic analysis of population health data. *Lancet*. 2006;367(9524):1747-1757.
124. Michelson AD. Antiplatelet therapies for the treatment of cardiovascular disease. *Nat Rev Drug Discov*. 2010;9(2):154-169.
125. Stoll G, Kleinschnitz C, Nieswandt B. Molecular mechanisms of thrombus formation in ischemic stroke: novel insights and targets for treatment. *Blood*. 2008;112(9):3555-3562.
126. Group TNiONDaSr-PSS. Tissue plasminogen activator for acute ischemic stroke. . *N Engl J Med*. 1995;333(24):1581-1587.
127. Dirnagl U, Iadecola C, Moskowitz MA. Pathobiology of ischaemic stroke: an integrated view. *Trends Neurosci*. 1999;22(9):391-397.
128. Wojda U, Salinska E, Kuznicki J. Calcium ions in neuronal degeneration. *IUBMB Life*. 2008;60(9):575-590.

129. Nieswandt B, Kleinschnitz C, Stoll G. Ischaemic stroke: a thrombo-inflammatory disease? *J Physiol.* 2011;589(Pt 17):4115-4123.
130. del Zoppo GJ, Mabuchi T. Cerebral microvessel responses to focal ischemia. *J Cereb Blood Flow Metab.* 2003;23(8):879-894.
131. Braeuninger S, Kleinschnitz C, Nieswandt B, Stoll G. Focal cerebral ischemia. *Methods Mol Biol.* 2012;788:29-42.
132. Heemskerk JW, Bevers EM, Lindhout T. Platelet activation and blood coagulation. *Thromb Haemost.* 2002;88(2):186-193.
133. Muller F, Mutch NJ, Schenk WA, Smith SA, Esterl L, Spronk HM, Schmidbauer S, et al. Platelet polyphosphates are proinflammatory and procoagulant mediators in vivo. *Cell.* 2009;139(6):1143-1156.
134. Muller F, Renne T. Novel roles for factor XII-driven plasma contact activation system. *Curr Opin Hematol.* 2008;15(5):516-521.
135. Stoll G, Jander S, Schroeter M. Inflammation and glial responses in ischemic brain lesions. *Prog Neurobiol.* 1998;56(2):149-171.
136. Gelderblom M, Leypoldt F, Steinbach K, Behrens D, Choe CU, Siler DA, Arumugam TV, et al. Temporal and spatial dynamics of cerebral immune cell accumulation in stroke. *Stroke.* 2009;40(5):1849-1857.
137. Iadecola C, Anrather J. The immunology of stroke: from mechanisms to translation. *Nat Med.* 2011;17(7):796-808.
138. Yilmaz G, Arumugam TV, Stokes KY, Granger DN. Role of T lymphocytes and interferon-gamma in ischemic stroke. *Circulation.* 2006;113(17):2105-2112.
139. Kleinschnitz C, Schwab N, Kraft P, Hagedorn I, Dreykluft A, Schwarz T, Austinat M, et al. Early detrimental T-cell effects in experimental cerebral ischemia are neither related to adaptive immunity nor thrombus formation. *Blood.* 2010;115(18):3835-3842.
140. Kleinschnitz C, Kraft P, Dreykluft A, Hagedorn I, Gobel K, Schuhmann MK, Langhauser F, et al. Regulatory T cells are strong promoters of acute ischemic stroke in mice by inducing dysfunction of the cerebral microvasculature. *Blood.* 2012;10.1182/blood-2012-04-426734.
141. Berridge MJ, Bootman MD, Roderick HL. Calcium signalling: dynamics, homeostasis and remodelling. *Nat Rev Mol Cell Biol.* 2003;4(7):517-529.
142. Barritt GJ. Receptor-activated Ca²⁺ inflow in animal cells: a variety of pathways tailored to meet different intracellular Ca²⁺ signalling requirements. *Biochem J.* 1999;337 (Pt 2):153-169.
143. Potier M, Trebak M. New developments in the signaling mechanisms of the store-operated calcium entry pathway. *Pflugers Arch.* 2008;457(2):405-415.
144. Liou J, Kim ML, Heo WD, Jones JT, Myers JW, Ferrell JE, Jr., Meyer T. STIM is a Ca²⁺ sensor essential for Ca²⁺-store-depletion-triggered Ca²⁺ influx. *Current biology : CB.* 2005;15(13):1235-1241.
145. Roos J, DiGregorio PJ, Yeromin AV, Ohlsen K, Liudyno M, Zhang S, Safrina O, et al. STIM1, an essential and conserved component of store-operated Ca²⁺ channel function. *The Journal of cell biology.* 2005;169(3):435-445.
146. Feske S, Gwack Y, Prakriya M, Srikanth S, Puppel SH, Tanasa B, Hogan PG, et al. A mutation in Orai1 causes immune deficiency by abrogating CRAC channel function. *Nature.* 2006;441(7090):179-185.

147. Vig M, Peinelt C, Beck A, Koomoa DL, Rabah D, Koblan-Huberson M, Kraft S, et al. CRACM1 is a plasma membrane protein essential for store-operated Ca²⁺ entry. *Science*. 2006;312(5777):1220-1223.
148. Cahalan MD. STIMulating store-operated Ca(2+) entry. *Nat Cell Biol*. 2009;11(6):669-677.
149. Feske S. Calcium signalling in lymphocyte activation and disease. *Nat Rev Immunol*. 2007;7(9):690-702.
150. Mignen O, Thompson JL, Shuttleworth TJ. Orai1 subunit stoichiometry of the mammalian CRAC channel pore. *J Physiol*. 2008;586(2):419-425.
151. Varnai P, Hunyady L, Balla T. STIM and Orai: the long-awaited constituents of store-operated calcium entry. *Trends Pharmacol Sci*. 2009;30(3):118-128.
152. Brandman O, Liou J, Park WS, Meyer T. STIM2 is a feedback regulator that stabilizes basal cytosolic and endoplasmic reticulum Ca²⁺ levels. *Cell*. 2007;131(7):1327-1339.
153. Berna-Ero A, Braun A, Kraft R, Kleinschnitz C, Schuhmann MK, Stegner D, Wultsch T, et al. STIM2 regulates capacitive Ca²⁺ entry in neurons and plays a key role in hypoxic neuronal cell death. *Sci Signal*. 2009;2(93):ra67.
154. Gwack Y, Srikanth S, Feske S, Cruz-Guilloty F, Oh-hora M, Neems DS, Hogan PG, Rao A. Biochemical and functional characterization of Orai proteins. *J Biol Chem*. 2007;282(22):16232-16243.
155. Mercer JC, Dehaven WI, Smyth JT, Wedel B, Boyles RR, Bird GS, Putney JW, Jr. Large store-operated calcium selective currents due to co-expression of Orai1 or Orai2 with the intracellular calcium sensor, Stim1. *J Biol Chem*. 2006;281(34):24979-24990.
156. Gross SA, Wissenbach U, Philipp SE, Freichel M, Cavalie A, Flockerzi V. Murine ORAI2 splice variants form functional Ca²⁺ release-activated Ca²⁺ (CRAC) channels. *J Biol Chem*. 2007;282(27):19375-19384.
157. Vig M, DeHaven WI, Bird GS, Billingsley JM, Wang H, Rao PE, Hutchings AB, et al. Defective mast cell effector functions in mice lacking the CRACM1 pore subunit of store-operated calcium release-activated calcium channels. *Nat Immunol*. 2008;9(1):89-96.
158. Bandyopadhyay BC, Pingle SC, Ahern GP. Store-operated Ca(2)+ signaling in dendritic cells occurs independently of STIM1. *J Leukoc Biol*. 2011;89(1):57-62.
159. Takahashi Y, Murakami M, Watanabe H, Hasegawa H, Ohba T, Munehisa Y, Nobori K, et al. Essential role of the N-terminus of murine Orai1 in store-operated Ca²⁺ entry. *Biochem Biophys Res Commun*. 2007;356(1):45-52.
160. Nagy A, Rossant J, Nagy R, Abramow-Newerly W, Roder JC. Derivation of completely cell culture-derived mice from early-passage embryonic stem cells. *Proc Natl Acad Sci U S A*. 1993;90(18):8424-8428.
161. Nieswandt B, Bergmeier W, Rackebrandt K, Gessner JE, Zirngibl H. Identification of critical antigen-specific mechanisms in the development of immune thrombocytopenic purpura in mice. *Blood*. 2000;96(7):2520-2527.
162. Gruner S, Prostredna M, Schulte V, Krieg T, Eckes B, Brakebusch C, Nieswandt B. Multiple integrin-ligand interactions synergize in shear-resistant platelet adhesion at sites of arterial injury in vivo. *Blood*. 2003;102(12):4021-4027.
163. May F, Hagedorn I, Pleines I, Bender M, Vogtle T, Eble J, Elvers M, Nieswandt B. CLEC-2 is an essential platelet-activating receptor in hemostasis and thrombosis. *Blood*. 2009;114(16):3464-3472.

164. Hofmann S, Vogtle T, Bender M, Rose-John S, Nieswandt B. The SLAM family member CD84 is regulated by ADAM10 and calpain in platelets. *J Thromb Haemost.* 2012;10(12):2581-2592.
165. Unkeless JC. Characterization of a monoclonal antibody directed against mouse macrophage and lymphocyte Fc receptors. *The Journal of experimental medicine.* 1979;150(3):580-596.
166. Bergmeier W, Schulte V, Brockhoff G, Bier U, Zirngibl H, Nieswandt B. Flow cytometric detection of activated mouse integrin alphaIIb beta3 with a novel monoclonal antibody. *Cytometry.* 2002;48(2):80-86.
167. Fassler R, Schnegelsberg PN, Dausman J, Shinya T, Muragaki Y, McCarthy MT, Olsen BR, Jaenisch R. Mice lacking alpha 1 (IX) collagen develop noninflammatory degenerative joint disease. *Proc Natl Acad Sci U S A.* 1994;91(11):5070-5074.
168. Dirnagl U. Bench to bedside: the quest for quality in experimental stroke research. *J Cereb Blood Flow Metab.* 2006;26(12):1465-1478.
169. Bederson JB, Pitts LH, Tsuji M, Nishimura MC, Davis RL, Bartkowski H. Rat middle cerebral artery occlusion: evaluation of the model and development of a neurologic examination. *Stroke.* 1986;17(3):472-476.
170. Moran PM, Higgins LS, Cordell B, Moser PC. Age-related learning deficits in transgenic mice expressing the 751-amino acid isoform of human beta-amyloid precursor protein. *Proc Natl Acad Sci U S A.* 1995;92(12):5341-5345.
171. Savage B, Shattil SJ, Ruggeri ZM. Modulation of platelet function through adhesion receptors. A dual role for glycoprotein IIb-IIIa (integrin alpha IIb beta 3) mediated by fibrinogen and glycoprotein Ib-von Willebrand factor. *J Biol Chem.* 1992;267(16):11300-11306.
172. Tucker KL, Sage T, Gibbins JM. Clot retraction. *Methods Mol Biol.* 2012;788:101-107.
173. Bender M, Hofmann S, Stegner D, Chalaris A, Bosl M, Braun A, Scheller J, Rose-John S, Nieswandt B. Differentially regulated GPVI ectodomain shedding by multiple platelet-expressed proteinases. *Blood.* 2010;116(17):3347-3355.
174. Wang KK, Villalobo A, Roufogalis BD. Calmodulin-binding proteins as calpain substrates. *Biochem J.* 1989;262(3):693-706.
175. DuVerle DA, Ono Y, Sorimachi H, Mamitsuka H. Calpain cleavage prediction using multiple kernel learning. *PLoS One.* 2011;6(5):e19035.
176. Schoenwaelder SM, Burridge K. Evidence for a calpeptin-sensitive protein-tyrosine phosphatase upstream of the small GTPase Rho. A novel role for the calpain inhibitor calpeptin in the inhibition of protein-tyrosine phosphatases. *J Biol Chem.* 1999;274(20):14359-14367.
177. Stoll G, Kleinschnitz C, Nieswandt B. Combating innate inflammation: a new paradigm for acute treatment of stroke? *Ann N Y Acad Sci.* 2010;1207:149-154.
178. Arumugam TV, Granger DN, Mattson MP. Stroke and T-cells. *Neuromolecular Med.* 2005;7(3):229-242.
179. Mombaerts P, Iacomini J, Johnson RS, Herrup K, Tonegawa S, Papaioannou VE. RAG-1-deficient mice have no mature B and T lymphocytes. *Cell.* 1992;68(5):869-877.
180. Gwack Y, Srikanth S, Oh-Hora M, Hogan PG, Lamperti ED, Yamashita M, Gelinas C, et al. Hair loss and defective T- and B-cell function in mice lacking ORAI1. *Molecular and cellular biology.* 2008;28(17):5209-5222.

181. Sachs UJ, Nieswandt B. In vivo thrombus formation in murine models. *Circ Res.* 2007;100(7):979-991.
182. Oliver-Vila I, Saborit-Villarroya I, Engel P, Martin M. The leukocyte receptor CD84 inhibits Fc epsilon RI-mediated signaling through homophilic interaction in transfected RBL-2H3 cells. *Mol Immunol.* 2008;45(8):2138-2149.
183. Dhanjal TS, Ross EA, Auger JM, McCarty OJ, Hughes CE, Senis YA, Buckley CD, Watson SP. Minimal regulation of platelet activity by PECAM-1. *Platelets.* 2007;18(1):56-67.
184. von Hundelshausen P, Weber C. Platelets as immune cells: bridging inflammation and cardiovascular disease. *Circ Res.* 2007;100(1):27-40.
185. Zarbock A, Polanowska-Grabowska RK, Ley K. Platelet-neutrophil-interactions: linking hemostasis and inflammation. *Blood Rev.* 2007;21(2):99-111.
186. Weyrich AS, Zimmerman GA. Platelets: signaling cells in the immune continuum. *Trends Immunol.* 2004;25(9):489-495.
187. Berndt MC, Shen Y, Dopheide SM, Gardiner EE, Andrews RK. The vascular biology of the glycoprotein Ib-IX-V complex. *Thromb Haemost.* 2001;86(1):178-188.
188. Li N. Platelet-lymphocyte cross-talk. *J Leukoc Biol.* 2008;83(5):1069-1078.
189. Hu H, Zhu L, Huang Z, Ji Q, Chatterjee M, Zhang W, Li N. Platelets enhance lymphocyte adhesion and infiltration into arterial thrombus. *Thromb Haemost.* 2010;104(6):1184-1192.
190. Soriano SG, Coxon A, Wang YF, Frosch MP, Lipton SA, Hickey PR, Mayadas TN. Mice deficient in Mac-1 (CD11b/CD18) are less susceptible to cerebral ischemia/reperfusion injury. *Stroke.* 1999;30(1):134-139.
191. Al-Tamimi M, Gardiner EE, Thom JY, Shen Y, Cooper MN, Hankey GJ, Berndt MC, Baker RI, Andrews RK. Soluble glycoprotein VI is raised in the plasma of patients with acute ischemic stroke. *Stroke.* 2011;42(2):498-500.
192. Al-Tamimi M, Tan CW, Qiao J, Pennings GJ, Javadzadegan A, Yong AS, Arthur JF, et al. Pathologic shear triggers shedding of vascular receptors: a novel mechanism for down-regulation of platelet glycoprotein VI in stenosed coronary vessels. *Blood.* 2012;119(18):4311-4320.
193. Bergmeier W, Rackebrandt K, Schroder W, Zirngibl H, Nieswandt B. Structural and functional characterization of the mouse von Willebrand factor receptor GPIb-IX with novel monoclonal antibodies. *Blood.* 2000;95(3):886-893.
194. Bergmeier W, Burger PC, Piffath CL, Hoffmeister KM, Hartwig JH, Nieswandt B, Wagner DD. Metalloproteinase inhibitors improve the recovery and hemostatic function of in vitro-aged or -injured mouse platelets. *Blood.* 2003;102(12):4229-4235.
195. Andrews RK, Munday AD, Mitchell CA, Berndt MC. Interaction of calmodulin with the cytoplasmic domain of the platelet membrane glycoprotein Ib-IX-V complex. *Blood.* 2001;98(3):681-687.
196. Berndt MC, Karunakaran D, Gardiner EE, Andrews RK. Programmed autologous cleavage of platelet receptors. *J Thromb Haemost.* 2007;5 Suppl 1:212-219.
197. Chalaris A, Gewiese J, Paliga K, Fleig L, Schneede A, Krieger K, Rose-John S, Scheller J. ADAM17-mediated shedding of the IL6R induces cleavage of the membrane stub by gamma-secretase. *Biochimica et biophysica acta.* 2010;1803(2):234-245.
198. Weskamp G, Cai H, Brodie TA, Higashiyama S, Manova K, Ludwig T, Blobel CP. Mice lacking the metalloprotease-disintegrin MDC9 (ADAM9) have no evident major

- abnormalities during development or adult life. *Molecular and cellular biology*. 2002;22(5):1537-1544.
199. Boylan B, Berndt MC, Kahn ML, Newman PJ. Activation-independent, antibody-mediated removal of GPVI from circulating human platelets: development of a novel NOD/SCID mouse model to evaluate the in vivo effectiveness of anti-human platelet agents. *Blood*. 2006;108(3):908-914.
200. Boilard E, Nigrovic PA, Larabee K, Watts GF, Coblyn JS, Weinblatt ME, Massarotti EM, et al. Platelets amplify inflammation in arthritis via collagen-dependent microparticle production. *Science*. 2010;327(5965):580-583.
201. Berna-Erro A. Generation and characterization of Stromal Interaction Molecule 2 (STIM2) deficient mice. Chair of Experimental Biomedicine: University of Würzburg; 2009.
202. Morris R. Developments of a water-maze procedure for studying spatial learning in the rat. *J Neurosci Methods*. 1984;11(1):47-60.
203. Ramanathan G, Gupta S, Thielmann I, Pleines I, Varga-Szabo D, May F, Mannhalter C, et al. Defective diacylglycerol-induced Ca²⁺ entry but normal agonist-induced activation responses in TRPC6-deficient mouse platelets. *J Thromb Haemost*. 2012;10(3):419-429.
204. Arundine M, Tymianski M. Molecular mechanisms of glutamate-dependent neurodegeneration in ischemia and traumatic brain injury. *Cell Mol Life Sci*. 2004;61(6):657-668.
205. Zalk R, Lehnart SE, Marks AR. Modulation of the ryanodine receptor and intracellular calcium. *Annu Rev Biochem*. 2007;76:367-385.
206. Putney JW, Jr. Capacitative calcium entry in the nervous system. *Cell Calcium*. 2003;34(4-5):339-344.
207. Parvez S, Beck A, Peinelt C, Soboloff J, Lis A, Monteilh-Zoller M, Gill DL, Fleig A, Penner R. STIM2 protein mediates distinct store-dependent and store-independent modes of CRAC channel activation. *FASEB journal : official publication of the Federation of American Societies for Experimental Biology*. 2008;22(3):752-761.
208. Ginsberg MD. Neuroprotection for ischemic stroke: past, present and future. *Neuropharmacology*. 2008;55(3):363-389.

6 Appendix

6.1 Abbreviations

[Ca ²⁺] _i	intracellular Ca ²⁺ concentration
°C	degree Celsius
μ	micro
aa	amino acid(s)
ADAM	a disintegrin and metalloproteinase
APC	antigen-presenting cell
APS	ammonium peroxodisulphate
bidest.	double distilled
BM	bone marrow
BMc	bone marrow chimeric
bp	base pair
BSA	bovine serum albumin
CD40L	CD40 ligand
cm ²	square centimeter
CPA	cyclopiazonic acid
CRP	collagen related peptide
CVX	convulxin
DMEM	Dulbecco's Modified Eagle's Medium
DMSO	dimethylsulfoxide
EAT-2	Ewing's sarcoma activated transcript 2
ECL	enhanced Chemiluminescence
ECM	extracellular matrix
EDTA	ethylenediaminetetraacetic acid
EF	embryonic feeder (cells)
EGTA	ethylene glycol tetraacetic acid
ERT	Eat-2-related transducer
ES (cell)	embryonic stem (cell)
<i>et al.</i>	<i>et alteri</i>
f	femto
Fab	fragment, antigen binding
Fc	fragment, crystallizable
FCS	fetal calf (bovine) serum
FITC	Fluorescein isothiocyanate

FSC	forward scatter
g	gram
G-418	Geneticin
GP	glycoprotein
h	hour(s)
H ₂ O	water
HCl	hydrogen chloride
HRP	horseradish peroxidase
Ig	immunoglobulin
IP	immunoprecipitation
IP ₃	inositol-1,4,5-trisphosphate
IRES	internal ribosome entry site
ITAM	Immunoreceptor tyrosine based activation motif
ITIM	Immunoreceptor tyrosine based inhibition motif
ITSM	Immunoreceptor tyrosine based switch motif
kb	kilo base (pair)
kDa	kilo Dalton
ko	knockout
L	liter
LB medium	Luria Bertani Medium
LIF	Leukaemia inhibitory factor
LPS	Lipopolysaccharide
M	Molar
mA	milliampere
MFI	mean fluorescence intensity
min	minute(s)
mL	milliliter
mm	millimeter
n	nano
NaCl	sodium chloride
NaOH	sodium hydroxide
NCBI	National Center for Biotechnology Information
Neo	neomycin
o/n	overnight
OGD	oxygen-glucose deprivation
PBS	phosphate buffered saline
PBS	phosphate-buffered saline

PCR	polymerase chain reaction
PE	phycoerythrin
PFA	paraformaldehyde
PKC	protein kinase C
PL	phospholipase
PRP	platelet-rich plasma
RC	rhodocytin
rpm	rounds per minute
RT	room temperature
s	second
SAP	SLAM-associated protein
sCD84	soluble CD84
SD	standard deviation
SDS	sodium dodecyl sulfate
SDS-PAGE	sodiumdodecylsulfate polyacrylamide gel electrophoresis
sGPVI	soluble GPVI
SH2	Src homology 2
SLAM	signaling lymphocyte activation molecule
SOC(E)	store operated calcium (entry)
SSC	side scatter
TAE	TRIS acetate EDTA buffer
TBS	Tris buffered saline
TE	TRIS EDTA buffer
tMCAO	transient middle cerebral artery occlusion
TNF	Tumor necrosis factor
TRAP	Thrombin receptor activating peptide
TRIS	Tris(hydroxymethyl)-aminomethane
TTC	2,3,5-triphenyltetrazolium chloride
TxA ₂	thromboxane A ₂
U	units
Uniprot	Universal Protein Resource
vWF	von Willebrand factor
wt	wild-type

6.2 Curriculum Vitae

Name	Sebastian Hofmann
Date of birth	October 6, 1982
Place of birth	Coburg
Nationality	German

School education

1989-2002	Primary, secondary and high school in Sesslach and Coburg
2002	German high school diploma (Abitur)

University education

2003-2009	Studies in Biology, Julius-Maximilians-Universität Würzburg
2009	Graduation - Diploma in Biology (Dipl. Biol.), Julius-Maximilians-Universität Würzburg

Postgraduate education

2009-now	PhD student in the group of Prof. Dr. Bernhard Nieswandt, Chair of Experimental Biomedicine, University Hospital and Rudolf Virchow Center for Experimental Biomedicine, Julius-Maximilians-Universität Würzburg
----------	--

Würzburg, March 11, 2013.....

Signature

6.3 Publications

Articles

Hofmann S, Vögtle T, Bender M, Rose-John S, Nieswandt B. The SLAM family member CD84 is regulated by ADAM10 and calpain in platelets. *J Thromb Haemost.* 2012;10(12):2581-2592.

Bender M, **Hofmann S**, Stegner D, Chalaris A, Bösl M, Braun A, Scheller J, Rose-John S, Nieswandt B. Differentially regulated GPVI ectodomain shedding by multiple platelet-expressed proteinases. *Blood.* 2010;116(17):3347-3355.

Oral Presentations

International Symposium of the Graduate School of Life Sciences, Würzburg, Oct 2012 Regulation and function of the SLAM family member CD84

Annual Retreat of the Rudolf-Virchow-Center, Kloster Schöntal, Sept 2011 Soluble CD84-a potential biomarker for thrombotic events?

Poster Presentations

EUPLAN Platelet Conference, Maastricht, the Netherlands, Sept 2012 Dual regulation of CD84 by ADAM10 and calpain in platelets

SFB688-CHFC Symposium, Würzburg, June 2012 Regulation and function of CD84 in platelets -a role beyond thrombus formation?

Jahrestagung der Gesellschaft für Thrombose und Hämostase, St.Gallen, Switzerland, Feb 2012 CD84 deficient mice are protected from ischemic stroke

International Symposium of SFB 487, "Molecular Pharmacology of Receptors, Channels and Transporters", Würzburg, July 2011 STIM2 and Orai2 are mediators of ischemic stroke

International Symposium of the Graduate
School of life Sciences, Würzburg, Oct 2010

Studies on the SLAM family member CD84
in mice

GPCR Dimer Symposium, Würzburg,
Oct 2009

Molecular studies on the SLAM family
member CD84 in mice

Award

Award for Best Poster Presentation at the EUPLAN Platelet Conference,
Maastricht, the Netherlands, Sept 2012

6.4 Acknowledgements

The work presented here was accomplished in the group of Prof. Dr. Bernhard Nieswandt at the Department of Experimental Biomedicine, University Hospital and the Rudolf Virchow Center, DFG Research Center for Experimental Biomedicine, University of Würzburg.

During the period of my PhD work (2009 - 2013), many people helped and supported me.

I would like to express my thanks to the following people:

- My supervisor, Prof. Dr. Bernhard Nieswandt, for giving me the opportunity to work in his laboratory, for his constant support, his enthusiasm and great scientific ideas. Without this, accomplishing this work would not have been possible. I would also like to thank him for allowing me to present my work at international conferences and symposia which enabled me to get to know many people in the scientific community and gather experience important for my future professional life.
- Dr. Heike Hermanns for the helpful scientific discussions and for reviewing my thesis.
- Prof. Dr. Guido Stoll for the helpful scientific discussions and for reviewing my thesis.
- My colleagues Dr. Markus Bender, Timo Vögtle and Dr. David Stegner for the close collaboration especially in the world-famous “shedding”-projects, support and for carefully proofreading my thesis.
- My colleague Dr. Attila Braun for support and help with molecular biologic issues.
- Sylvia Hengst and Birgit Midloch their support in the molecular biology lab.
- All present and former members of the group, who have not been mentioned here by name for the enjoyable working atmosphere and fun in the lab.
- All external collaborators who contributed to this work.
- Most importantly I would like to thank Hannah, my parents, my brother and my friends for their constant encouragement, support and patience.

6.5 Affidavit

I hereby confirm that my thesis entitled “Studies on the function and regulation of CD84, GPVI and Orai2 in genetically modified mice” is the result of my own work. I did not receive any help or support from commercial consultants. All sources and/or materials applied are listed and specified in the thesis.

Furthermore, I confirm that this thesis has not yet been submitted as part of another examination process neither in identical nor in similar form.

Würzburg, March 11, 2013.....

Signature

Eidesstattliche Erklärung

Hiermit erkläre ich an Eides statt, die Dissertation „Untersuchungen zur Funktion und Regulation von CD84, GPVI und Orai2 in genetisch veränderten Mäusen“ eigenständig, d.h. insbesondere selbständig und ohne Hilfe eines kommerziellen Promotionsberaters, angefertigt und keine anderen als die von mir angegebenen Quellen und Hilfsmittel verwendet zu haben.

Ich erkläre außerdem, dass die Dissertation weder in gleicher noch in ähnlicher Form bereits in einem anderen Prüfungsverfahren vorgelegen hat.

Würzburg, 11. März 2013

Unterschrift